HARVARD UNIVERSITY
Graduate School of Arts and Sciences

DISSERTATION ACCEPTANCE CERTIFICATE

The undersigned, appointed by the

Department of Chemistry & Chemical Biology

have examined a dissertation entitled:

Hydrodynamic Analysis and Protein Interactions of the Chromosomal Passenger Complex

presented by : Mariah Hanley

candidate for the degree of Doctor of Philosophy and hereby certify that it is worthy of acceptance.

Signature _____

Typed name: Professor Timothy J Mitchison

Signature _____

Typed name: Professor Emily Balskus

Signature _____

Typed name: Professor Daniel Kahne

Date: 21 November 2016

Hydrodynamic Analysis and Protein Interactions of the Chromosomal Passenger Complex

A DISSERTATION PRESENTED

BY

MARIAH L. HANLEY

TO

THE DEPARTMENT OF CHEMISTRY AND CHEMICAL BIOLOGY

IN PARTIAL FULFILLMENT OF THE REQUIREMENTS

FOR THE DEGREE OF

DOCTOR OF PHILOSOPHY

IN THE SUBJECT OF

CHEMISTRY

HARVARD UNIVERSITY

CAMBRIDGE, MASSACHUSETTS

NOVEMBER 2016

Thesis advisor: Professor Timothy J. Mitchison Mariah L. Hanley

Hydrodynamic Analysis and Protein Interactions of the Chromosomal Passenger Complex

Abstract

The chromosomal passenger complex (CPC) is a conserved protein complex regulating cell division. Although the kinase subunit, Aurora B (AURKB), self-activates through autophosphorylation, it remains unclear how this happens and more broadly how phosphorylation regulates CPC function. There are also outstanding questions about CPC structure, protein-protein interactions, and transport along microtubules.

In Chapter 1, I analyzed CPC hydrodynamic behavior to discover novel interacting partners with inactive CPC. Phosphorylated CPC in clarified mitotic and interphase *Xenopus laevis* egg extracts had a lower sedimentation coefficient on sucrose density gradients than unphosphorylated CPC. Therefore, phosphorylated CPC either is lighter or is in a more extended conformation. The addition of AURKB inhibitors prevented phosphorylation-induced sedimentation change, emphasizing the role of AURKB activity on CPC structure and function.

I tagged the CPC subunit CDCA8 with GFP-3xFLAG in HeLa cells using CRISPR/Cas9. CPC diffusion speed, measured by fluorescence correlation spectroscopy, underwent an AURKB kinase activity-dependent increase upon phosphorylation, indicating a decrease in complex size. This would

not be possible if phosphorylated CPC adopted a more extended conformation, which in conjunction with prior density sedimentation data implies that it must decrease in mass.

The nucleophosmin/nucleoplasmin family of proteins were identified to be candidates for this mass decrease using immunoprecipitation-mass spectrometry in both *X. laevis* extract and HeLa cell lysate. As known oligomeric chaperones, binding and unbinding of these proteins may be large enough to cause observed changes in CPC sedimentation and diffusion. Nucleophosmin/nucleoplasmin may inhibit CPC activity or prevent complex aggregation as a means of regulation.

In Chapter 2, I discussed tools developed to study CPC structure and function, including attempted targeting of the CPC to artificial lipid bilayers and purification of several recombinant CPC subunits and subunit domains. I also enumerated several efforts to isolate the CPC from biological sources.

In Chapter 3, I identified two additional potential CPC interacting partners, myosin II and the kinesin KIF20AE, through sucrose density gradient analysis and conduct preliminary examinations of the effects of these interactions on cell division.

Contents

Listing of figures

Acknowledgments

There are many people and organizations without whom this work would not have been possible. I would like to thank Timothy Mitchison, who kindly agreed to mentor me midway through graduate school. His near-constant wellspring of experiment ideas was an invaluable asset. Christine Field in many ways was a second mentor always available for advice, particularly about working with the frogs.

Arguably Tim's greatest strength is recruiting excellent people, and I benefited tremendously from the advice and support of members of the Mitchison lab, past and present. I particularly thank Keisuke Ishihara and Aaron Groen, who introduced me to the frog egg extract, and other members who got me up to speed quickly after I joined, including Martin Loose, a wonderful bay mate. Kristin Krukenberg, Nefeli Georgoulia, Alexandra Zidovska, Hallie Kuhn, and Sujeong Kim were also instrumental in creating a positive and productive lab environment and went on to amazing and inspirational careers. Peg Coughlin was always game for electron microscopy experiments, and Kathy Buhl, our indefatigable laboratory manager, kept the lab clean and tidy and accommodated equipment and materials requests with a smile. More recently, Matt Sonnett and members of the Mitchison family tree Tae Yeon Yoo

and Dan Needleman provided critical experimental support, and Elizabeth Van Itallie, Jui-Hsia Weng, James Pelletier, Elvan Boke, Zoltan Maliga, and Peter Koch provided assistance in manuscript and dissertation preparation and constant encouragement.

I would not have ended up at the Mitchison lab without support from key individuals in my first few years of graduate school, particularly Herschel Mukherjee, with whom I worked closely in the Myers lab, Allen Aloise, who provided support when I wanted to change things up, and Emily Balskus, who has kindly served on my advising committee throughout the entire process.

I met many wonderful people through my involvement in graduate student organizations, which allowed me to expand my Harvard network beyond the biochemistry community. The Harvard Women in Chemistry group welcomed me to Harvard and on the leadership board I met other thoughtful chemists with whom I had many lively discussions. I feel quite privileged to have helped the Journal of Emerging Investigators emerge from its infancy as Editor-in-Chief and am indebted to other graduate students who donated their time. Through the Harvard Graduate Consulting Club I found others who shared similar post-graduate visions and helped make those visions into reality.

Lastly, my family and friends provided a great deal of emotional support throughout my time at Harvard. You know who you are. Thank you.

0

Introduction

Proteins are defined by three principal attributes: amino acid sequence, posttranslational modifications, and the biological molecules with which they interact. This work concerned itself with how the latter two properties influence each other in an important mitotic protein complex, the chromosomal passenger complex (CPC). In particular, I focused on how adding phosphate groups affects the number and type of proteins with which the CPC interacts and described a novel interacting partner of inactive, unphosphorylated CPC.

0.1 Phosphorylation impacts protein behavior and structure

Of the great variety of possible posttranslational modifications, phosphorylation is both extremely common and also critical for proper cell function. A residue of a protein is phosphorylated when a kinase enzyme transfers a phosphate group from ATP. The phosphate group can then be removed by a phosphatase. The addition of the small phosphate molecule, with its four exposed oxygen atoms, can dramatically increase the hydrophilicity of that portion of the protein, resulting in a large change in protein structure and behavior (some examples of which are discussed below). Developing kinase inhibitors to modulate phosphorylation levels of key proteins has been a powerful way of treating of many diseases.

Phosphorylation can activate kinases, leading to a series of phosphorylation events known as a phosphorylation signaling cascade. One common function for such cascades is to generate a cellular response to external triggers. For instance, binding of epidermal growth factor to its receptor EGFR activates the receptor's cytoplasmic tyrosine kinase domain, which phosphorylates tyrosine residues on itself (Mitsudomi & Yatabe, 2010). After a few non-phosphorylation steps, RAF, MEK1/2, and MAPK kinases are all activated in turn. MAPK then phosphorylates many other proteins which regulate activity of transcription factors and ribosomal proteins, ultimately promoting cell growth (Avruch, 2007).

Alterations to this signaling cascade can have significant effects both on the single cell and on the host organism. Defects in this pathway alter the rate of cell growth, which can result in the development of cancer as the mutated cells proliferate (Zhang et al., 2007). While there are numerous drugs available modifying the EGFR/RAF/MEK/MAPK pathway, developing increasingly specific drugs with fewer off-target effects and fewer potential mechanisms for resistance, as well as identifying new pathways and connections, are still (and will likely remain for some time) important research areas.

Phosphorylation can also negatively regulate kinase activity. c-Src, a kinase influencing a range of

cellular functions from growth to motility and adhesion (Bjorge, Jakymiw, & Fujita, 2000), contains a SH2 domain, a SH3 domain, and a tyrosine kinase domain. When the kinase is inactive, a phosphorylated tyrosine group near the C-terminus, approximately 40 Å away from the catalytic site, interacts with the SH2 domain (Cooper, Gould, Cartwright, & Hunter, 1986; Okada & Nakagawa, 1989; Sicheri & Kuriyan, 1997; Haskell, Slack, Parsons, & Parsons, 2001). This in turn causes the SH3 domain interact with a linker region to keep the entire kinase tightly folded and the catalytic site hidden. The kinase is activated when the phosphate is removed and the protein opens up. Like many proteins, however, c-Src possesses multiple phosphorylation sites. A second site blocks the catalytic site when unphosphorylated. Phosphorylation shifts the residue away, allowing substrate access (Bjorge et al., 2000). Such "activation loops" are common regulatory elements for kinases (Schwartzberg, 1998). As with the kinases in the EGFR/MAPK pathway, numerous inhibitors have been developed to inhibit its activity for clinical use (Schenone, Brullo, Musumeci, Radi, & Castagnolo, 2011).

0.2 Regulation of the cell cycle by phosphorylation

Proper regulation of phosphorylation is particularly critical for successful progression through the cell cycle. This is guided primarily through cyclin-dependent kinases (CDKs). CDKs are active when bound to cyclins, proteins whose expression levels change throughout the cell cycle. For instance, cyclin B, which binds and activates Cdk1, is highly expressed at the beginning of the mitosis. In addition to regulation by cyclin B binding, Cdk1 itself is also phosphoregulated; similarly to c-Src, it must be phosphorylated on a threonine on its activation loop to have any kinase activity (Desai, Gu, & Morgan, 1992; Russo, Jeffrey, & Pavletich, 1996). Cdk1 phosphorylates a vast number of proteins, causing the dramatic changes required for the cell to enter mitosis (Petrone, Adamo, Cheng, & Kettenbach, 2016).

Phosphorylation also guides the location of the cleavage furrow. In late mitosis, two microtubule

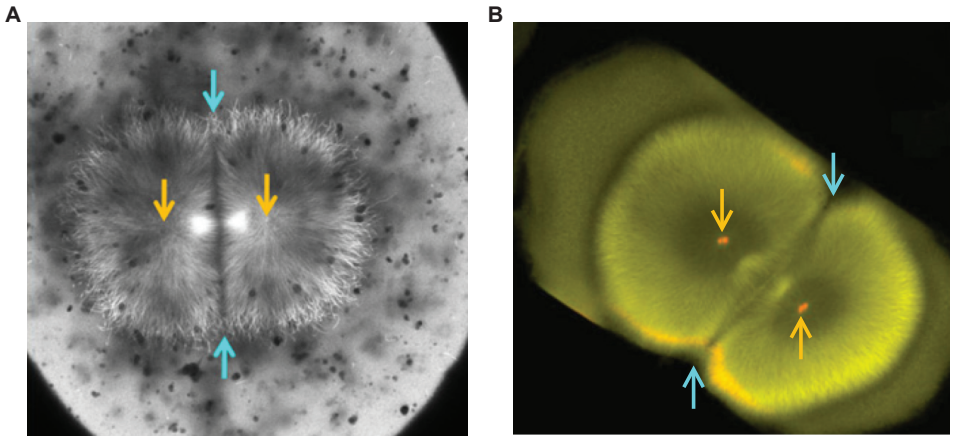

Figure 0.1: **Microtubule asters span cells and guide the location of the cleavage furrow.** (A) A live EMTB-3GFP zebrafish embryo showing the microtubules of a dividing cell. (B) A fixed *X. laevis* embryo immunostained for α-tubulin (yellow) and γ-tubulin (red). Blue arrows indicate midzone and orange arrows indicate centrosomes. Figures adapted from Wuhr, Tan, Parker, Detrich, & Mitchison, 2010.

asters form, which together spread across the entire area of the cell even in organisms with large eggs, such as zebrafish and *Xenopus laevis* (Figure 0.1) (Mitchison et al., 2012). At the midplane of the cell, the small area of microtubule overlap from the two asters forms a zone where many proteins localize. These proteins then communicate to the cortex to induce invagination of the plasma membrane, partially through phosphorylation. At the highest level of regulation, Cdk1 inhibits the growth of aster microtubules (Wuhr et al., 2008). Degradation of cyclin B by the anaphase promoting complex inactivates Cdk1 kinase and allows asters to form.

However, Cdk1 is too general a kinase to guide specific details of aster-cortex communication. Instead, other kinases fulfill this role. For instance, PLK1 (polo-like kinase 1) phosphorylates and is recruited to the midzone between microtubule asters by PRC1 (protein regulator of cytokinesis 1), a protein which bundles antiparallel microtubules (Hu, Ozlu, Coughlin, Steen, & Mitchison, 2012). PLK1 also phosphorylates RACGAP1 (Rac GTPase-activating protein 1), promoting the association of RAC-

GAP1 and ECT2 (protein Ect2), activating RHOA (transforming protein RhoA), and ultimately initiating actomyosin contraction and furrow invagination (Tatsumoto, Xie, Blumenthal, Okamoto, & Miki, 1999; Petronczki, Glotzer, Kraut, & Peters, 2007; Kim, Guo, Brahma, Xing, & Burkard, 2014).

0.3 Structure and function of the CPC

Another mitotically active kinase that influences microtubule-cortex communication is Aurora B kinase (AURKB). AURKB phosphorylates other mitotic proteins, including MCAK (Sampath et al., 2004), stathmin/Op18 (Belmont & Mitchison, 1996; Kelly et al., 2007), MKLP1 (Guse, Mishima, & Glotzer, 2005), histone H3 (Crosio et al., 2002), RACGAP1 (Hsu et al., 2000; Minoshima et al., 2003), and myosin II regulatory light chain (Murata-Hori et al., 2000), among others. These phosphorylations then impact protein function. For instance, MCAK (also known as KIF2C) is a kinesin that depolymerizes the plus ends of microtubules. This activity is suppressed by AURKB-dependent phosphorylation, which allows large microtubule asters to form (Andrews et al., 2004; Lan et al., 2004, Ohi et al., 2004). AURKB also phosphorylates itself on a threonine residue within its activation loop to activate its kinase activity, in a manner similar to c-Src and Cdk1 kinases (Yasui et al., 2004). Inhibition of AURKB via small molecules prevents mitosis and cytokinesis from progressing properly (Hu, Coughlin, Field, & Mitchison, 2008; Nguyen et al., 2014).

AURKB exists in a complex called the chromosomal passenger complex (CPC) containing three other proteins: CDCA8 (Dasra/borealin), BIRC5 (survivin) and INCENP (inner centromere protein). Together, these four proteins form the CPC, the focus of this work. The CPC has a variety of roles throughout mitosis, including promoting chromosome condensation (Mackay, Ainsztein, Eckley, & Earnshaw, 1998) and regulating the spindle assembly checkpoint (Tseng, Tan, Kapoor, & Funabiki, 2010) in metaphase (Figure 0.2A) and later in mitosis localizing to the midzone between microtubule asters and the cleavage furrow (Figure 0.2B) and triggering furrow ingression (Nguyen et al., 2014).

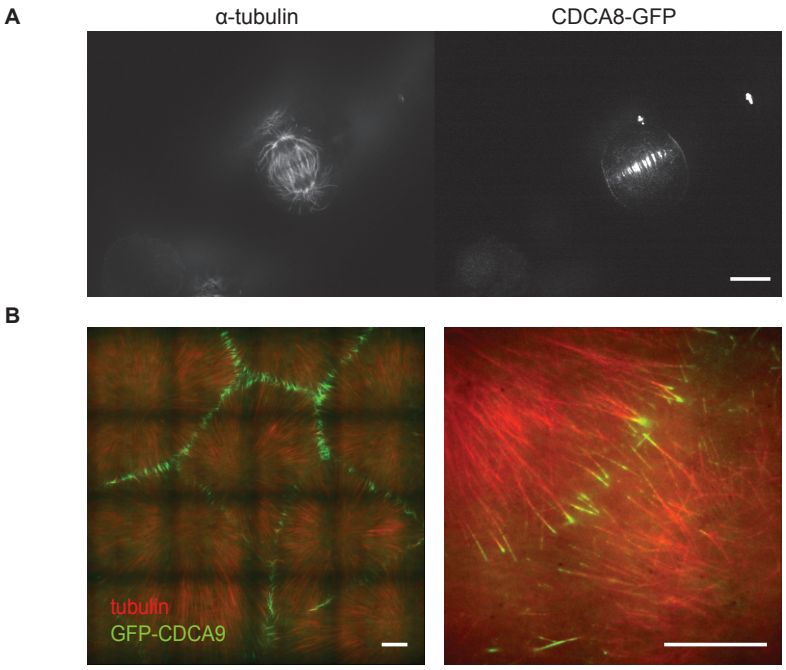

Figure 0.2: **Localization of the CPC in mitosis.** (A) The CPC subunit CDCA8 localizes to the center of spindles in HeLa cells (adapted from Figure 1.3). (B) The CPC subunit CDCA9 (the maternally loaded version of CDCA8 in *X. laevis*) localizes to the plus ends of microtubules in the midzone between microtubule asters in *X. laevis* extract on artificial supported lipid bilayers (adapted from Figure 2.1). Scale bars represent 10 μm.

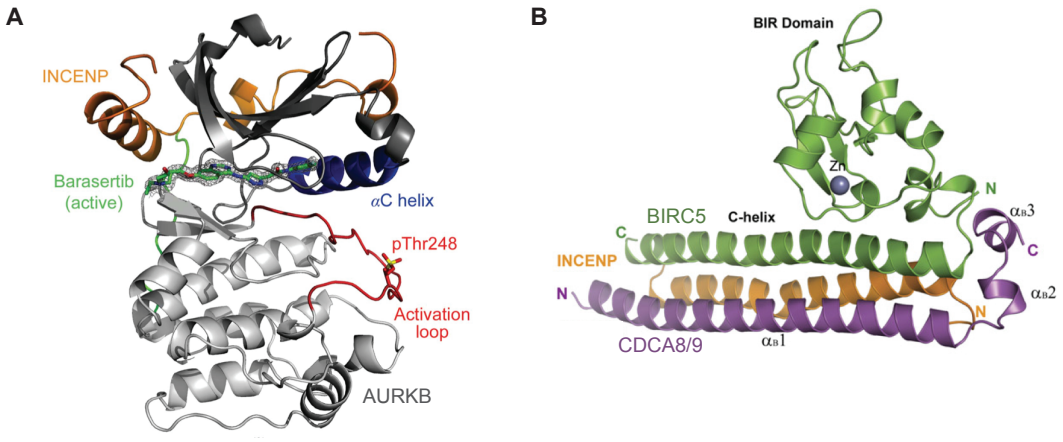

Figure 0.3: **Crystal structures of portions of the CPC.** (A) INCENP C-terminus with AURKB and the AURKB inhibitor barasertib, adapted from Sessa & Villa, 2014. (B) N-terminus with BIRC5 and CDCA8, adapted from Jeyaprakash et al., 2007. In between these two termini of the CPC is a section of INCENP that remains structurally uncharacterized, although it has recently been suggested to be partially a long single alpha helix (Samejima et al., 2015).

INCENP (inner centromere protein) is a large 110 kDa scaffolding protein containing a microtubule binding site (Mackay et al., 1998; Wheatley, Kandels-Lewis, Adams, Ainsztein, & Earnshaw, 2001; van der Horst et al., 2015) and an AURKB phosphorylation site near the C-terminus that allosterically regulates AURKB (Adams et al., 2000; Bishop & Schumacher, 2002; Honda, Koerner, & Nigg, 2003; Sessa et al., 2005). A long region in the middle contains a potential actin binding site (Landino & Ohi, 2016), and a helix on the N-terminus binds CDCA8 and BIRC5 (Jeyaprakash et al., 2007). While crystal structures of both termini of INCENP and its binding partners have been obtained (Sessa et al., 2005; Jeyaprakash et al., 2007; Sessa & Villa, 2014) (Figure 0.3), the structure of the inner section is still under investigation. Although previously thought to contain a coiled coil domain, recent evidence, primarily circular dichroism spectroscopy, suggests that this region may in fact be a single alpha helix 32 nm long, capable of stretching up to 80 nm, which may assist with a conformational change (Samejima et al., 2015; van der Horst et al., 2015).

CDCA8 binds DNA (Klein, Nigg, & Gruneberg, 2006) and dimerizes (Bekier, Mazur, Rashid, & Taylor, 2015), which may help cluster and anchor the CPC to biological structures, directing AURKB activity. In fact, artificially clustering the CPC by immunoprecipitating the complex on beads or by binding with certain antibodies (in particular, with antibodies raised against a peptide of the INCENP C-terminus) can activate AURKB (Kelly et al., 2007). CDCA8 is phosphorylated at numerous sites by multiple kinases including AURKB, but the purpose of these phosphorylations is not understood (Gassmann et al., 2004). In some eukaryotes, a separate isoform, CDCA9, replaces CDCA8 in early stage oogenesis.

BIRC5 is more notorious as an anti-apoptotic protein than as a member of the CPC (Athanasoula et al., 2014). Overexpression of BIRC5 in a variety of cancers correlates with decreased survival rate, and as such there are active efforts to develop therapeutics to modulate BIRC5 activity. During mitosis, however, it is affiliated with the other three CPC proteins. A subcomplex of INCENP, CDCA8, and BIRC5 can target independently to the centromere (Klein et al., 2006), and AURKB subcomplexes lacking CDCA8 and BIRC5 fail to target to any defined structures in mitosis, evidence that one or both of these proteins attach the complex to other biological structures (Jeyaprakash et al., 2007). BIRC5 is also phosphorylated by other mitotic proteins including PLK1, but as with CDCA8 phosphorylations their purpose is unclear (Chu et al., 2011). Similarly to CDCA8, some eukaryotes have different maternally loaded and embryonically expressed versions of BIRC5. The functional differences of the different versions of both BIRC5 and CDCA8/9 have not yet been investigated to any appreciable extent.

0.4 *Xenopus laevis* extract as a model system for cell division

To study the CPC, I made extensive use of extracts prepared from the eggs of *Xenopus laevis*. These eggs are easy to obtain, requiring only an injection of hormone into female frogs, and easy to manip-

ulate due to their large size (approximately 1 mm in diameter). To prepare cytoplasmic extract, the protective jelly coat is chemically removed and the unprotected eggs centrifuged, separating the cytoplasm from the yolk and membranes (Figure 0.4A) (Field, Nguyen, Ishihara, Groen, & Mitchison, 2014). The resulting undiluted extract is arrested in mitosis and can form both microtubule spindles and, when cycled into interphase, microtubule asters. The polymerizing ability of actin and other cortical proteins can also be observed microscopically if actin-intact extract is placed on supported lipid bilayers on glass coverslips. Because proteins are present in high concentrations and behave similarly to how they do in the egg, *X. laevis* extract is also a useful source of material for biochemical assays (Nguyen et al., 2014). These properties have been used to answer a number of important questions about the process of mitosis and cytokinesis.

Centrifuging the extract with greater force results in additional separation of cytoplasmic components (Groen, Ngyuen, Field, Ishihara, & Mitchison, 2014). Glycogen, which serves as an energy source for the egg, sediments at the bottom. Membranous organelles also separate from the rest of the extract, which forms a clear layer called high-speed supernatant (HSS). Proteins in HSS remain active, and, unlike crude extract, HSS can be frozen and thawed without any appreciable loss of activity. With the addition of energy supplements, taxol (a small molecule that stabilizes microtubules) and DMSO, ordered circular microtubule structures called pineapples form where the plus ends of the microtubules are oriented inwards and the minus ends outward toward the remainder of the solution (Figure 0.4B) (Mitchison, Nguyen, Coughlin, & Groen, 2013). The same proteins that localize to the midzone between asters in crude extract also localize to the pineapple centers, seemingly an apparent model for the midzone.

The *X. laevis* extract system has been used to great effect in studying CPC behavior, both through understanding CPC localization with microscopy experiments and through investigating CPC biochemical activity. (Sampath et al., 2004; Kelly et al., 2007; Nguyen et al., 2014). However, most studies have either looked at the CPC in relation to its effect on other mitotic proteins or at individual

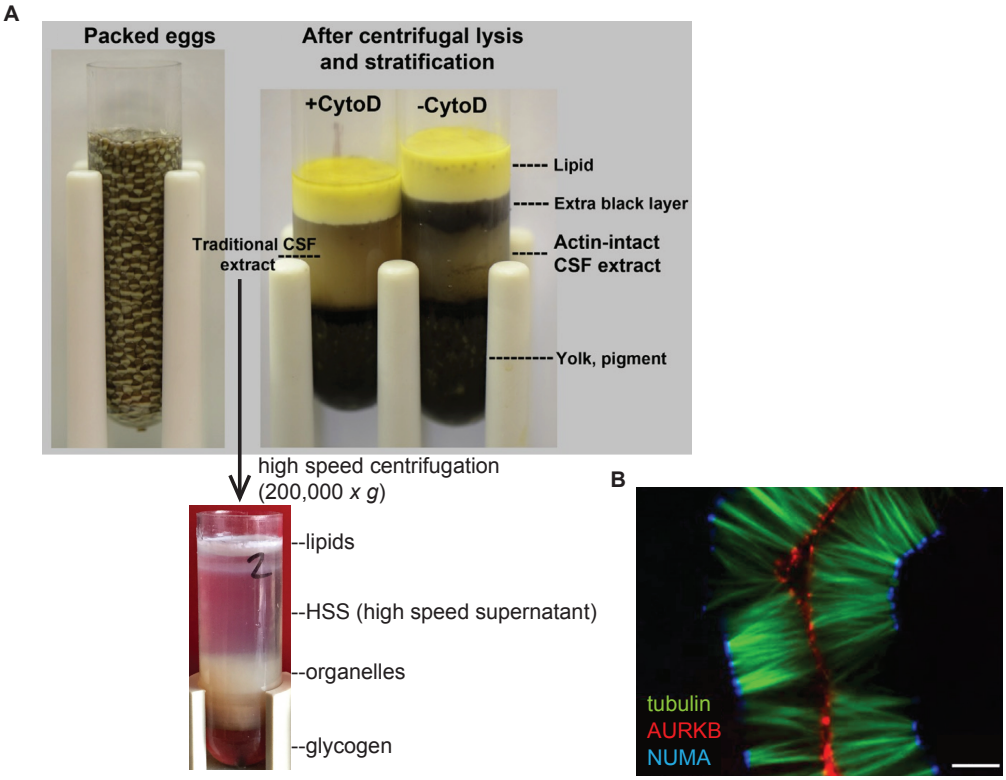

Figure 0.4: ***X. laevis* extract and HSS preparation** (A) Dejellied *X. laevis* eggs are crushed by centrifugation to generate crude extract, with or without intact actin polymerization based on the optional addition of cytochalasin D. An additional higher speed centrifugation of CSF extract further separates extract components. Most cytoplasmic protein is in the clear high speed supernatant (HSS) layer (adapted from Field, Nguyen, Ishihara, Groen, & Mitchison, 2014). (B) Example of a microtubule pineapple formed from HSS by adding 5% DMSO and 5 μM taxol (adapted from Mitchison, Nguyen, Coughlin, & Groen, 2013). Scale bar represents 10 μm.

subunits. In this work, I focus on the gap between these two areas of research and look primarily at the relationship between the subunits of the CPC and how phosphorylation influences the behavior of the complex as a whole.

0.5 Dissertation Scope

This work focused on expanding our knowledge of the function and regulation of the CPC and its subunits. I used primarily *X. laevis* HSS in my investigations but also expanded my work on certain occasions to include pure protein assays and mammalian tissue culture cells.

It was previously reported that the sedimentation coefficient of the CPC increased as the cell shifted from mitosis to interphase (Bolton et al., 2002). In Chapter 1, my collaborators and I addressed two primary questions related to this observation using a combination of biochemical assays and hydrodynamic analyses.

We felt that analyzing hydrodynamic changes of the CPC would be illuminating in light of the recent discovery of the long single alpha helix in the middle of INCENP. It was previously thought that this domain was a coiled-coil, which would suggest that the CPC formed dimers or multimers. However, this discovery opens up the possibility that the CPC may undergo conformational changes or have other, more complex mechanisms of oligomerization. Examining the hydrodynamic behavior of the CPC allowed us to distinguish between some of these possibilities.

Hydrodynamic analysis encompasses a range of techniques to determine the size and shape of proteins and complexes, including density gradient sedimentation and fluorescence correlation spectroscopy (Cantor & Schimmel, 1980). Density gradient sedimentation, for instance, involves centrifuging a biological sample on a gradient of low to high density. Proteins or protein complexes that are heavier or more compact will sediment in denser fractions. Fluorescence correlation spectroscopy allow us to determine the spatial size of the protein or complex by measuring how fast the molecule(s)

diffuse through solution. This is done by using a microscope to observe intensity fluctuations generated by movement of fluorescently-tagged molecules through a femtoliter-sized volume. When these techniques are combined, we can learn more about the structure of a protein or complex and investigate how these parameters change with different stimuli.

We first confirmed the previously observed change in the sedimentation coefficient of the CPC. We treated HSS with a phosphatase inhibitor, an AURKB inhibitor, or a combination of the two and sedimented HSS on sucrose gradients. CPC proteins in both mitotic and interphase HSS treated with phosphatase inhibitor sedimented significantly higher up on the gradient than those in HSS without drug treatment, with AURKB inhibitor or with both drugs. This suggested that the shift of the CPC sedimentation coefficient is guided by AURKB phosphorylation and that the complex is either changing in mass or changing in conformation. We then generated and used a CDCA8-GFP-3xFLAG tagged HeLA cell line in fluorescence correlation spectroscopy (FCS) experiments, where the addition of a phosphatase inhibitor caused the CPC to move faster, meaning that the CPC had decreased in size. This effect was prevented by the concurrent addition of an AURKB inhibitor. Therefore, AURKB activity is also required for the decrease in the size of the CPC.

Based on the change in the sedimentation coefficient, the phosphorylated complex either lost mass or adopted a more extended conformation. However, it moved faster when phosphorylated and thus could not have adopted a more extended conformation. Therefore, the phosphorylated complex has less mass, either because it is no longer an oligomer or because it has lost other associated proteins.

We used immunoprecipitation-mass spectrometry (IP-MS) from HSS to identify proteins that only associate with inactive, dephosphorylated CPC. The nucleophosmin/nucleoplasmin family of proteins (NPMs) was an attractive set of hits because they are present in high abundance in both *X. laevis* eggs and tissue culture cells and form large hetero-oligomeric pentameric and decameric complexes (Namboodiri, Akey, Schmidt-Zachmann, Head, & Akey, 2004; Platonova, Akey, Head, & Akey, 2011). The association between NPMs and the CPC is only present when AURKB is inhibited or

inactive, suggesting that NPM may regulate CPC activity.

Nucleophosmin/nucleoplasmin proteins are already known to chaperone other proteins, particularly histones (Okuwaki, Matsumoto, Tsujimoto, & Nagata, 2001; Gadad et al., 2011; Fernandez-Rivero et al., 2016). In fact, the term "molecular chaperone" was first coined in 1978, when Laskey found that nucleoplasmin helps stop unwanted histone-DNA aggregation (Laskey, Honda, Mills, & Finch, 1978). It has since been expanded to encompass a wide range of proteins that typically prevent aggregation, most commonly by sequestering hydrophobic patches on the target protein (Sousa, 2014). For instance, the chaperonins form hollow cylinders where only unfolded proteins can enter, promoting their own folding by isolating them from other proteins (Langer, Pfeifer, Martin, Baumeister, & Hartl, 1992; Martin, Mayhew, Langer, & Hartl, 1993). Heat shock proteins, in particular Hsp70, also protect proteins from aggregation. In the case of Hsp70, a clamshell-like binding pocket opens and closes around singular proteins to isolate them. Hsp70 can also disaggregate proteins, particularly when used in combination with another family member Hsp110 (Shaner, Trott, Goeckeler, Brodsky, & Morano, 2004; Hrizo et al., 2007). NPM proteins may protect the CPC from associating with other CPCs. A signal may then initiate NPM-CPC dissociation, promoting AURKB activity.

In Chapter 2, I presented some tools developed to explore the behavior and function of the CPC and its subunits. In the first section, I discussed attempts to develop a system to artificially target mitotically important proteins to supported lipid bilayers. AURKB activity is required for proper positioning of the cleavage furrow (Nguyen et al., 2014), so I wondered if by targeting the CPC to an artificial lipid bilayer using a light-inducible recruitment system in the presence of *X. laevis* extract, I could recruit active RHOA without microtubule asters.

I attempted to use a system based on a light-sensitive LOV domain caging a protein-binding peptide in yeast (Strickland et al., 2012), but it did not translate well to purified proteins in the extract system. When LOV was used to cage a different protein-binding peptide which forms a covalent bond, a light-induced dimerization was observed. However, the binding took roughly 30 minutes to reach

maximum binding and there was a large proportion of unbound protein remaining. Interphase *X. laevis* extracts tend to lose potency after about 45 minutes, so this system was ultimately not practical for the desired targeting experiments on supported lipid bilayers in *X. laevis* extract.

In addition to studying the interactions of the complex with other proteins, I wanted to examine the interactions between complex subunits. I cloned, expressed, and purified versions of fluorescently tagged CDCA8, CDCA9 (the maternally loaded version of CDCA8 in *X. laevis* eggs) and BIRC5 as well as several CDCA8/9 domain mutants. The CDCA8/9 proteins, and, surprisingly, the domain mutants, localized to pineapple microtubules, but only some convincingly localized to microtubule plus ends (where the complete CPC localizes). In contrast, BIRC5 proteins only localized to microtubule plus ends. Further optimization and mutational analysis may yield new information about the function of CPC subunit domains.

Lastly, I attempted to purify whole CPC from biological sources for both biochemical assays and electron microscopy. From *X. laevis* extract, I recruited the CPC to magnetic beads coated with an AURKB inhibitor or antibodies against CPC subunits, but neither method gave clean and abundant complex. A modification where the antibody was conjugated with a cleavable peptide attached to beads was more promising but additional optimization of this strategy is still required. I also isolated the CPC from lysates of the CDCA8-GFP-3xFLAG HeLa cell line with the FLAG tag. Unfortunately, many other proteins were obtained, many likely non-specific, and an additional tag on a different CPC subunit will almost certainly be required for successful CPC isolation.

In Chapter 3, I described additional experiments exploring CPC properties and behavior. When fractions from sucrose gradient sedimentation experiments described in Chapter 1 were analyzed with quantitative mass spectrometry, two proteins were identified that may associate with the CPC and have some affect on its behavior: myosin II and KIF20AE (the maternally loaded isoform of KIF20A).

I wondered if the binding and contraction of myosin II was driving the observed CPC shifts on sucrose gradients, but found that myosin II heavy chain did not co-sediment with the CPC when the

CPC is phosphorylated. I also tested if AURKB activity was required for actomyosin contractility in interphase extract. When interphase extract is treated with phosphatase inhibitors at room temperature, it rapidly contracts. Inhibition of AURKB did indeed slow down this contraction. However, drugs inhibiting the activity of PLK1 or microtubule polymerization also influenced interphase extract contractility. The regulatory networks guiding myosin behavior are complex, and substantial effort will need to be invested to fully understand the implications of these observations.

There has been some evidence that KIF20AE, a maternally loaded kinesin, is responsible for CPC transport along microtubules in mitosis (Nguyen et al., 2014). CPC subunits in KIF20AE-depleted HSS did not sediment any differently than regular HSS. Pineapple formation and localization of CDCA9 to the center of pineapples was similarly unaffected by KIF20AE depletion. CDCA9 actually recruited to pineapples earlier that KIF20AE, although it did not localize to the center of pineapples until KIF20AE did, leaving open the question of CPC transport by KIF20AE in this system.

In this work, I have demonstrated that the CPC binds to the nucleophosmin/nucleoplasmin family of proteins only when AURKB is inactive. The most important next step will be to investigate the functional significance of this interaction. Opportunities based on this work also exist to isolate the CPC from biological extracts, to study individual CPC subunits using pure proteins, and to explore the effects the CPC has on actomyosin contractility.

0.6 References

Adams, R. R., Wheatleya, S. P., Gouldsworthy, A. M., Kandels-Lewis, S. E., Carmena, M., Smythe, C., Gerloff, D. L., & Earnshaw, W. C. (2000). INCENP binds the Aurora-related kinase AIRK2 and is required to target it to chromosomes, the central spindle and cleavage furrow. Curr. Biol., 10(17), 1075-1078.

Andrews, P.D., Ovechkina, Y., Morrice, N., Wagenbach, M., Duncan, K., Wordeman, L., & Swedlow, J.R. (2004). Aurora B regulates MCAK at the mitotic centromere. Dev. Cell 6, 253-268.

Athanasoula, K. C., Gogas, H., Polonifi, K., Vaiopoulos, A. G., Polyzos, A., & Mantzourani, M. (2014). Survivin beyond physiology: Orchestration of multistep carcinogenesis and therapeutic potentials. Cancer Lett., 347(2), 175-182.

Avruch, J. (2007). MAP kinase pathways: The first twenty years. Biochim. Biophys. Acta, Mol. Cell Res., 1773(8), 1150-1160.

Bekier, M. E., Mazur, T., Rashid, M. S., & Taylor, W. R. (2015). Borealin dimerization mediates optimal CPC checkpoint function by enhancing localization to centromeres and kinetochores. Nat. Commun., 6, 6775.

Belmont, L. D., & Mitchison, T. J. (1996). Identification of a protein that interacts with tubulin dimers and increases the catastrophe rate of microtubules. Cell, 84(4), 623-631.

Bishop, J. D., & Schumacher, J. M. (2002). Phosphorylation of the carboxyl terminus of inner centromere protein (INCENP) by the Aurora B kinase stimulates Aurora B kinase activity. J. Biol. Chem., 277(31), 27577-27580.

Bjorge, J. D., Jakymiw, A., & Fujita, D. J. (2000). Selected glimpses into the activation and function of Src kinase. Oncogene, 19(49), 5620-5635.

Bolton, M. A., Lan, W., Powers, S. E., McCleland, M. L., Kuang, J., & Stukenberg, P. T. (2002). Aurora B kinase exists in a complex with survivin and INCENP and its kinase activity is stimulated by survivin binding and phosphorylation. Mol. Biol. Cell, 13(9), 3064-3077.

Cantor, C. R., & Schimmel, P. R. (1980). Biophysical Chemistry. New York, NY: W. H. Freeman and Company.

Chu, Y., Yao, P. Y., Wang, W., Wang, D., Wang, Z., Zhang, L., Huang, Y., Ke, Y., Ding, X., & Yao, X. (2011). Aurora B kinase activation requires survivin priming phosphorylation by PLK1. J. Mol. Cell Biol., 3(4), 260-267.

Cooper, J. A., Gould, K. L., Cartwright, C. A., & Hunter, T. (1986). Tyr527 is phosphorylated in pp60c-src: implications for regulation. Science, 231(4744), 1431-1434.

Crosio, C., Fimia, G. M., Loury, R., Kimura, M., Okano, Y., Zhou, H., Sen, S., Allis, C. D., & Sassone-Corsi, P. (2002). Mitotic phosphorylation of histone H3: spatio-temporal regulation by mammalian aurora kinases. Mol. Cell. Biol., 22(3), 874-885.

Desai, D., Gu, Y., & Morgan, D. O. (1992). Activation of human cyclin-dependent kinases in vitro. Mol. Biol. Cell, 3(5), 571-582.

Fernandez-Rivero, N., Franco, A., Velazquez-Campoy, A., Alonso, E., Muga, A., & Prado, A. (2016). A quantitative characterization of nucleoplasmin/histone complexes reveals chaperone versatility. Sci. Rep., 6, 32114.

Field, C. M., Nguyen, P. A., Ishihara, K., Groen, A. C., & Mitchison, T. J. (2014). Xenopus egg cytoplasm with intact actin. Methods Enzymol., 540, 399-415.

Gadad, S. S., Senapati, P., Syed, S. H., Rajan, R. E., Shandilya, J., Swaminathan, V., Chatterjee, S., Colombo, E., Dimitrov, S., Pelicci, P. G., Ranga, U., & Kundu, T. K. (2011). The multifunctional protein nucleophosmin (NPM1) is a human linker histone H1 chaperone. Biochemistry, 50(14), 2780-2789.

Gassmann, R., Carvalho, A., Henzing, A. J., Ruchaud, S., Hudson, D. F., Honda, R., Nigg, E. A., Gerloff, D. L., & Earnshaw, W. C. (2004). Borealin: A novel chromosomal passenger required for stability of the bipolar mitotic spindle. J. Cell Biol., 166(2), 179-191.

Groen, A. C., Ngyuen, P. A., Field, C. M., Ishihara, K., & Mitchison, T. J. (2014). Glycogen-supplemented mitotic cytosol for analyzing Xenopus egg microtubule organization. Methods Enzymol., 540, 417-433.

Guse, A., Mishima, M., & Glotzer, M. (2005). Phosphorylation of ZEN-4/MKLP1 by Aurora B regulates completion of cytokinesis. Curr. Biol., 15(8), 778-786.

Haskell, M. D., Slack, J. K., Parsons, J. T., & Parsons, S. J. (2001). c-Src tyrosine phosphorylation of epidermal growth factor receptor, P190 RhoGAP, and focal adhesion kinase regulates diverse cellular processes. Chem. Rev., 101(8), 2425-2440.

Honda, R., Koerner, R., & Nigg, E. A. (2003). Exploring the functional interactions between Aurora B, INCENP, and survivin in mitosis. Mol. Biol. Cell, 14(8), 3325-3341.

Hrizo, S. L., Gusarova, V., Habiel, D. M., Goeckeler, J. L., Fisher, E. A., & Brodsky, J. L. (2007).

The Hsp110 molecular chaperone stabilizes apolipoprotein B from endoplasmic reticulum-associated degradation (ERAD). J. Biol. Chem., 282(45), 32665-32675.

Hsu, J.-Y., Sun, Z.-W., Li, X., Reuben, M., Tatchell, K., Bishop, D. K., Grushcow, J. M., Brame, C. J., Caldwell, J. A., Hunt, D. F., Lin, R., Smith, M. M., & Allis, C. D. (2000). Mitotic phosphorylation of histone H3 is governed by Ipl1/aurora kinase and Glc7/PP1 phosphatase in budding yeast and nematodes. Cell, 102(3), 279-291.

Hu, C.-K., Ozlu, N., Coughlin, M., Steen, J. J., & Mitchison, T. J. (2012). Plk1 negatively regulates PRC1 to prevent premature midzone formation before cytokinesis. Mol. Biol. Cell, 23(14), 2702-2711.

Hu, C. K., Coughlin, M., Field, C. M., & Mitchison, T. J. (2008). Cell polarization during monopolar cytokinesis. J. Cell. Biol., 181(2), 195-202.

Jeyaprakash, A. A., Klein, U. R., Lindner, D., Ebert, J., Nigg, E. A., & Conti, E. (2007). Structure of a survivin-borealin-INCENP core complex reveals how chromosomal passengers travel together. Cell, 131(2), 271-285.

Kelly, A. E., Sampath, S. C., Maniar, T. A., Woo, E. M., Chait, B. T., & Funabiki, H. (2007). Chromosomal enrichment and activation of the Aurora B pathway are coupled to spatially regulate spindle assembly. Dev. Cell, 12, 31-43.

Kim, H., Guo, F., Brahma, S., Xing, Y., & Burkard, M. E. (2014). Centralspindlin assembly and 2 phosphorylations on MgcRacGAP by Polo-like kinase 1 initiate Ect2 binding in early cytokinesis. Cell Cycle, 13(18), 2952-2961.

Klein, U. R., Nigg, E. A., & Gruneberg, U. (2006). Centromere targeting of the chromosomal passenger complex requires a ternary subcomplex of Borealin Survivin, and the N-terminal domain of INCENP. Mol. Biol. Cell, 17, 2547-2558.

Lan, W., Zhang, X., Kline-Smith, S.L., Rosasco, S.E., Barrett-Wilt, G.A., Shabanowitz, J., Hunt, D.F., Walczak, C.E., and Stukenberg, P.T. (2004). Aurora B phosphorylates centromeric MCAK and regulates its localization and microtubule depolymerization activity. Curr. Biol. 14, 273-286.

Landino, J., & Ohi, R. (2016). The timing of midzone stabilization during cytokinesis depends on myosin II activity and an interaction between INCENP and actin. Curr. Biol., 26(5), 698-706.

Langer, T., Pfeifer, G., Martin, J., Baumeister, W., & Hartl, F. U. (1992). Chaperonin-mediated protein folding: GroES binds to one end of the GroEL cylinder, which accommodates the protein substrate within its central cavity. EMBO J., 11(13), 4757-4765.

Laskey, R. A., Honda, B. M., Mills, A. D., & Finch, J. T. (1978). Nucleosomes are assembled by an acidic protein which binds histones and transfers them to DNA. Nature, 275(5679), 416-420.

Mackay, A. M., Ainsztein, A. M., Eckley, D. M., & Earnshaw, W. C. (1998). A dominant mutant of inner centromere protein (INCENP), a chromosomal protein, disrupts prometaphase congression and cytokinesis. J. Cell Biol., 140(5), 991-1002.

Martin, J., Mayhew, M., Langer, T., & Hartl, F. U. (1993). The reaction cycle of GroEL and GroES in chaperonin-assisted protein folding. Nature, 366(6452), 228-233.

Minoshima, Y., Kawashima, T., Hirose, K., Tonozuka, Y., Kawajiri, A., Bao, Y. C., Deng, X., Tatsuka, M., Narumiya, S., May, W. S., Jr., Nosaka, T., Semba, K., Inoue, T., Satoh, T., Inagaki, M., & Kitamura, T. (2003). Phosphorylation by Aurora B converts MgcRacGAP to a RhoGAP during cytokinesis. Dev. Cell, 4(4), 549-560.

Mitchison, T., Wuehr, M., Nguyen, P., Ishihara, K., Groen, A., & Field, C. M. (2012). Growth, interaction, and positioning of microtubule asters in extremely large vertebrate embryo cells. Cytoskeleton, 69(10), 738-750.

Mitchison, T. J., Nguyen, P., Coughlin, M., & Groen, A. C. (2013). Self-organization of stabilized microtubules by both spindle and midzone mechanisms in Xenopus egg cytosol. Mol. Biol. Cell, 24(10), 1559-1573.

Mitsudomi, T., & Yatabe, Y. (2010). Epidermal growth factor receptor in relation to tumor development: EGFR gene and cancer. FEBS J., 277(2), 301-308.

Murata-Hori, M., Fumoto, K., Fukuta, Y., Iwasaki, T., Kikuchi, A., Tatsuka, M., & Hosoya, H. (2000). Myosin II regulatory light chain as a novel substrate for AIM-1, an Aurora/Ipl1p-related kinase from rat. J. Biochem., 128(6), 903-907.

Namboodiri, V. M. H., Akey, I. V., Schmidt-Zachmann, M. S., Head, J. F., & Akey, C. W. (2004). The structure and function of Xenopus NO38-core, a histone chaperone in the nucleolus. Structure, 12(12), 2149-2160.

Nguyen, P. A., Groen, A. C., Loose, M., Ishihara, K., Wuehr, M., Field, C. M., & Mitchison, T. J. (2014). Spatial organization of cytokinesis signaling reconstituted in a cell-free system. Science, 346(6206), 244-247.

Ohi, R., Sapra, T., Howard, J., and Mitchison, T.J. (2004). Differentiation of cytoplasmic and meiotic spindle assembly MCAK functions by Aurora B-dependent phosphorylation. Mol. Biol. Cell, 5(2), 309-321.

Okada, M., & Nakagawa, H. (1989). A protein tyrosine kinase involved in regulation of pp60c-src function. J. Biol. Chem., 264(35), 20886-20893.

Okuwaki, M., Matsumoto, K., Tsujimoto, M., & Nagata, K. (2001). Function of nucleophosmin/B23, a nucleolar acidic protein, as a histone chaperone. FEBS Lett., 506(3), 272-276.

Petronczki, M., Glotzer, M., Kraut, N., & Peters, J.-M. (2007). Polo-like kinase 1 triggers the initiation of cytokinesis in human cells by promoting recruitment of the RhoGEF Ect2 to the central spindle. Dev. Cell, 12, 713-725.

Petrone, A., Adamo, M. E., Cheng, C., & Kettenbach, A. N. (2016). Identification of candidate cyclin-dependent kinase 1 (Cdk1) substrates in mitosis by quantitative phosphoproteomics. Mol. Cell. Proteomics, 15(7), 2448-2461.

Platonova, O., Akey, I. V., Head, J. F., & Akey, C. W. (2011). Crystal structure and function of human nucleoplasmin (Npm2): A histone chaperone in oocytes and embryos. Biochemistry, 50(37), 8078-8089.

Russo, A. A., Jeffrey, P. D., & Pavletich, N. P. (1996). Structural basis of cyclin-dependent kinase activation by phosphorylation. Nat. Struct. Biol., 3(8), 696-700.

Samejima, K., Platani, M., Wolny, M., Ogawa, H., Vargiu, G., Knight, P. J., Peckham, M., & Earnshaw, W. C. (2015). The inner centromere protein (INCENP) coil is a single alpha-helix (SAH) domain that binds directly to microtubules and is important for chromosome passenger complex (CPC) localization and function in mitosis. J. Biol. Chem., 290, 21460-21472.

Sampath, S. C., Ohi, R., Leismann, O., Salic, A., Pozniakovski, A., & Funabiki, H. (2004). The chromosomal passenger complex is required for chromatin-induced microtubule stabilization and spindle assembly. Cell, 118(2), 187-202.

Schenone, S., Brullo, C., Musumeci, F., Radi, M., & Castagnolo, D. (2011). Src kinase inhibitors: an update on patented compounds. Curr. Med. Chem., 18(33), 5061-5078.

Schwartzberg, P. L. (1998). The many faces of Src: multiple functions of a prototypical tyrosine kinase. Oncogene, 17(11), 1463-1468.

Sessa, F., Mapelli, M., Ciferri, C., Tarricone, C., Areces, L. B., Schneider, T. R., Stukenberg, P. T., & Musacchio, A. (2005). Mechanism of Aurora B activation by INCENP and inhibition by hesperadin. Mol. Cell, 18(3), 379-391.

Sessa, F., & Villa, F. (2014). Structure of Aurora B-INCENP in complex with barasertib reveals a po-

tential transinhibitory mechanism. Acta Crystallogr. F: Struct. Biol. Commun., 70(3), 294-298.

Shaner, L., Trott, A., Goeckeler, J. L., Brodsky, J. L., & Morano, K. A. (2004). The function of the yeast molecular chaperone Sse1 Is mechanistically distinct from the closely related Hsp70 family. J. Biol. Chem., 279(21), 21992-22001.

Sicheri, F., & Kuriyan, J. (1997). Structures of Src-family tyrosine kinases. Curr. Opin. Struct. Biol., 7(6), 777-785.

Sousa, R. (2014). Structural mechanisms of chaperone mediated protein disaggregation. Front. Mol. Biosci., 1, 12/11-12/18.

Strickland, D., Lin, Y., Wagner, E., Hope, C. M., Zayner, J., Antoniou, C., Sosnick, T. R., Weiss, E. L., & Glotzer, M. (2012). TULIPs: tunable, light-controlled interacting protein tags for cell biology. Nat. Methods, 9, 379-384.

Tatsumoto, T., Xie, X., Blumenthal, R., Okamoto, I., & Miki, T. (1999). Human ECT2 is an exchange factor for Rho GTPases, phosphorylated in G2/M phases, and involved in cytokinesis. J. Cell Biol., 147(5), 921-927.

Tseng, B. S., Tan, L., Kapoor, T. M., & Funabiki, H. (2010). Dual detection of chromosomes and microtubules by the chromosomal passenger complex drives spindle assembly. Dev. Cell, 18, 903-912.

van der Horst, A., Vromans, M. J. M., Bouwman, K., van der Waal, M. S., Hadders, M. A., & Lens, S. M. A. (2015). Inter-domain cooperation in INCENP promotes Aurora B relocation from centromeres to microtubules. Cell Rep., 12(3), 380-387.

Wheatley, S. P., Kandels-Lewis, S. E., Adams, R. R., Ainsztein, A. M., & Earnshaw, W. C. (2001). INCENP binds directly to tubulin and requires dynamic microtubules to target to the cleavage furrow. Exp. Cell Res., 262(2), 122-127.

Wuhr, M., Chen, Y., Dumont, S., Groen, A. C., Needleman, D. J., Salic, A., & Mitchison, T. J. (2008). Evidence for an upper limit to mitotic spindle length. Curr. Biol., 18(16), 1256-1261.

Wuhr, M., Tan, E. S., Parker, S. K., Detrich, H. W., 3rd, & Mitchison, T. J. (2010). A model for cleavage plane determination in early amphibian and fish embryos. Curr. Biol., 20(22), 2040-2045.

Yasui, Y., Urano, T., Kawajiri, A., Nagata, K.-i., Tatsuka, M., Saya, H., Furukawa, K., Takahashi, T., Izawa, I., & Inagaki, M. (2004). Autophosphorylation of a newly identified site of Aurora-B Is indispensable for cytokinesis. J. Biol. Chem., 279, 12997-13003.

Zhang, H., Berezov, A., Wang, Q., Zhang, G., Drebin, J., Murali, R., & Greene, M. I. (2007). ErbB receptors: from oncogenes to targeted cancer therapies. J. Clin. Invest., 117(8), 2051-2058.

1

CPC Hydrodynamic Analysis Reveals Inactive State Association with Nucleoplasmin / Nucleophosmin

Mariah L. Hanley, Tae Yeon Yoo, Matthew Sonnett, Daniel J. Needleman, and Timothy J. Mitchison

Manuscript in Preparation

1.1 Abstract

The chromosomal passenger complex (CPC) is a conserved, essential regulator of cell division. As such, significant anti-cancer drug development efforts have been focused on targeting the CPC, most notably by inhibiting the AURKB kinase subunit. The CPC is activated by AURKB-catalyzed autophosphorylation on multiple subunits, but how this regulates CPC interactions with other mitotic proteins remains unclear. We investigated the hydrodynamic behavior of the CPC in *Xenopus laevis* egg cytosol using sucrose gradient sedimentation and in HeLa cells using fluorescence correlation spectroscopy (FCS). We found that autophosphorylation of the CPC decreases its sedimentation coefficient (S-value) in egg cytosol and increases its diffusion coefficient in live cells, indicating a decrease in mass. Using immunoprecipitation coupled with mass spectrometry and immunoblots, we discovered that inactive, unphosphorylated CPC binds to nucleophosmin/nucleoplasmin proteins, which are known to oligomerize into large complexes. Autophosphorylation of the CPC causes it to dissociate from nucleophosmin/nucleoplasmin. We propose that nucleophosmin/nucleoplasmin complexes serve as chaperones that stabilize the inactive form of the CPC, preventing CPC autophosphorylation and recruitment to chromatin and microtubules in mitosis.

1.2 Introduction

The four-protein chromosomal passenger complex (CPC) is essential for proper cell division in many eukaryotes (Nguyen et al., 2014; Sampath et al., 2004). Comprising one each of AURKB (AuroraB kinase), INCENP (inner centromere protein), CDCA8 (borealin/DasraB), and BIRC5 (survivin) subunits, the complex localizes to mitotic chromosomes during metaphase, where it is involved in chromosome condensation (Mackay, Ainsztein, Eckley, & Earnshaw, 1998) and the spindle assembly checkpoint (Tseng, Tan, Kapoor, & Funabiki, 2010). During anaphase and cytokinesis, the CPC redistributes to the midzone between microtubule asters where it assists in localizing the cleavage furrow and triggering its ingression (Cooke, Heck, & Earnshaw, 1987; Field, Groen, Nguyen, & Mitchison, 2015).

The CPC and its individual subunits have been extensively studied, both to understand their biological function and to investigate AURKB as a potential drug target for cancer treatment (Portella, Passaro, & Cheiffi, 2011). AURKB is a critical mitotic kinase that phosphorylates many mitotic proteins (Carmena, Wheelock, Funabiki, & Earnshaw, 2012) including the CPC components INCENP (Adams et al., 2000; Bishop & Schumacher, 2002; Honda, Koerner, & Nigg, 2003; Sessa et al., 2005) and CDCA8 (Gassmann et al., 2004). AURKB also phosphorylates itself on Thr232 within its activation loop (Yasui et al., 2004). Clustering the CPC on chromatin or microtubules or multimerizing it with antibodies triggers activating autophosphorylation of AURKB, suggesting that this occurs *in trans* (Kelly et al., 2007). Additionally, AURKB phosphorylation of INCENP allosterically activates AURKB (Adams et al., 2000; Bishop & Schumacher, 2002; Honda et al., 2003; Sessa et al., 2005).

Crystal structures of both termini of INCENP and its CPC binding partners have been obtained, but the structure of the entire complex remains elusive (Sessa et al., 2005; Jeyaprakash et al., 2007; Sessa & Villa, 2014). The middle region of INCENP was previously thought to contain a coiled coil domain, but recent evidence suggests that this region may in fact be a single alpha helix 32 nm long

that is capable of stretching up to 80 nm, allowing CDCA8 and BIRC5 to anchor the complex while AURKB phosphorylates other proteins in the vicinity (Samejima et al., 2015). A long single alpha helix may be prone to degradation and might need to be stabilized when the complex is inactive. Inactive CPC is unphosphorylated on key residues of AURKB and INCENP, but whether posttranslational modifications or chaperone proteins assist in stabilizing the inactive state is unknown. Stabilization of an inactive state by these mechanisms is common in other kinases (Shalloway & Taylor, 1997), other cytokinesis proteins (Staus, Taylor, & Mack, 2011), and other protein complexes (Berrabah, Aumercier, Lefebvre, & Staels, 2011; Koryakina, Ta, & Gioeli, 2014).

Hydrodynamic measurements provide a classic approach to elucidating regulatory mechanisms of protein complexes. Comparison of the CPC sedimentation coefficient in interphase and mitotic *Xenopus laevis* extracts revealed slower sedimentation rate in mitosis which was attributed to cell cycle regulation (Bolton et al., 2002). However, in that study, the mitotic extract was treated with the phosphatase inhibitor microcystin and diluted into buffer containing additional phosphatase inhibitors, whereas the interphase extract was not treated with phosphatase inhibitors at any step. Therefore, the reported difference in sedimentation coefficient between mitotic and interphase CPC could have been caused by artificial induction of CPC autophosphorylation and activation in the mitotic sample, rather than by the cell cycle state difference. Below, we show that this is indeed the case, and we use the resulting hydrodynamic information to gain additional insights about how the CPC is regulated.

The *X. laevis* egg extract system is ideal for studying the CPC, as it is arrested in a mitotic state and contains a relatively high concentration of CPC proteins (estimated between 55-155 nM based on mass spectrometry of individual subunits) (Wuhr et al., 2014). *X. laevis* has different maternally stored and embryonically expressed forms of CDCA8 and BIRC5; we will refer to the maternally stored forms analyzed in this work as CDCA9 (also known as DasraA) and BIRC5.1, respectively. Here, we use high speed supernatant (HSS) of *X. laevis* egg extract lacking glycogen or membranous organelles prepared such that the cell cycle state (mitotic or interphase) was retained (Groen, Coughlin, & Mitchison, 2011;

Mitchison, Nguyen, Coughlin, & Groen, 2013). In particular, we added a degradation-resistant form of CDK1 to the extract before the high-speed spin to stabilize the mitotic state of HSS without the use of phosphatase inhibitors. A major downside to the *X. laevis* extract system is its lack of genetic tractability, which makes tagging of endogenous proteins with GFP variants difficult. We therefore also investigated CPC behavior in mitotic HeLa cells, using the CRISPR-Cas9 system to tag endogenous proteins with GFP (Cong et al., 2013). Although CPC protein sequences vary between the *X. laevis* and *Homo sapiens* (ranging from 70% identical for AURKB to only 24% for CDCA8/9, see Methods), the overall architecture and regulation of the complex is highly conserved.

We report that the CPC hydrodynamic profile changes with autophosphorylation and not with cell cycle state and that this change occurs in both *X. laevis* extract and live mitotic HeLa cells. We then provide evidence that the hydrodynamic change is due to a direct physical interaction between the CPC in its inactive state and the nucleophosmin/nucleoplasmin (NPM) family of oligomeric histone chaperones. We propose that NPM complexes are regulatory chaperones that stabilize the inactive state of the CPC.

1.3 Results

1.3.1 CPC autophosphorylation causes a decrease in sedimentation coefficient

Human AURKB is controlled in part by autophosphorylation on T232 in its activation loop, which activates the kinase (Yasui et al., 2004). To examine phosphoregulation of *X. laevis* AURKB and the CPC as a whole, we used a phosphatase inhibitor, okadaic acid, in combination with AURKB inhibitors (barasertib, ZM447439, and VX680, listed here from most to least specific) in a variety of applications. We first wanted to confirm that autophosphorylation of this site occurs in *X. laevis* HSS (clarified extract from eggs) (Groen et al., 2011). We incubated HSS with AURKB inhibitors, okadaic

acid, or sequential treatment with AURKB inhibitors followed by okadaic acid. AURKB phosphosites will be blocked from phosphorylation by pretreatment with AURKB inhibitors, but all other phosphosites will become phosphorylated in response to okadaic acid. We performed immunoblot analysis of the treated extracts for pThr232-AURKB and STMN (stathmin/Op18), a known AURKB target that undergoes a gel shift upon phosphorylation (Gadea & Ruderman, 2006). The pThr232-AURKB antibody was raised to the activation loop phosphosite in humans with high homology in *X. laevis* AURKA and AURKB (Figure 1.1A). As anticipated, okadaic acid addition promoted AURKB and STMN phosphorylation (Figure 1.1B). These phosphorylations were blocked by pre-treatment with AURKB inhibitors, indicating that AURKB and STMN phosphorylation require AURKB activity in HSS.

To test if AURKB autophosphorylation is due to cis- or trans-action of the kinase, we diluted HSS with S-CSF-XB-phosphate, a buffer previously developed to maintain the mitotic state of HSS (Groen et al., 2011). In the presence of okadaic acid, HSS dilution reduced AURKB phosphorylation (Figure 1.1C), suggesting that two CPCs may interact to promote AURKB phosphorylation in trans.

Using the drug treatments characterized in Figure 1.1B, we probed the hydrodynamic properties of the CPC in mitotic HSS as a function of its activity state. Following drug treatment, we diluted HSS 1:1 in S-CSF-XB-phosphate, fractionated on 5-40% sucrose gradients and blotted fractions with antibodies raised against *X. laevis* INCENP and CDCA9 (Figure 1.1D, top bracket) (Sampath et al., 2004). In all cases INCENP and CDCA9 co-fractionated, suggesting that the complex stays intact during centrifugation. There was no notable difference in sedimentation between basal state of HSS and HSS pre-incubated with barasertib, a highly specific AURKB inhibitor. However, when HSS was preincubated with okadaic acid, the CPC proteins sedimented substantially higher up on the sucrose gradient (Figure 1.1D, second bracket from bottom). The shift in sedimentation coefficient (S-value) is similar to that previously observed based on bovine serum albumin (4S) and bovine γ-globulin (7S) standards run on a parallel gradient (Bolton et al., 2002). This shift could be due to a decrease in mass upon phosphorylation or to a conformational change to a more extended conformation with a higher frictional coefficient.

To test if AURKB activity is necessary for the observed phosphorylation-induced hydrodynamic shift of the CPC, we employed the same two drug strategy used in Figure 1.1B, sequentially dosing with barasertib and okadaic acid followed by sucrose gradient sedimentation. The CPC proteins had the same S-value as in the basal and AURKB inhibited states (Figure 1.1D, bottom). Therefore, AURKB activity is required to reduce the value of the sedimentation coefficient of the CPC in response to okadaic acid treatment.

Figure 1.1 *(following page)*: **Phosphatase inhibition activates AURKB and causes a change in the hydrodynamic properties of its associated protein complex.** (A) Sequences of human and *X. laevis* AURKB and *X. laevis* AURKA. Differences are highlighted in red and the key phosphorylated threonine highlighted in turquoise. (B) Mitotic HSS was incubated with kinase inhibitors and okadaic acid. Equal reaction volumes were run on an SDS-PAGE gel and immunoblotted with antibodies against pT232-AURKB, STMN, and α-tubulin. Blots were quantified by comparing band intensities of pAURKB normalized to α-tubulin. Reactions were repeated four times with two biological and two technical replicates, blot shown is representative. (C) Mitotic HSS was diluted 1, 2, 3, 4, or 5-fold in S-CSF-XB-phosphate buffer, okadaic acid was added at a constant concentration, and the reactions were incubated at room temperature for 25 minutes. Reaction aliquots containing the same amount of HSS were immunoblotted with the antibody against the pT232-AURKB epitope (sample blot at top). The intensity of the samples was normalized by α-tubulin intensity and across each biological replicate (dilution reaction with highest phosphorylated AURKB was set at 100% activity). Graph represents average of four biological replicates; error bars represent standard deviations. (D) HSS was incubated with kinase inhibitor or DMSO for 25 minutes, followed by okadaic acid or DMSO for an additional 25 minutes. Equal volumes were sedimented on 5-40% sucrose gradients for 6 hours at 237,000 *x g* and 4 °C. The indicated fractions were separated on SDS-PAGE gels and immunoblotted with antibodies raised against C-terminal peptides of INCENP and CDCA9. Full blots with molecular weight markers available in Appendix A. Experiments were repeated with three biological replicates. (E) Sucrose gradient blots in (D) were quantified and normalized to the total amount of the indicated protein in the gradient.

Figure 1.1: (continued)

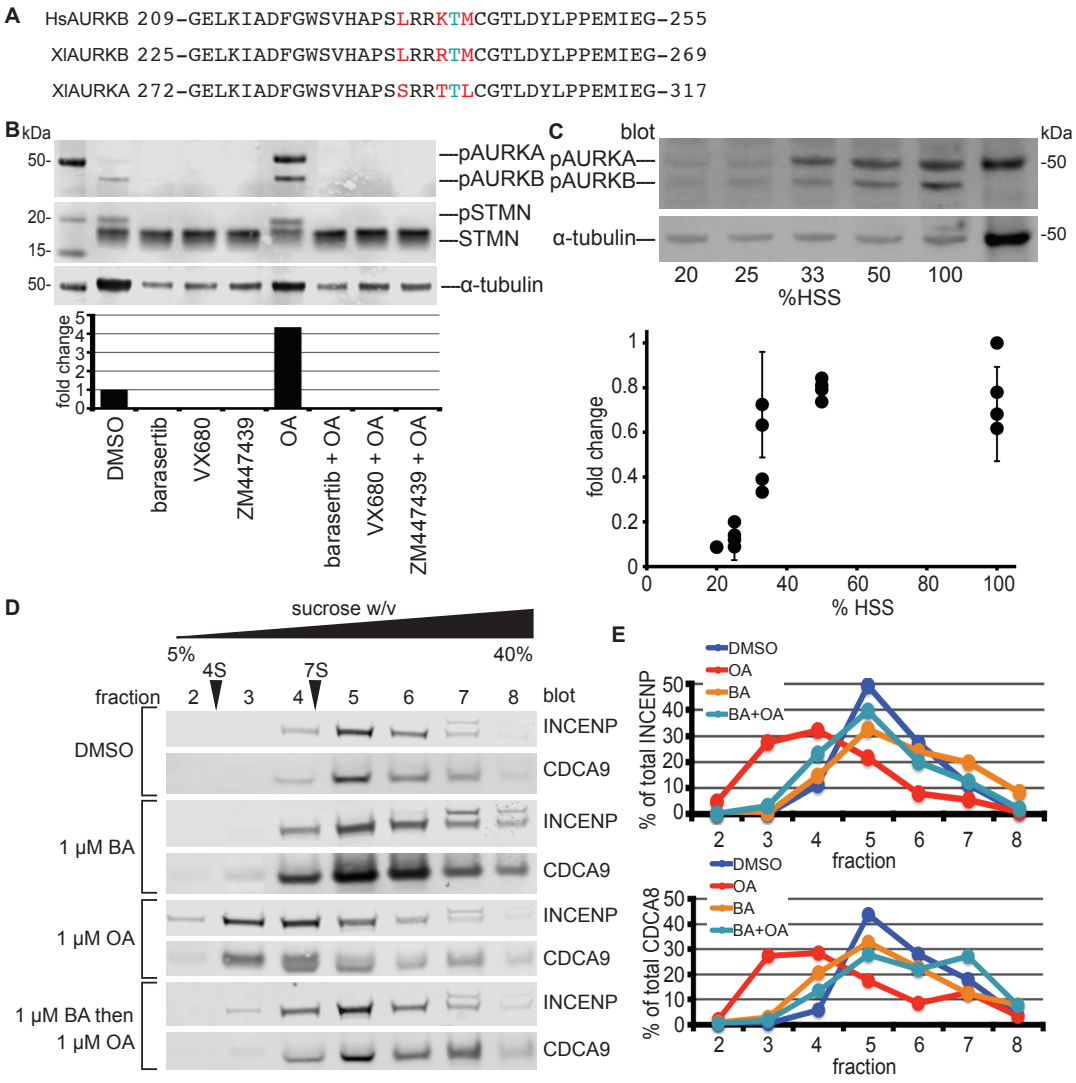

1.3.2 CPC hydrodynamic properties are not cell cycle regulated

Similar basal hydrodynamic properties of the CPC in *X. laevis* were previously reported, and a shift from the high to low S-value form was attributed to cell cycle regulation (Bolton et al., 2002). In those experiments, a phosphatase inhibitor was added to mitotic but not interphase samples, so it is possible that the observed S-value shifts were instead due to phosphorylation effects as we observed in Figure 1D. The mitotic HSS used in Figure 1 was prepared using methods that do not require phosphatase inhibitors to stabilize the mitotic state by adding recombinant CDK1 Δ90 to the crude extract prior to centrifugation (Groen et al., 2011). To test the effect of cell cycle on CPC hydrodynamic behavior and AURKB phosphorylation, we prepared interphase HSS by first cycling crude mitotic extract into interphase with the addition of calcium and then preventing any further protein translation with the addition of cycloheximide prior to the centrifugation step that transforms crude extract into HSS. To confirm the cell cycle state of mitotic and interphase HSS, we immunoblotted with an antibody against phosphorylated epitopes of MPM2 target sites, which are more abundant in mitosis (Figure 1.2A). Substantially less protein phosphorylated by MPM2 was recognized in the interphase than in the mitotic sample, showing that the cell cycle state had been maintained throughout the HSS preparation without the use of phosphatase inhibitors.

We repeated the sucrose gradient experiments to probe the effects of kinase and phosphatase inhibitors on the CPC, comparing interphase and mitotic HSS prepared from the same extract. Treatment with 1 μM okadaic acid was sufficient to shift mitotic CPC to the low S-value form, but 10 μM was required to shift interphase CPC (Figure 1.2B, C). We therefore concluded that the basal state of the CPC is the same in both cell cycle states and can undergo similar phosphorylation-driven shifts to the lower S-value form, although less phosphatase inhibition is required in mitosis. We next tested the levels of AURKB phosphorylation at Thr232 in response to inhibitors (Figure 1.2D). Unsurprisingly, AURKB phosphorylation was promoted by okadaic acid and inhibited by barasertib in both cell cycle states. We concluded that autophosphorylation drives the CPC to a lower S-value independent of cell cycle state.

We attempted to measure the Stokes radius of the native and phosphorylated CPC using gel filtration chromatography to compare changes in size with the hydrodynamic behavior observed on sucrose gradients. However, during gel filtration in a wide range of buffers and on a wide range of resins the CPC smeared out on the column. Blots of the fractions for CPC subunits suggested that the complex dissociated, potentially in response to dilution or to nonspecific interactions with the resin. Similar results were seen in a previous study (Bolton et al., 2002). We therefore turned to a less perturbing method, fluorescence correlation spectroscopy (FCS), to further probe CPC hydrodynamics (see below).

1.3.3 Hydrodynamic CPC regulation occurs in live HeLa cells

We next investigated if hydrodynamic regulation of the CPC also occurs in human cells. To test if CPC autophosphorylation can be triggered by okadaic acid in HeLa cells we synchronized cells in mitosis by overnight treatment with the kinesin-5 inhibitor STLC (Hu, Ozlu, Coughlin, Steen, & Mitchison, 2012). This arrests cells in monopolar mitosis while minimally perturbing microtubule dynamics. We then incubated with barasertib, okadaic acid, or both drugs concurrently and lysed cells with SDS-

Figure 1.2 *(following page)*: **CPC hydrodynamic properties are similar in interphase and mitotic HSS.** (A) Interphase HSS was prepared by cycling CSF *X. laevis* egg extract into interphase with calcium and then adding cycloheximide, followed by the high speed spin. Equal amounts of interphase and mitotic HSS prepared from the same extract were blotted with an antibody against phospho-MPM2 epitopes, which are known to be more prevalent in mitosis. Interphase extract was prepared over five times and compared to mitotic HSS prepared from the same crude extract using MPM2 blots twice. (B) Sucrose gradients were run as in Figure 1.1. Mitotic and interphase HSS were prepared from the same extract. Fractions were blotted with antibodies raised against INCENP and CDCA9. Experiment was repeated with two biological replicates. Full blots with molecular weight markers are available in Appendix A. (C) Sucrose gradient blots from (B) were quantified as in Figure 1.1E. (D) Mitotic and interphase HSS samples prepared from the same extract were incubated with the indicated drugs as in Figure 1.1. The reactions were then blotted with antibodies against pT232-AURKB and α-tubulin and pAURKB levels quantified by normalizing to α-tubulin. Experiment was repeated with three biological replicates.

Figure 1.2: (continued)

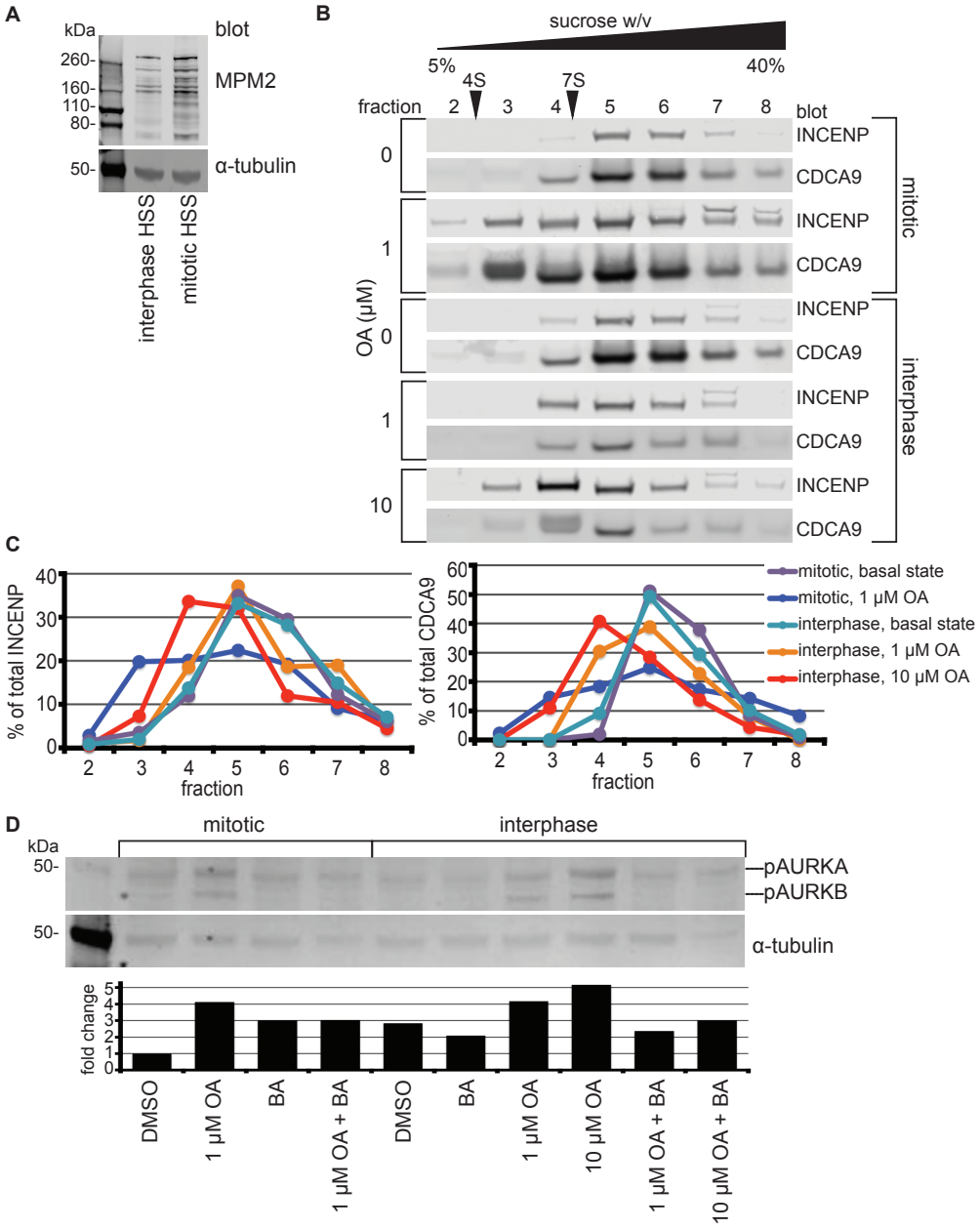

PAGE running buffer. We then blotted with the antibody against pThr232-AURKB used previously (Figure 1.3A). Mitotic cells had minimal phosphorylated AURKB, presumably because the bulk of the complex is in an inactive, soluble pool, and only a small fraction is active at specific sites on chromatin or microtubules. Phosphatase inhibition by okadaic acid increased AURKB phosphorylation levels, which was counteracted by pretreatment with barasertib. These effects are identical to those observed in *X. laevis* HSS and suggest that similar autophosphorylation regulates CPC kinase activity across organisms. In preliminary biochemical studies we were unable to observe auto-phosphorylation of AURKB in response to phosphatase inhibition in cell lysates, potentially as a result of greater dilution in HeLa lysates as compared to *X. laevis* HSS. This prevented the use of sucrose gradients to measure hydrodynamic regulation of the CPC, so we instead used FCS to obtain hydrodynamic information in live cells.

FCS measures movement of fluorescent molecules in and out of a small illuminated volume, and thus measures diffusion coefficients in live cells (Kim, Heinze, & Schwille, 2007). FCS requires a cell line where the CPC is fluorescently tagged, but with minimal artifacts resulting from overexpression of a single CPC subunit. Ideally, cells should also have a high fluorescence signal per particle to maximize detection but a low concentration of tagged particles to facilitate measurement of intensity fluctuations. We tagged the C-terminus of the CDCA8 subunit in HeLa cells with a GFP-3xFLAG tag using a CRISPR/Cas9 strategy and sorted GFP-positive cells with FACS to obtain a cell line with stable expression (Cong et al., 2013). The concentration of tagged CDCA8 was too low to be detected in blots of whole cell lysates; however, when the 3xFLAG tag was immunoprecipitated from both the tagged cell line and the parent line and blotted with an antibody against FLAG, only the tagged cell line exhibited a clear band at the expected molecular weight (62 kDa) without any other significant bands (Figure 1.3B). Similarly, immunoprecipitation of the FLAG tag or random IgG from whole cell lysates of the tagged cell line followed by an anti-FLAG blot showed a protein band at 62 kDa only in the FLAG IP, indicating that the tagging was successful (Figure 1.3C). We also obtained HeLa cell lines expressing GFP-tagged INCENP and CDCA8 from BAC constructs as a generous gift from Tony Hyman (MPI Dresden) (Poser et al., 2008). These express the tagged subunit from its endogenous promoter, but this expression occurs in addition to endogenous gene expression. Cell populations from each of the three cell types were fixed with paraformaldehyde and imaged by confocal microscopy (Figure 1.3D). All three lines showed the expected localization of the tagged CPC subunit to centromeres during metaphase and to midzone microtubules during anaphase/cytokinesis. The new CDCA8-GFP-3xFLAG CRISPR cell line exhibited significantly less background fluorescence than the BAC cell lines and had no expression in interphase cells, suggesting a larger fraction of the tagged subunit was successfully incorporated into the CPC. We therefore selected the CRISPR tagged line for FCS experiments.

Figure 1.3 *(following page)*: **Tagging of CDCA8 in HeLa cells with GFP-3xFLAG.** (A) HeLa cells were arrested in mitotis by overnight treatment with STLC and collected via mitotic shakeoff, followed by washing with PBS. The indicated drugs were added to the final wash of the cells, after which the cells were lysed with freeze-thaw cycles. Cell lysates were then immunoblotted for pT232-AURKB and α-tubulin. Experiment was repeated three times with different biological replicates. (B) Lysates of the parent and tagged cell line were prepared as in A. Magnetic beads preloaded with an antibody against FLAG were used to immunoprecipitate (IP) tagged proteins from the lysates, and the resulting proteins were blotted for FLAG following separation via SDS-PAGE gel electrophoresis. Experiment was repeated twice with two biological replicates. (C) Lysates of the tagged cell line were prepared as in (A) and IPs were done with beads loaded with antibodies against random IgG or FLAG, followed by blotting for FLAG as in (A). Experiment was repeated three times with different biological replicates. (D) HeLa cells expressing GFP-tagged CPC were fixed with 4% paraformaldehyde, stained with an antibody against α-tubulin and imaged with a spinning disk confocal microscope at 60x magnification. Scale bars represent 10 μm. Cells were imaged on three separate occasions.

Figure 1.3: (continued)

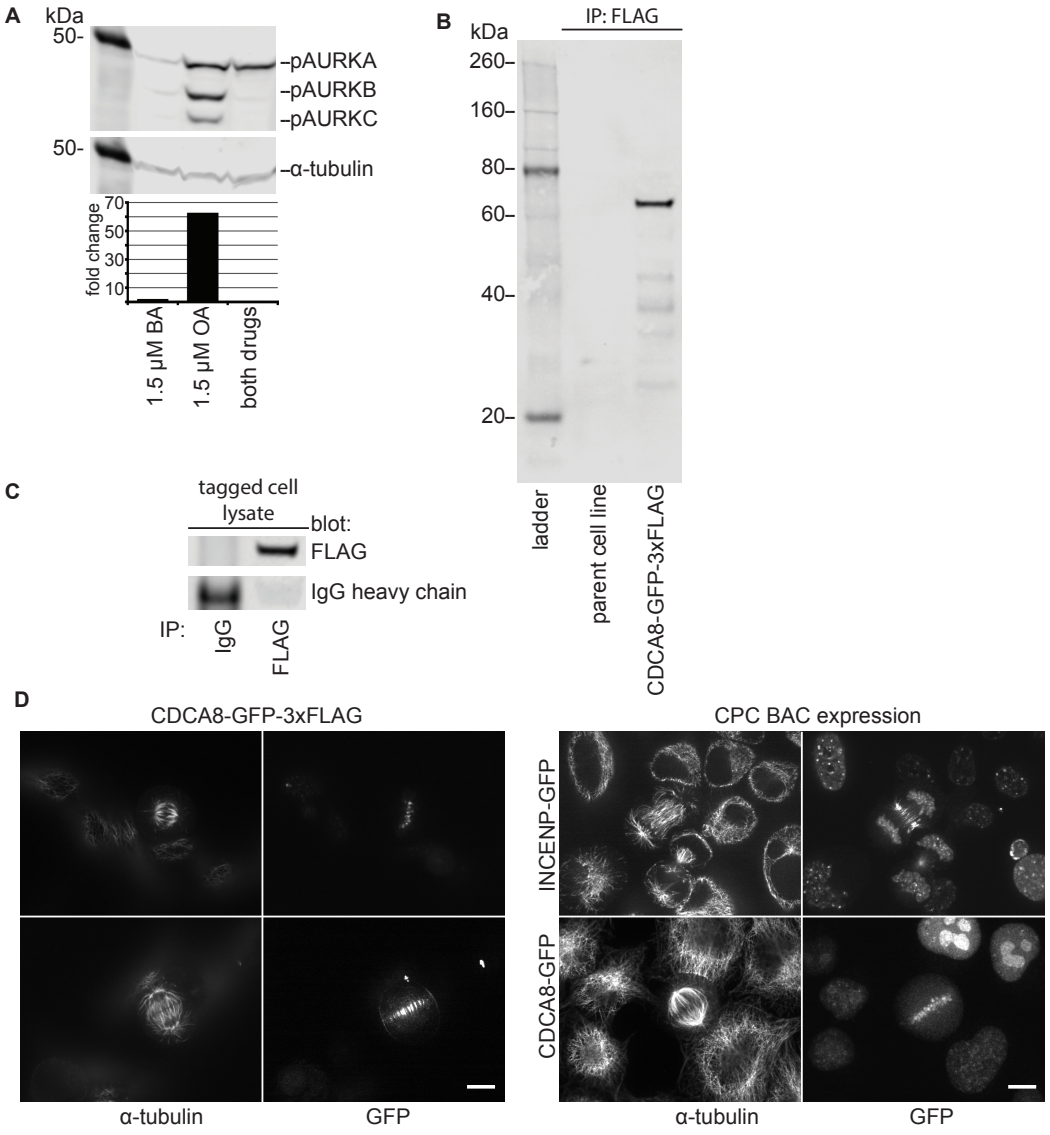

To measure the diffusion of GFP-tagged CDCA8 in live mitotic cells we applied two-photon confocal FCS using previously described methods (Needleman, Xu, & Mitchison, 2009). Mitotic cells were identified in unsynchronized cells by morphology. Conventional two-photon confocal imaging before FCS revealed CPC localization to centromeres as in Figure 1.3D. We then focused the FCS beam away from chromatin and other static bodies which might affect the measurement. Due to the rapid timescales probed, FCS only provides information on the soluble pool of CPC. Representative primary FCS data presented as autocorrelation curves are shown in Figure 1.4A (top). The grey line is the best fit to a model over multiple autocorrelation measurements. We used a model with two distinct populations undergoing normal diffusion (Kim et al., 2007) with four fitting parameters, the two diffusion coefficients of each population (D_{slow} and D_{fast}) and the amplitudes of the autocorrelation functions of each population (G_{slow} and G_{fast}). A model with a single diffusing species did not fit the data, whereas a two species model gave a good fit in all cases. An example of low residuals with this fit is shown in Figure 1.4A (bottom). We found that adding nocodazole to prevent astral microtubules from moving into the FCS voxel strongly reduced noise in autocorrelation graphs, so we added nocodazole to all subsequent experiments, which did not appear to affect the hydrodynamics of the soluble pool of CPC. The diffusion coefficient of the fast-diffusing population was roughly three times smaller than that of monomeric GFP (Kuhn et al., 2011) and is therefore likely the monomeric GFP-tagged CDCA8 outside of the CPC. The slow population, therefore, is presumed to be the complete CPC. Given large uncertainties in size-dependent viscosity in live cells, we did not attempt to calculate a hydrodynamic radius of the large complex.

With a live cell hydrodynamic assay in hand we added kinase (barasertib) and phosphatase (okadaic acid) inhibitors to test the effect of autophosphorylation on diffusion rates of the CPC. There was no systematic effect of okadaic acid or both drugs combined on G_{slow}/G_{fast}, suggesting the drugs did not cause dissociation of the CPC into its subunits (Figure 1.4B). D_{fast} exhibited no systematic changes in response to drugs, suggesting that unincorporated CDCA8 does not undergo hydrodynamic changes

Figure 1.4 *(following page)*: **Fluorescence correlation spectroscopy of HeLa CDCA8-GFP-3xFLAG cells.** (A) Example autocorrelation curves (top, black circles represent averages and grey line represents the fitted two-component FCS model) and weighted residual (bottom). (B) Ratio of amplitudes of slow to fast components over time after drug treatment. Amplitudes are proportional to the number of molecules in a focal volume and molecular brightness squared. (C) Diffusion coefficients over time following drug treatment of fast and slow populations in the presence of 1 μM nocodazole, with no further drug treatment (blue circles), or following the treatment with only 250 nM okadaic acid (OA, green squares) or with both 250 nM OA and 250 nM barasertib (BA, red triangles). Each data point represents one mitotic cell, identified by observing round cell morphology and chromosomes in phase contrast, and averages were obtained by taking multiple measurements in each cell at each time point. All FCS experiments were repeated twice on different days with the same cell line.

Figure 1.4: (continued)

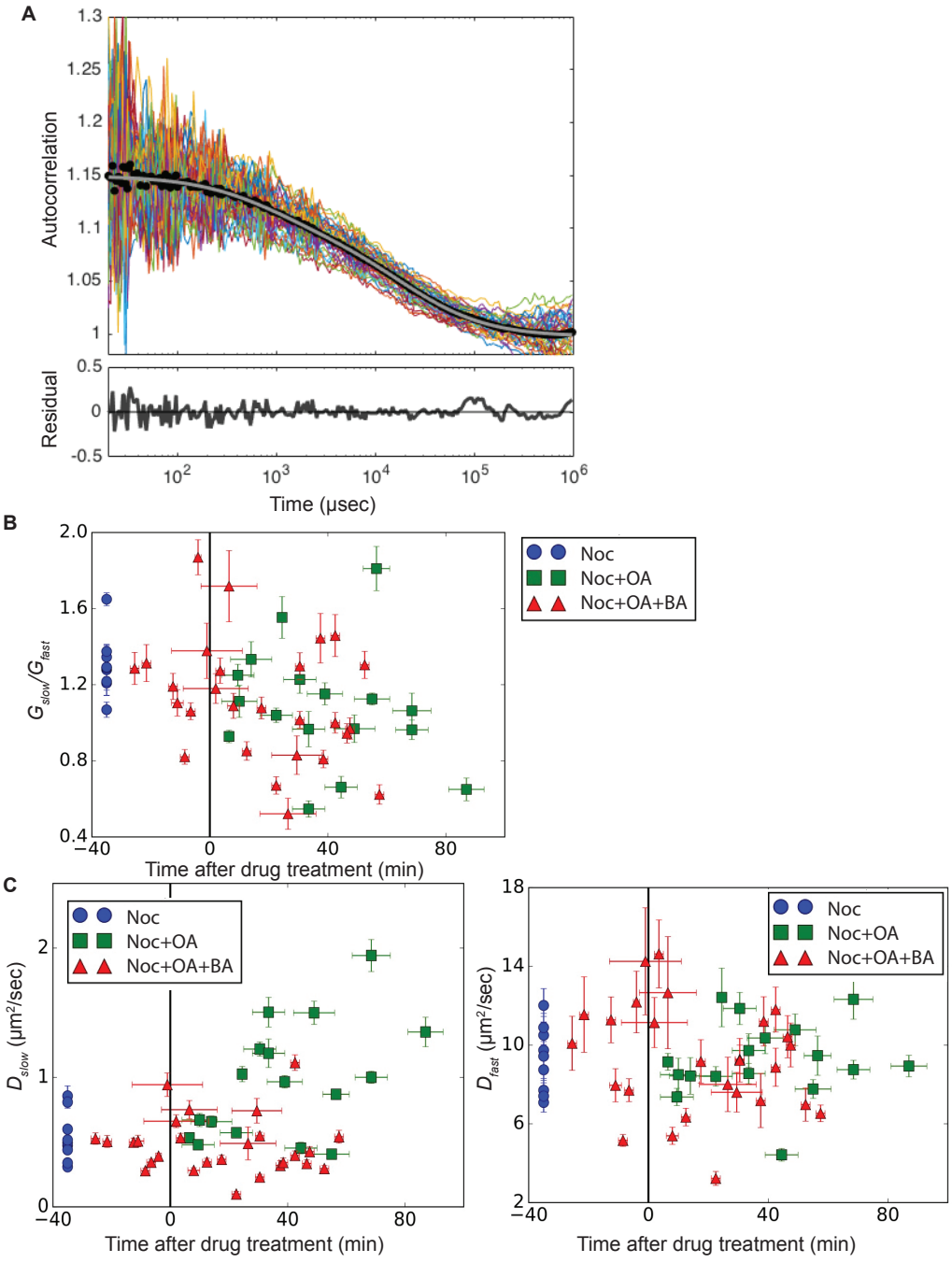

alone in response to phosphoryation (Fig 1.4C, right). However, D_{slow}, presumably corresponding to the diffusion constant of the native CPC, exhibited a time-dependent increase in response to okadaic acid, indicating that the complex diffuses faster as it becomes phosphorylated (Figure 1.4C, left, green squares). When barasertib was added in addition to okadaic acid, no increase in diffusion coefficient was observed, indicating the OA-induced change was due to autophosphorylation and requires AURKB activity (Figure 1.4C, left, red triangles).

We believe that the okadaic acid-induced, barasertib-inhibited increase in CPC diffusion rate measured by FCS is due to the same biochemistry as the okadaic acid-induced, barasertib-inhibited decrease of the sedimentation coefficient of the CPC. An increase in diffusion coefficient upon phosphorylation is not consistent with an increased frictional coefficient of the complex and instead implies a shift to a lower molecular weight. Autophosphorylation could cause the CPC to shift to a lower molecular weight for two reasons: when inactive, the CPC could either be oligomerized or be bound to some large, unknown factor. The FCS data allows us to distinguish between these possibilities. G_{slow}/G_{fast} is equivalent to the ratio of fluorescent particles in each population multiplied by the ration of the brightness of each population squared. If dephosphorylated CPC is an oligomer then, in that state, one oligomer would contain multiple units of CDCA8-GFP, but would only contribute one count to G_{slow}. Upon dissociation due to autophosphorylation, the apparent number of particles in the slow fraction would increase because each CPC containing one CDCA8-GFP subunit would be counted. The brightness of each particle in the slow fraction would decrease by the same ratio. Therefore, when cells are treated with okadaic acid, G_{slow} would decrease, and G_{slow}/G_{fast} would decrease correspondingly. However, G_{slow}/G_{fast} did not change regardless of drug treatment (Figure 1.4B). This suggests an absence of phospho-regulated oligomerization. Therefore, the observed changes in hydrodynamic properties of the CPC are more likely due to its binding to some other large factor(s) when inactive, and this complex dissociates upon autophosphorylation.

1.3.4 Inactive CPC binds to nucleoplasmin/nucleophosmin

To identify candidate inactive CPC binding proteins we returned to *X. laevis*, employing an immunoprecipitation-mass spectrometry (IP-MS) strategy in both HSS and crude extract. Mitotic HSS was treated with barasertib, okadaic acid, or both drugs as in Figure 1.1B. We then immunopreciptiated INCENP and CDCA9 from separate samples in tandem and subjected the samples to quantitative mass spectrometry analysis. We used tandem mass tags (TMT) after proteolysis to differentially label samples. Samples were then pooled and analyzed using multi-notch MS3 methods to quantify the amount of each peptide that came from each sample (Wuhr et al., 2014). We ranked proteins by their enrichment on IPs with AURKB inhibition over AURKB activation (Appendix A). Highly ranked candidates had to meet two additional criteria: first, that they are abundant enough in frog eggs to bind all the CPC molecules (Wuhr et al., 2014) and secondly, that they have a large native molecular weight, sufficient to significantly increase the S-value and decrease the diffusion coefficient of inactive CPC through binding. Applying these criteria, the nucleoplasmin/nucleophosmin family of proteins (NPM) were clear hits (Figure 1.5A). Similar results were seen in IP-MS experiments done in crude extract, where we compared IPs without drug, where complex activation is induced by clustering on beads, and in the presence of ZM447439, an AURKB inhibitor (Appendix A). In addition to being highly enriched in IPs of CPC under inactive versus activating conditions, NPM family members are known to assemble into large homo- and hetero-pentameric and -decameric complexes (Namboodiri, Akey, Schmidt-Zachmann, Head, & Akey, 2004; Platonova, Akey, Head, & Akey, 2011). They are also abundant in frog eggs. We observed peptides from both NPM2 and NPM3 in IP-MS experiments, but not from the somatic isoform NPM1 which is not expressed in eggs. NPM2 is an embryonic isoform that is highly abundant in *X. laevis* eggs (∼2000 nM), which is more than enough to sequester all the CPC in the egg (∼100 nM) (Wuhr et al., 2014). NPM3, which is much less abundant in eggs than NPM2 (∼150 nM), likely hetero-oligomerizes with NPM2, so it is not clear if it interacts independently with the

CPC. Other proteins that were identified as potential CPC inactive state binding partners through IP-MS include PARD3, a protein involved in asymmetrical cell division and the chromatin protein CBX3. These were less reproducible interactions than with NPMs 2 and 3 when compared to previous experiments in crude extract (Appendix A), the proteins are less abundant in eggs (as indicated by the size of the bubbles in Figure 1.5A), and their native molecular weight is uncharacterized. We therefore focused on NPMs, though we suspect additional or alternative proteins may exhibit similar behavior.

We next used IP-immunoblots from HSS to confirm IP-MS findings. Immunoprecipitations of random IgG, INCENP, CDCA9, and NPM2 from HSS dosed with no drug, barasertib, okadaic acid, or barasertib followed by okadaic acid were blotted with antibodies against INCENP and NPM2. We observed very strong interactions between both CPC components and NPM2 under AURKB inhibited conditions, but no interaction when phosphatases were inhibited and AURKB is active (Figure 1.5B). The only exception was the immunoprecipitation of INCENP without any drugs. In this case, low levels of NPM2 were observed (much lower than in the barasertib-inhibited cases). We suspect this is because the well-known AURKB activating properties of the antibody raised against INCENP cause this sample to behave more like the okadaic acid treated sample (Kelly et al., 2007).

Similar IP-immunoblots were done from HeLa lysates. When cells arrested in mitosis were treated with barasertib prior to lysis, a small amount of NPM1 was observed when antibody against BIRC5 was used to IP the CPC. Much less NPM1 was observed in BIRC5 IPs from cells were treated with okadaic acid (Figure 1.5C). However, treatment of cells with barasertib in addition to okadaic acid was able to preserve the association of NPM1 with the CPC, suggesting that, as in *X. laevis* HSS, this interaction is dependent on AURKB inactivity.

Samples of barasertib- and okadaic-acid treated HSS were centrifuged as in Figure 1.1, and smaller fractions were taken to see if NPM2 sedimentation changed with CPC inhibition or activation. However, there was no appreciable difference in NPM2 sedimentation with different drug treatments (Figure 1.5D). While NPM2 that dissociates from the CPC would have a lower sedimentation coefficient, we suspect that the markedly higher abundance of NPM2 in the egg relative to CPC proteins (roughly 20 times) masks any shift in NPM2 sedimentation coefficient. Notably, NPM2 is minimally present in fractions 5 and 7 in the okadaic acid sample, whereas there are significant amounts of CPC proteins in these fractions, suggesting that there is potentially no interaction between the CPC and NPM2 in this sample as corroborated by IP-MS and IP-immunoblot experiments. However, NPM2 is present in all the fractions that CPC subunits are in the barasertib-treated sample, and as such the CPC and

Figure 1.5 *(following page)*: **NPM1 and NPM2 interact with inactive CPC.** (A) Antibodies against INCENP or CDCA9 were used to IP proteins from HSS, which were then analyzed via quantitative mass spectrometry. Protein counts were normalized to IgG IPs and the amount of target protein (INCENP or CDCA9). Plotted ratios for each protein were generated by dividing protein count from barasertib-treated samples by count from okadaic acid-treated samples. Gridlines on plot are at a ratio value of 1. Proteins with a ratio above 1 indicate enrichment in barasertib-treated samples over okadaic acid-treated samples. Labeled proteins are those with ratios above 1 in both CDCA8 and INCENP IPs. Size of bubbles are proportional to the measured amount of protein in *X. laevis* extract (Wuhr et al., 2014). IP-MS experiments were done once due to cost of materials and availability of equipment time. (B) HSS was incubated with barasertib (BA), okadaic acid (OA), both, or neither as in Figure 1.1. Beads loaded with antibodies against *X. laevis* INCENP, CDCA9, and NPM2 were used for immunoprecipitations from treated HSS, and then the proteins on the beads were blotted with antibodies against INCENP and NPM2. Blots were quantified by dividing levels of the blotted protein by levels of the IP target protein. Fold change represents change in NPM2 levels (left eight bars) or INCENP levels (right four bars). Experiment was repeated twice with two biological replicates. (C) HeLa cell lysates were generated as in Figure 1.3, with the indicated drugs added just before lysis. BIRC5 was immunoprecipitated from the lysates, and the resulting protein mixtures blotted for NPM1 and BIRC5. The same INCENP blots from Figure 1.1D are shown for ease of comparison. (D) Sucrose gradients of barasertib (BA) or okadaic acid (OA)-treated HSS were run as in Figure 1.1, except fractions were a third smaller. Every other fraction was immunoblotted for NPM2, INCENP, or CDCA8. NPM2 blots had 7.5 times less total protein concentration in each lane. Experiment was repeated twice with biological replicates. NPM2 blots were quantified as in Figure 1.1.

Figure 1.5: (continued)

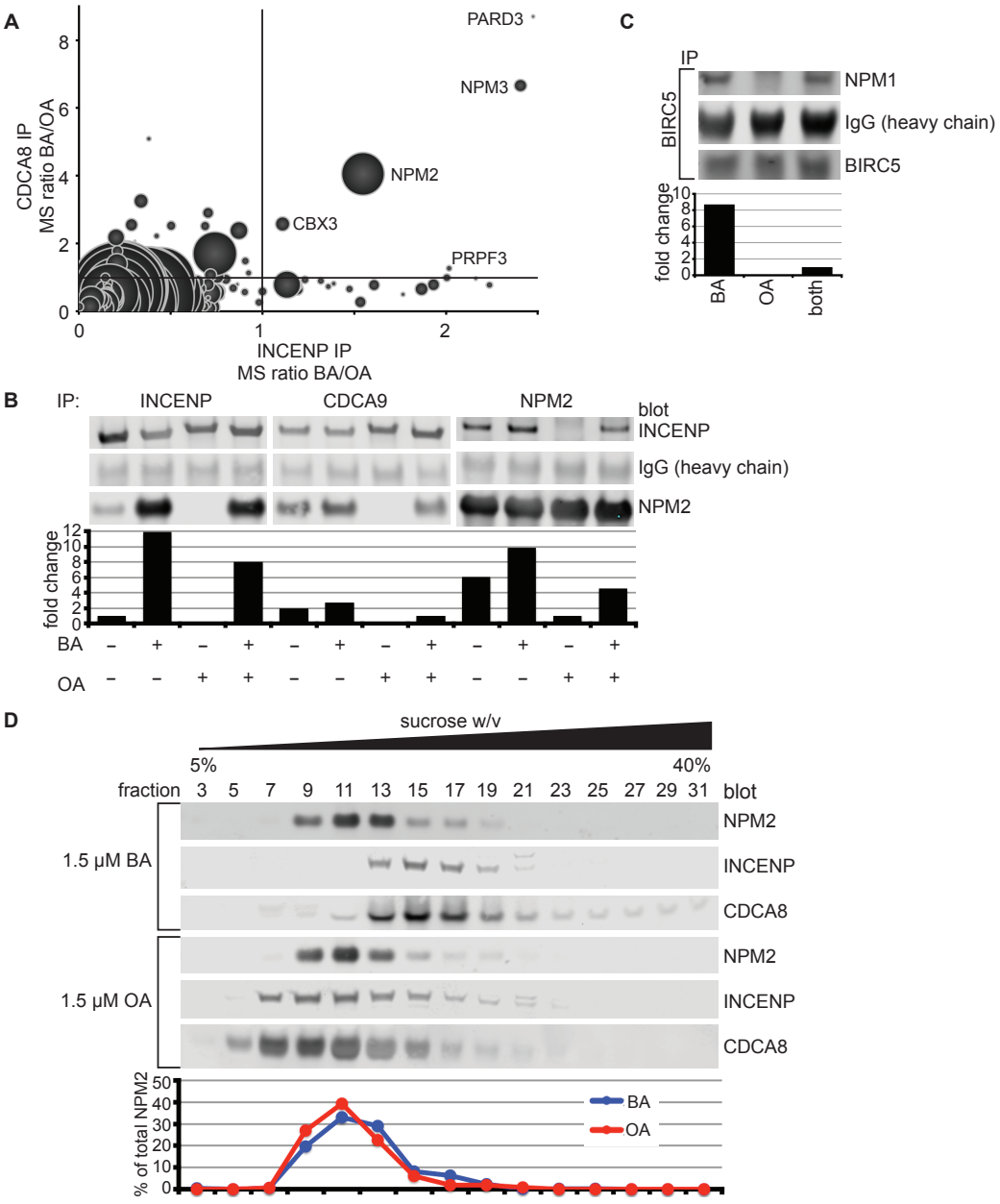

NPM2 could be interacting in the AURKB-inhibited HSS as IP-MS and IP-immunblot experiments suggest.

Although not the focus of our analysis, our IP-MS data also revealed candidate proteins that interact more with active CPC than inactive (Appendix A). These included KIF20A, a kinesin that is thought to transport CPC towards microtubule plus ends during cytokinesis (Nguyen et al., 2014). Further experimentation is required to evaluate the significance of these proteins.

1.4 Discussion

We used a combination of nonspecific phosphatase inhibitor and specific kinase inhibitors to confirm previous studies showing that the CPC can be activated by autophosphoylation, most likely *in trans* (Yasui et al., 2004; Kelly et al., 2007). We then investigated the effect of autophosphorylation on hydrodynamic behavior of the CPC in HSS from *Xenopus laevis* eggs and live HeLa cells. We confirmed that the CPC can undergo a regulated change in hydrodynamic behavior (Bolton et al., 2002), but we showed this change was triggered by autophosphorylation and not by cell cycle regulation. Combining data from sucrose gradient and FCS data, we concluded that autophosphorylation caused a decrease in native molecular weight which was not due to reversal of an oligomeric state, but rather to dissociation of a complex between inactive CPC and a second large but diffusible factor. IP-MS and IP-immunoblot analysis suggested that this second factor was the abundant, oligomeric histone chaperone complex nucleoplasmin/nucleophosmin. Thus, we hypothesize that inactive CPC is chaperoned by NPM complexes. Other kinases are known to complex with additional factors in their inactive state, and these interactions play an important role in regulation of kinase activity. For example, in the inactive form of Src kinase the kinase domain complexes with SH2 and SH3 domains in the same polypeptide, which helps keep the kinase inactive (Shalloway & Taylor, 1997). In general, the biochemistry of the native state of kinases tends to get less experimental attention than it deserves.

NPM family members have well-established chaperone activity; indeed, the term "molecular chaperone" was first coined in 1978 by Laskey to describe the histone chaperone activity of nucleoplasmin (Laskey, Honda, Mills, & Finch, 1978). NPM1 was shown to protect a number of different proteins from aggregation during thermal denaturation (Szebeni & Olson, 1999) and to escort ribosomal subunits from the nucleus to the cytoplasm (Maggi et al., 2008). Both NPM1 and NPM2 bind histones H2A and H2B (Okuwaki, Matsumoto, Tsujimoto, & Nagata, 2001; Gadad et al., 2011; Fernandez-Rivero et al., 2016). NPM2 is particularly abundant in *X. laevis* eggs and is thought to store histones, catalyze their assembly into chromatin, and assist in transcription repression prior to the mid-blastula transition through histone sequestration.

We imagine several reasons inactive CPC might be sequestered by NPM complexes. Most obviously, this may prevent inactive CPC competing with active CPC for binding to AURKB targets such as chromatin and microtubules. It may also slow auto-activation of the CPC. The CPC functions in a highly dynamic system where its inactive and active forms rapidly interconvert, leading to local gradients in substrate phosphorylation on a micron scale (Afonso et al., 2014). NPM sequestration of the inactive state may assist in tuning this delicate balance. NPM interactions may also catalyze nucleus-cytoplasm trafficking of the CPC; during interphase, NPMs are substrates for nuclear import through the Ran-KPNB1 system (Quensel, Friedrich, Sommer, Hartmann, & Kohler, 2004) and interacts with exportin, ultimately localizing to nucleoli (Bolli et al., 2007). Nucleus-cytoplasm shuttling of the CPC is probably important in prophase regulation of chromatin and the nuclear envelope, and there are hints that the CPC is involved in nuclear pore reformation late in cytokinesis (Afonso et al., 2014). NPM also reportedly has important roles in mitosis; disrupting the protein with (+)-avrainvillamide, a small molecule that binds NPM1, results in supernumerary chromosomes (Mukherjee et al., 2015). This may be a result of disrupting its inhibition of the CPC, although direct actions of this abundant protein in mitotic progression is also a plausible explanation. We suspect that NPMs bind the CPC near the AURKB subunit near the C-terminus of INCENP for a few reasons. To have inhibitory func-

tion on AURKB, it is much more likely to be bound at or near the kinase in the complex. Secondly, the antibody against INCENP was raised from a C-terminal peptide, and this antibody is known to turn on AURKB activity (Kelly et al., 2007). It may do this by knocking off inhibitory NPMs. Genetic analysis of the function of the CPC-NPM interaction will be challenging since both are essential for cell growth (Cutts et al., 1999). Progress will likely depend on precise mapping, followed by mutation, of regions involved in the interaction. Depletion of NPM2 might be feasible in egg extract, though its abundance and the high likelihood that depleting NPM2 would co-deplete CPC present significant experimental challenges.

The exact nature of the CPC-NPM interaction still remains to be understood. We did not observe histone enriched in IPs of inactive CPC by MS, suggesting binding of CPC and H2A/H2B to NPM2 might be mutually exclusive. However, histones can be difficult to detect by mass spectrometry, and this point requires further investigation. Also unclear is if NPM2 recognizes some structural characteristic of the CPC only present when AURKB is inactive or if NPM2 actually holds it in an inactive state. We also do not know the extent of phosphorylation of CPC subunits or NPM family members by AURKB. Understanding the mechanistic implications of the NPM-CPC relationship will provide additional insight about cell division as a whole and potentially establish new proteins as drug targets for modulating cell division. Finally, our work extends the idea of NPM complexes as chaperones to a new substrate, the CPC. It will be interesting to ask what other substrates are chaperoned by NPM members in vivo and whether chaperone activity plays a role in the function of NPM1 mutants as oncogenes in acute myeloid leukemia (Bolli et al., 2007).

1.5 Experimental Procedures

Materials: All chemicals were purchased from Sigma Aldrich unless otherwise noted.

Antibodies: Antibodies against *X. laevis* INCENP and CDCA8 and human AURKB were raised

against C-terminal peptides as previously described (Kelly et al., 2007; Ozlu et al., 2010). The antibody against *X. laevis* NPM2 was a generous gift of David Shetcher (Albert Einstein College of Medicine). Antibodies were purchased from commercial sources for pThr232-AURKB (Cell Signaling #2914S), MPM2 (Millipore #16-155), BIRC5 (Cell Signaling #2808S), FLAG (Cell Signaling #2368P), α-tubulin (Sigma #T6199) and random rabbit IgG (Jackson Immunoresearch #011-000-003), goat anti-mouse DyLight 680 conjugated (Thermo #35518), goat anti-rabbit DyLight 800 conjugated (Thermo #35571), AlexaFluor-568 goat anti-mouse (Life Technologies #A-11004).

Western Blots: Protein solutions were diluted in sample buffer (5X: 200 mM Tris-HCl pH 6.8, 20% glycerol, 25% β-mercaptoethanol, 100 mg/mL SDS, 0.5 mg/mL Bromophenol Blue (Fluka)) and heated at 85-90 °C for 5 (pAURKB blots) or 10 minutes (all other blots). The solutions were then separated on 4-12% NuPAGE Bis-Tris gels (Life Technologies) in MES buffer (Life Technologies). Following gel electrophoresis, proteins were transferred to a nitrocellulose membrane (0.2 μm, Biorad) via wet transfer in 25 mM Tris base, 30 mM glycine, 20% methanol buffer at 100 V for 2 hours or 35 mA for 12-16 hours at 4 °C. Membranes were stained with Ponceau S stain (0.5% w/v Ponceau S (Mallinckrodt), 1% acetic acid (JT Baker)) prior to cutting the membrane into strips for analysis with multiple antibodies (if necessary). Membranes were blocked with Odyssey Blocking Buffer (PBS, LI-COR) for one hour at room temperature or overnight at 4 °C. Membranes were incubated with primary and secondary antibodies for one hour at room temperature. Primary antibodies were used at 1:1000 (commercial) or 1 μg/mL (produced in-lab) and secondary antibodies were used at 1:10000. Between the primary and secondary antibodies and after the secondary antibody, membranes were washed briefly with TBST (50 mM Trizma base pH 7.6, 155 mM NaCl, 1% TWEEN 20) followed by TBST and two rounds of TBS (50 mM Trizma base pH 7.6, 155 mM NaCl) for ten minutes each at room temperature. Membranes were imaged with an Odyssey Infrared Imager (LI-COR), adjusting intensity of illumination to just below the oversaturation point. Blots were quantified using the gel analysis tools in ImageJ and plotted using Microsoft Excel. Any bands that were undetectable above background intensity by

ImageJ were assumed to have a value of zero. All other band intensities were normalized across the blot by setting the value of the lowest to one and dividing the values of all others by the value of the lowest intensity.

Homology Analysis: Sequences of *X. laevis* and human CPC subunits were obtained from the UniProt database and compared using the NCBI BLAST tool, reporting the percent identical.

HSS Preparation: Mitotic HSS was prepared as previously described (Groen et al., 2011). S-CSF-XB-phosphate buffer (10 mM HEPES, pH 7.7, 100 mM KCl, 5 mM EGTA, 1 mM $MgCl_2$, 1 mM ATP, 1 mM GTP, 1 mM DTT, 5 mM glucose-6-phosphate, 1 mM creatine phosphate) was used for any dilutions. Interphase HSS was prepared as mitotic HSS, with the addition of cycling crude extract into interphase with calcium and adding 2 μg/mL cyclohexamide prior to the hard spin. HSS was aliquotted and frozen in liquid nitrogen and stored at -80 °C until use.

HeLa Cell Culture and Lysate Preparation: HeLa cells were cultured in DMEM (Corning), 10% FBS (Gibco) and 1% 100X penicillin/streptomycin solution (Corning) at 37 °C, 5% CO_2, 85% relative humidity. Mitotic HeLa lysates were prepared by dosing cells at ~70-80% confluency for 16 hours with 3 μM S-trityl-L-cysteine (STLC, Sigma) and then isolating mitotic cells via vigorous shakeoff. The mitotic cells were washed 3 times with cold PBS (Corning) supplemented with STLC. After the removal of the final wash, protease inhibitors (leupeptin, pepstatinA, and chymostatin, 10 μg each as a 10 mg/mL mixture of all three in DMSO, Sigma), cytochalasin D (10 μg from a 10 mg/mL solution in DMSO, Sigma), and nocodazole (7.5 μg as a 25 mM solution in DMSO) were added to the pellet, which was subsequently frozen in liquid nitrogen and thawed at room temperature three times to lyse cells. The lysate was then spun at 20000 *x g* for 30 minutes at 4 °C and the supernatant immediately used in experiments. For cells treated with okadaic acid (1 μM, Enzo) or barasertib (1 μM, ApexBio), the drug(s) was added to the final wash of the cells as well as just prior to lysis after removal of the final PBS wash.

Sucrose Gradients: For each gradient (5%-40% w/w in S-CSF-XB-phosphate), five step gradients

(5, 14, 23, 32, and 40% sucrose) of equal volume (950 µL) were gently layered, highest density on the bottom, by pipetting into 1/2 x 2 inch ultra-clear centrifuge tubes (Beckman Coulter) and allowed to diffuse overnight at 4 °C into a continuous gradient. 50 µL HSS was treated with DMSO, barasertib, okadaic acid, or a combination of drugs for 25 minutes per drug at room temperature prior to diluting in half with S-CSF-XB-phosphate and pipetting gently onto the sucrose gradient. The sucrose gradients were then spun in tandem at 237,000 *x g* for 6 hours at 4 °C in an SW55Ti rotor (Beckman Coulter). Gradients were fractionated from the top by pipetting 130 or 400 µL and the indicated fractions were blotted for INCENP, CDCA9, and NPM2. Bovine serum albumin (4S) and bovine γ-globulin (7S) standards were run on parallel gradients and their fractionation determined by SDS-PAGE gel electrophoresis of all fractions followed by staining with Coomassie Blue (45% methanol (BDH), 10% glacial acetic acid (JT Baker), 0.25 g Coomassie Blue (Fluka)) and destaining with an aqueous solution of 7.5% acetic acid and 20% methanol.

Tagging of CDCA8-GFP-3xFLAG in HeLa cells: Guide RNA to cut at the C-terminal endogenous locus of CDCA8 in HeLa cells were designed using the tools at crispr.mit.edu. The top five hits were selected, and oligos (CACCGAATGAGACACCAAAGTTGAC, CACCGAGACACCAAAGTTGACAGGA, CACCGCAACTTTGGTGTCTCATTTG, CACCGAACTTTGGTGTCTCATTTGT, CACCGAAAGTCCATCCTGTCAACTT and reverse complements, IDT) to generate guide RNAs were cloned into the pX330-U6-Chimeric_BB-CBh-hSpCas9 plasmid (Addgene) following the depositing lab's instructions at crispr.genome-engineering.org (Cong et al. 2013). Successful cloning was confirmed by sequencing using a U6 sequencing primer (Genewiz). Donor DNA was generated via isothermal assembly (Gibson et al., 2009) of two Geneblocks (IDT) and a modified pET21a(+) backbone (Novagen) with a 650 bp homology arm on the N-terminal side of the insert and a 597 bp homology arm on the C-terminal side of the insert. The backbone was cut using EcoRI and ZraI restriction enzymes (NEB) for 2 hours at 37 °C. The Geneblocks were amplified in PCR reactions using oligos with 30 bp overlaps with the

backbone and 20 bp priming sequences in Phusion high fidelity PCR master mix with HF buffer using the program 1) 94 °C, 2 minutes, 2) 94 °C, 30 seconds, 3) 54 °C, 30 seconds, 4) 72 °C, 2 minutes, 5) repeat steps 2-4 9 more times, 6) 94 °C, 30 seconds, 7) 72 °C, 2 minutes, 8) repeat steps 6-7 24 more times, 9) 72 °C, 10 minutes. Cut backbone and PCR products were purified on 1% agarose (Lonza) gels in TAE buffer (40 mM Tris base, 1 mM EDTA, 5.7% acetic acid) followed by DNA isolation using the QIAquick Gel Extraction kit (Qiagen) according to the manufacturer□s instructions. Backbone (3 μL) and inserts (1 μL each) were combined and annealed together at 50 °C for 30 minutes in 15 μL isothermal assembly buffer (Gibson et al., 2009). The reaction was then transformed into 5-alpha competent E. coli (high efficiency, NEB) according to the manufacturer□s instructions. Cloning was confirmed by sequencing using a T7 reverse primer (Genewiz). HeLa cells (24 x 104 per well of a 6-well plate (Corning)) were transfected simultaneously with the two plasmids using Lipofectamine 3000 (Life Technologies) according to the manufacturer□s instructions (2 μg donor DNA, 1 μg guide/Cas9 pX330 DNA, 3.75 μg Lipofectamine 3000, and 6 μL P3000). Cells were then selected by FACS using a BD FACSAria IIu-3 Laser with a 488 nm laser. All guides produced fluorescent cells with proper localization of GFP to the midzone in mitosis (see confocal microscopy, below). The population with the most cells after FACS sorting from the first guide sequence listed above were used for subsequent experiments.

Confocal Microscopy: Cells were grown on glass coverslips (22 x 22 mm, no. 1.5, VWR), fixed with 4% paraformaldehyde in PBS (Corning) for 15 minutes at room temperature, permeabilized with 0.2% Triton-X 100 in PBS (PBST) for 20 minutes at room temperature and immunostained with antibodies against α-tubulin (1:400 in PBST, 1 hour, room temperature) and AlexaFluor-568 goat anti-mouse (1:400 in PBST, 1 hour, room temperature) followed by three 5 minute washes in PBST. The coverslips were then placed onto 10 μL droplets of 10% glycerol in PBST on clean coverslips and sealed with Valap (1:1:1 lanolin, paraffin (Fluka), and petroleum jelly). Images were obtained at room temperature at the Nikon Imaging Center at Harvard Medical School using a 60X oil Plan Apo 1.49 NA

objective lens (Nikon) on a confocal Nikon Ti motorized inverted microscope equipped with a Yokogawa CSU-X1 spinning disc (Spectral Applied Research Aurora Borealis modification), Perfect Focus, a Prior Proscan II motorized stage, a Spectral Applied Research LMM-5 laser merge module (Ex:Em 488:480/40, 561:620/60, 642:700/75) with AOTF controlled solid state lasers, a Hamamatsu ORCA-AG cooled CCD camera, and driven by Metamorph. Images were prepared for publication using ImageJ. No modifications were made to images beyond minor brightness and contrast adjustments and cropping to center image on mitotic cells.

Fluorescence Correlation Spectroscopy: FCS measurements were performed on a Nikon Eclipse Ti microscope using two-photon excitation from a Ti:Sapphire pulsed laser (Mai-Tai, Spectral-Physics) with a 80-MHz repetition rate and ~70-fs pulse width at an 920-nm wavelength. The excitation light was expanded and collimated to fully utilize the numerical aperture of the water immersion objective (CFI Apo 40x WI, NA 1.25, Nikon) that focuses the light into the sample. The intensity of excitation light was modulated to 3 mW at the objective by the combination of half-wave plate and polarizing beam splitter (Thorlab). Cells were grown to 80-90% confluency on glass coverslips with #1.5 thickness, 25 mm diameter, and poly-D-lysine coating (Neuvitro). During imaging, we used a home-built temperature controlled chamber to maintain cells at 37 °C in an imaging medium, FluoroBrite DMEM (Gibco) supplemented with 10 mM HEPES and 2 mM L-glutamine, covered with mineral oil. A hybrid detector (HPM-100-40, Becker & Hickl) with 510/42 bandpass filter (Chroma) and TCSPC module (SPC-150, Becker & Hickl) were used to collect GFP fluorescence and calculate the normalized autocorrelation function of the fluorescence intensity fluctuations.

FCS data analysis: Each autocorrelation function was collected for 10 seconds while the excitation beam was parked close to the edge of a mitotic cell. 20-50 autocorrelation functions were averaged after the outliers were removed. The following two-component FCS model, $G_D(\tau)$, was fitted to the

average autocorrelation function:

$$G_D(\tau) = \sum_{i=slow,fast} \left(\frac{1}{1+\tau/\tau_{D,i}}\right)\left(\frac{1}{1+S^2(\tau/\tau_{D,i})}\right)^{1/2} + G_\infty \tag{1.1}$$

are the amplitude and diffusion time of each component, respectively, and S the ratio between the equatorial w_{xy} and axial w_z radii of the focal volume. Prior to every FCS experiment, w_{xy} and w_z were determined from the FCS measurements on calibration samples, 9.7 nM and 97 nM Alexa 488 dye in water, assuming that the diffusion coefficient of Alexa 488 is 435 μm^2/sec (Petrasek & Schwille, 2008). The nonlinear fitting was performed by a MATLAB built-in function, *nlinfit*, with the observation weight specified to the inverse of the standard deviation of the autocorrelation functions. The diffusion time, $\tau_{D,i}$, was converted to the diffusion coefficient, D_i, using the relationship:

$$D_i = \frac{w_{xy}^2}{8\tau_{D,i}}, \qquad i = slow, fast \tag{1.2}$$

Immunoprecipitation: Anti-FLAG M2 beads (Sigma) or Dynabeads Protein A beads (Life Technologies), charged with INCENP, CDCA9, NPM1 and NPM2 antibody at saturating levels according to the manufacturer's instructions, were incubated end-over-end with lysate or HSS following drug treatment for at least 45 minutes at 4 °C. Beads were separated from the lysate on a DynaMag-2 Magnet (Life Technologies) and washed with cold 10 mM HEPES, 1 mM MgCl2, 25 mM KCl, 1 mM EGTA, 0.1% TWEEN 20, pH 7.7 at least four times and subjected to immunoblot analysis or quantitative mass spectrometry (TWEEN 20 omitted for mass spectrometry experiments).

Quantitative MS: IPs were performed as above. The beads were taken up in 5 µL 8M guanidine-HCl, incubated at 60 °C for 20 minutes, and diluted to 2 M guanidine-HCl with 20 mM HEPBS pH 9.0. 0.4 µL 2 mg/mL LysC (Wako Chemical) was added and incubated at room temperature for 14 hours. The slurry was then diluted again to 0.5 M guanidine-HCl with the same HEPBS solution and an additional 0.4 µL of 2 mg/mL LysC was added along with 0.8 µL or 0.5 mg/mL trypsin (Promega

sequencing grade) and the solution incubated at 37 °C for 8 hours. Following transfer to a fresh tube, the supernatant was removed by vacuum overnight. The pellets were diluted in 20 µL 300 mM HEPES pH 8.0 and 3 µL TMT tags (Thermo). 5 mg/250 µL dry acetonitrile was added to the solution which was then incubated at room temperature for 2 hours. 3 µL 5% hydroxylamine (Sigma 99.999% pure) was added followed by a 15 minute room temperature incubation after which the solvent was removed by vacuum overnight. The solution was acidified to pH ∼1 with phosphoric acid, and a C18 stage-tip was done to desalt the sample (Rappsilber, Mann, & Ishihama, 2007). All solvent was removed and the sample resuspended in 6 µL of 1% formic acid. 3 µL the sample was shot on an Orbitrap Lumos instrument as previously reported (Wuhr et al., 2015). Samples were normalized by IgG IPs and by the amount of target protein (INCENP or CDCA8). The normalized amount of protein in the barasertib-treated sample was divided by that in the okadaic acid-treated sample, and hits were considered to be those proteins which had values above 1.

1.6 Acknowledgements

We gratefully thank D. Shechter (Albert Einstein College of Medicine) for the gift of NPM2 antibody, T. Hyman (MPI Dresden) for BAC cell lines, and S. Gygi (HMS Cell Biology) for mass spectrometry resources. We thank the Nikon Imaging Center at Harvard Medical School for microscopy resources and assistance. We also thank C. Field for critical reading of the manuscript and E. Boke and J.-H. Wang for helpful discussions.

This work was supported in part by NIH-GM39565. FCS work (TYY and DJN) was supported National Science Foundation grants DBI-0959721 and DMR-0820484. MS was supported by Ruth L Kirschstein NIH F31 pre-doctoral fellowship 5F31GM116451. The content is solely the responsibility of the authors and does not necessarily represent the official views of the National Institutes of Health.

1.7 Author Contributions

MLH and TJM designed the study. MLH performed all experiments unless otherwise noted. TYY performed FCS experiments and TTY and DJN analyzed the results. MLH and MS performed and analyzed IP-MS experiments. MLH and TJM wrote the manuscript with assistance in figure preparation by TYY. TJM and DJN provided funding. All authors reviewed the results and approved the final version of the manuscript.

1.8 References

Adams, R. R., Wheatleya, S. P., Gouldsworthy, A. M., Kandels-Lewis, S. E., Carmena, M., Smythe, C., Gerloff, D. L., & Earnshaw, W. C. (2000). INCENP binds the Aurora-related kinase AIRK2 and is required to target it to chromosomes, the central spindle and cleavage furrow. Curr. Biol., 10(17), 1075-1078.

Afonso, O., Matos, I., Pereira, A. J., Aguiar, P., Lampson, M. A., & Maiato, H. (2014). Feedback control of chromosome separation by a midzone Aurora B gradient. Science, 345(6194), 332-336.

Berrabah, W., Aumercier, P., Lefebvre, P., & Staels, B. (2011). Control of nuclear receptor activities in metabolism by post-translational modifications. FEBS Lett., 585(11), 1640-1650.

Bishop, J. D., & Schumacher, J. M. (2002). Phosphorylation of the carboxyl terminus of inner centromere protein (INCENP) by the Aurora B kinase stimulates Aurora B kinase activity. J. Biol. Chem., 277(31), 27577-27580.

Bolli, N., Nicoletti, I., De Marco, M. F., Bigerna, B., Pucciarini, A., Mannucci, R., Martelli, M. P., Liso, A., Mecucci, C., Fabbiano, F., Martelli, M. F., Henderson, B. R., & Falini, B. (2007). Born to be exported: COOH-terminal nuclear export signals of different strength ensure cytoplasmic accumulation of nucleophosmin leukemic mutants. Cancer Res., 67(13), 6230-6237.

Bolton, M. A., Lan, W., Powers, S. E., McCleland, M. L., Kuang, J., & Stukenberg, P. T. (2002). Aurora B kinase exists in a complex with survivin and INCENP and its kinase activity is stimulated by survivin binding and phosphorylation. Mol. Biol. Cell, 13(9), 3064-3077.

Carmena, M., Wheelock, M., Funabiki, H., & Earnshaw, W. C. (2012). The chromosomal passenger complex (CPC): From easy rider to the godfather of mitosis. Nat. Rev. Mol. Cell Biol., 13(12), 789-803.

Cong, L., Ran, F. A., Cox, D., Lin, S., Barretto, R., Habib, N., Hsu, P. D., Wu, X., Jiang, W., Marraffini, L. A., & Zhang, F. (2013). Multiplex genome engineering using CRISPR/Cas systems. Science, 339(6121), 819-823.

Cooke, C. A., Heck, M. M. S., & Earnshaw, W. C. (1987). The inner centromere protein (INCENP) antigens: Movement from inner centromere to midbody during mitosis. J. Cell Biol., 105(5), 2053-2067.

Cutts, S. M., Fowler, K. J., Kile, B. T., Hii, L. L. P., O'Dowd, R. A., Hudson, D. F., Saffery, R., Kalitsis, P., Earle, E., & Choo, K. H. A. (1999). Defective chromosome segregation, microtubule bundling and nuclear bridging in inner centromere protein gene (Incenp)-disrupted mice. Hum. Mol. Genet.,

8(7), 1145-1155.

Fernandez-Rivero, N., Franco, A., Velazquez-Campoy, A., Alonso, E., Muga, A., & Prado, A. (2016). A quantitative characterization of nucleoplasmin/histone complexes reveals chaperone versatility. Sci. Rep., 6, 32114.

Field, C. M., Groen, A. C., Nguyen, P. A., & Mitchison, T. J. (2015). Spindle-to-cortex communication in cleaving, polyspermic Xenopus eggs. Mol. Biol. Cell, 26(20), 3628-3640.

Gadad, S. S., Senapati, P., Syed, S. H., Rajan, R. E., Shandilya, J., Swaminathan, V., Chatterjee, S., Colombo, E., Dimitrov, S., Pelicci, P. G., Ranga, U., & Kundu, T. K. (2011). The multifunctional protein nucleophosmin (NPM1) is a human linker histone H1 chaperone. Biochemistry, 50(14), 2780-2789.

Gadea, B. B., & Ruderman, J. V. (2006). Aurora B is required for mitotic chromatin-induced phosphorylation of Op18/Stathmin. Proc. Natl. Acad. Sci. U. S. A., 103(12), 4493-4498.

Gassmann, R., Carvalho, A., Henzing, A. J., Ruchaud, S., Hudson, D. F., Honda, R., Nigg, E. A., Gerloff, D. L., & Earnshaw, W. C. (2004). Borealin: A novel chromosomal passenger required for stability of the bipolar mitotic spindle. J. Cell Biol., 166(2), 179-191.

Gibson, D. G., Young, L., Chuang, R.-Y., Venter, J. C., Hutchison, C. A., and Smith, H. O. (2009) Enzymatic assembly of DNA molecules up to several hundred kilobases. Nat. Methods 6, 343-345.

Groen, A. C., Coughlin, M., & Mitchison, T. J. (2011). Microtubule assembly in meiotic extract requires glycogen. Mol. Biol. Cell, 22(17), 3139-3151.

Honda, R., Koerner, R., & Nigg, E. A. (2003). Exploring the functional interactions between Aurora B, INCENP, and survivin in mitosis. Mol. Biol. Cell, 14(8), 3325-3341.

Hu, C.-K., Ozlu, N., Coughlin, M., Steen, J. J., & Mitchison, T. J. (2012). Plk1 negatively regulates PRC1 to prevent premature midzone formation before cytokinesis. Mol. Biol. Cell, 23(14), 2702-2711.

Jeyaprakash, A. A., Klein, U. R., Lindner, D., Ebert, J., Nigg, E. A., & Conti, E. (2007). Structure of a survivin-borealin-INCENP core complex reveals how chromosomal passengers travel together. Cell, 131(2), 271-285.

Kelly, A. E., Sampath, S. C., Maniar, T. A., Woo, E. M., Chait, B. T., & Funabiki, H. (2007). Chromosomal enrichment and activation of the Aurora B pathway are coupled to spatially regulate spindle assembly. Dev. Cell, 12(1), 31-43.

Kim, S. A., Heinze, K. G., & Schwille, P. (2007). Fluorescence correlation spectroscopy in living cells. Nat. Methods, 4(11), 963-973.

Koryakina, Y., Ta, H. Q., & Gioeli, D. (2014). Androgen receptor phosphorylation: biological context and functional consequences. Endocr. Relat. Cancer, 21(4), T131-T145.

Kuhn, T., Ihalainen, T. O., Hyvaluoma, J., Dross, N., Willman, S. F., Langowski, J., Vihinen-Ranta, M., & Timonen, J. (2011). Protein diffusion in mammalian cell cytoplasm. PLoS One, 6(8), e22962.

Laskey, R. A., Honda, B. M., Mills, A. D., & Finch, J. T. (1978). Nucleosomes are assembled by an acidic protein which binds histones and transfers them to DNA. Nature, 275(5679), 416-420.

Mackay, A. M., Ainsztein, A. M., Eckley, D. M., & Earnshaw, W. C. (1998). A dominant mutant of inner centromere protein (INCENP), a chromosomal protein, disrupts prometaphase congression and cytokinesis. J. Cell Biol., 140(5), 991-1002.

Maggi, L. B., Jr., Kuchenruether, M., Dadey, D. Y. A., Schwope, R. M., Grisendi, S., Townsend, R. R., Pandolfi, P. P., & Weber, J. D. (2008). Nucleophosmin serves as a rate-limiting nuclear export chaperone for the mammalian ribosome. Mol. Cell. Biol., 28(23), 7050-7065.

Mitchison, T. J., Nguyen, P., Coughlin, M., & Groen, A. C. (2013). Self-organization of stabilized microtubules by both spindle and midzone mechanisms in Xenopus egg cytosol. Mol. Biol. Cell, 24(10), 1559-1573.

Mukherjee, H., Chan, K.-P., Andresen, V., Hanley, M. L., Gjertsen, B. T., & Myers, A. G. (2015). Interactions of the natural product (+)-avrainvillamide with nucleophosmin and exportin-1 mediate the cellular localization of nucleophosmin and its AML-associated mutants. ACS Chem. Biol., 10(3), 855-863.

Namboodiri, V. M. H., Akey, I. V., Schmidt-Zachmann, M. S., Head, J. F., & Akey, C. W. (2004). The structure and function of Xenopus NO38-core, a histone chaperone in the nucleolus. Structure, 12(12), 2149-2160.

Needleman, D. J., Xu, Y., & Mitchison, T. J. (2009). Pin-hole array correlation imaging: highly parallel fluorescence correlation spectroscopy. Biophys. J., 96(12), 5050-5059.

Nguyen, P. A., Groen, A. C., Loose, M., Ishihara, K., Wuehr, M., Field, C. M., & Mitchison, T. J. (2014). Spatial organization of cytokinesis signaling reconstituted in a cell-free system. Science, 346(6206), 244-247.

Okuwaki, M., Matsumoto, K., Tsujimoto, M., & Nagata, K. (2001). Function of nucleophosmin/B23,

a nucleolar acidic protein, as a histone chaperone. FEBS Lett., 506(3), 272-276.

Ozlu, N., Monigatti, F., Renard, B. Y., Field, C. M., Steen, H., Mitchison, T. J., & Steen, J. J. (2010). Binding partner switching on microtubules and Aurora-B in the mitosis to cytokinesis transition. Mol. Cell. Proteomics, 9(2), 336-350.

Petrasek, Z., & Schwille, P. (2008). Precise measurement of diffusion coefficients using scanning fluorescence correlation spectroscopy. Biophys. J., 94(4), 1437-1448.

Platonova, O., Akey, I. V., Head, J. F., & Akey, C. W. (2011). Crystal structure and function of human nucleoplasmin (Npm2): A histone chaperone in oocytes and embryos. Biochemistry, 50(37), 8078-8089.

Portella, G., Passaro, C., & Cheiffi, P. (2011). Aurora B: A new prognostic marker and therapeutic target in cancer. Curr. Med. Chem., 18(4), 482-496.

Poser, I., Sarov, M., Hutchins, J. R. A., Heriche, J.-K., Toyoda, Y., Pozniakovsky, A., Weigl, D., Nitzsche, A., Hegemann, B., Bird, A. W., Pelletier, L., Kittler, R., Hua, S., Naumann, R., Augsburg, M., Sykora, M. M., Hofemeister, H., Zhang, Y., Nasmyth, K., White, K. P., Dietzel, S., Mechtler, K., Durbin, R., Stewart, A. F., Peters, J.-M., Buchholz, F., & Hyman, A. A. (2008). BAC TransgeneOmics: A high-throughput method for exploration of protein function in mammals. Nat. Methods, 5(5), 409-415.

Quensel, C., Friedrich, B., Sommer, T., Hartmann, E., & Kohler, M. (2004). In vivo analysis of importin α proteins reveals cellular proliferation inhibition and substrate specificity. Mol. Cell. Biol., 24(23), 10246-10255.

Rappsilber, J., Mann, M., & Ishihama, Y. (2007). Protocol for micro-purification, enrichment, prefractionation and storage of peptides for proteomics using StageTips. Nat. Protoc., 2(8), 1896-1906.

Samejima, K., Platani, M., Wolny, M., Ogawa, H., Vargiu, G., Knight, P. J., Peckham, M., & Earnshaw, W. C. (2015). The inner centromere protein (INCENP) coil is a single α-helix (SAH) domain that binds directly to microtubules and is important for chromosome passenger complex (CPC) localization and function in mitosis. J. Biol. Chem., 290(35), 21460-21472.

Sampath, S. C., Ohi, R., Leismann, O., Salic, A., Pozniakovski, A., & Funabiki, H. (2004). The chromosomal passenger complex is required for chromatin-induced microtubule stabilization and spindle assembly. Cell, 118(2), 187-202.

Sessa, F., Mapelli, M., Ciferri, C., Tarricone, C., Areces, L. B., Schneider, T. R., Stukenberg, P. T., & Musacchio, A. (2005). Mechanism of Aurora B activation by INCENP and inhibition by hesperadin.

Mol. Cell, 18(3), 379-391.

Sessa, F., & Villa, F. (2014). Structure of Aurora B-INCENP in complex with barasertib reveals a potential transinhibitory mechanism. Acta Crystallogr. F: Struct. Biol. Commun., 70(3), 294-298.

Shalloway, D., & Taylor, S. J. (1997). Src: More than the sum of its parts. Trends Cell Biol., 7(6), 215-217.

Staus, D. P., Taylor, J. M., & Mack, C. P. (2011). Enhancement of mDia2 activity by Rho-kinase-dependent phosphorylation of the diaphanous autoregulatory domain. Biochem. J., 439(1), 57-65.

Szebeni, A., & Olson, M. O. J. (1999). Nucleolar protein B23 has molecular chaperone activities. Protein Sci., 8(4), 905-912.

Tseng, B. S., Tan, L., Kapoor, T. M., & Funabiki, H. (2010). Dual detection of chromosomes and microtubules by the chromosomal passenger complex drives spindle assembly. Dev. Cell, 18(6), 903-912.

Wuhr, M., Freeman, R. M., Jr., Presler, M., Horb, M. E., Peshkin, L., Gygi, S. P., & Kirschner, M. W. (2014). Deep proteomics of the Xenopus laevis egg using an mRNA-derived reference database. Curr. Biol., 24(13), 1467-1475.

Wuhr, M., Guttler, T., Peshkin, L., McAlister, G. C., Sonnett, M., Ishihara, K., Groen, A. C., Presler, M., Erickson, B. K., Mitchison, T. J., Kirschner, M. W., & Gygi, S. P. (2015). The nuclear proteome of a vertebrate. Curr. Biol., 25(20), 2663-2671.

Yasui, Y., Urano, T., Kawajiri, A., Nagata, K.-i., Tatsuka, M., Saya, H., Furukawa, K., Takahashi, T., Izawa, I., & Inagaki, M. (2004). Autophosphorylation of a newly identified site of Aurora-B Is indispensable for cytokinesis. J. Biol. Chem., 279(13), 12997-13003.

2

Development of Tools to Study the Chromosomal Passenger Complex

This chapter describes the development of tools intended to study the structure and function of the CPC and its subunits. These tools are based on recombinant, tagged proteins but vary significantly in application. While none of these tools have yet led to substantial advances in understanding of CPC biology, there may be opportunity for others to use them in the future, prompting this discussion of their development.

2.1 Recruitment of mitotic proteins to supported lipid bilayers

The CPC localizes at the site of furrow ingression during cytokinesis (Figure 2.1A), where RHOA is activated and induces actomyosin contractility. Inhibition of AURKB with small molecules prevents cytokinesis by preventing the formation of a proper midzone between microtubule asters in *X. laevis* egg extract on supported lipid bilayers (Nguyen et al., 2014). Conversely, activation of AURKB in *X. laevis* eggs by the addition of an antibody raised against the C-terminus of INCENP, known to stimulate AURKB activity, results in a large number of cleavage furrows (Field, Groen, Nguyen, & Mitchison, 2015). However, it is unclear if recruitment of the CPC to the cortex in the absence of microtubules is enough to induce a cleavage furrow. To test this, a system to attract the CPC to a specific location needed to be developed. Using light to attract the CPC was an obvious choice because supported lipid bilayers are built on glass coverslips and have already been extensively used for microscopic observation of midzones (Nguyen et al., 2014). The usage of light as an activating factor also does not require the introduction of any small molecules (like biotin or metals) into the extract which may affect extract function. Microtubules can easily be prevented from forming in the extract by the addition of the small molecule nocodazole.

Light-sensitive proteins have been previously used for location-specific protein recruitment. I selected a system reported in yeast using a LOV (light oxygen voltage) domain (Strickland et al., 2012). AsLOV2 is an oat plant kinase activated with blue light. Following the absorption of photons by a flavin cofactor, a reversible covalent bond is formed between the cofactor and the protein, inducing a conformational change. This results in the J-α helix at the C-terminus unhinging from the rest of the protein, exposing its caged element (in the case of the native protein, a kinase domain) (Harper, Neil, & Gardner, 2003; Harper, Christie, & Gardner, 2004; Halavaty & Moffat, 2007). This is thought to be a mechanism for the plant to follow the sun throughout the day. Since its discovery, the light activated portion of the kinase has been adapted for a number of other functions. For instance, the LOV do-

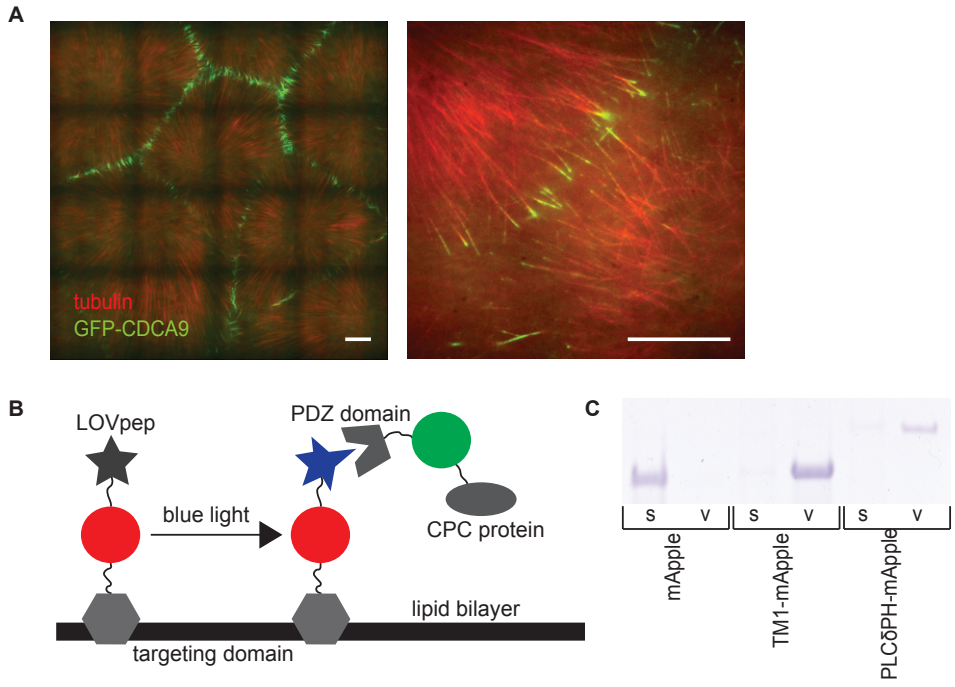

Figure 2.1: **LOV-based protein-bilayer recruitment scheme and development of a membrane targeting domain.** (A) GFP-CDCA9 localizes to the midzone between microtubule asters. Magnetic beads coated with an antibody against Aurora kinase A (AURKA) were added to interphase extract along with purified GFP-CDCA9 and imaged between two PLL-PEG-coated glass coverslips on a spinning disk confocal microscope. Scale bars represent 10 μm. (B) Scheme for the proposed targeting of proteins to a supported lipid bilayer using a LOV domain. (C) Vesicles were made from pure lipids and incubated with pure proteins. The vesicles were sedimented and isolated from the supernatant, after which the protein content of the separated protein fractions was analyzed via SDS-PAGE followed by staining with Coomassie Blue.

main can cage a short peptide, which binds to a separate protein when exposed. In the extract-bilayer system, a membrane-targeting domain could anchor the LOV domain caging a peptide, distributed uniformly across the bilayer. Then, when blue light is shone on a particular spot, the peptide binds to a PDZ domain in the extract. The PDZ domain could be attached to a protein of interest, such as CDCA9 of the CPC (Figure 2.1B).

I first developed a suitable membrane targeting domain. I tested two potential candidates with different mechanisms of action: a transmembrane helix adapted from the transmembrane receptor

FGFR3 and the plexstrin homology (PH) domain of PLCδ, which binds specifically to PI(4,5)P_2 lipids. Using isothermal assembly followed by expression and purification from bacterial culture, the candidate membrane targeting domains were produced attached to an mApple fluorophore.

I tested the membrane targeting abilities of these proteins with a vesicle sedimentation assay. Vesicles formed from a mixture of pure lipids were combined with the recombinant proteins and centrifuged so that the vesicles pelleted at the bottom. The protein content of the supernatant and the vesicle pellet was analyzed by SDS-PAGE followed by Coomassie Blue staining. Both membrane binding domains sedimented with vesicles, while a control mApple protein remained in the supernatant (Figure 2.1C). Either of these domains, therefore, could be used to attach a larger protein to a membrane.

I then turned my attention to the LOV domain. I first tested if a PDZ-binding peptide alone, uncaged by the LOV domain, could bind to reported PDZ domains (Strickland et al., 2012). The microtubule binding domain of ensconsin (MAP7) was attached to mApple and the PDZ-binding peptide with flexible linkers between each domain to create ensconsin-mApple-pep. The construct selectively bound to polymerized microtubules of bovine tubulin stabilized with taxol (Figure 2.2A). Three PDZ domains reported to bind to the peptide were cloned with GFP tags and expressed and purified from bacterial culture. The PDZ domains only colocalized with microtubules when added in conjunction with ensconsin-mApple-pep (Figure 2.2A). There was no substantial difference in binding ability between the three PDZ domains in this test system.

Caging the peptide with a LOV domain proved significantly more challenging. I initially tried to use a recombinant protein containing the LOV-peptide combination reported in yeast attached to the ensconsin microtubule binding domain (Strickland et al., 2012). However, no PDZ recruitment to purified microtubules in the presence of ensconsin-mApple-LOVpep was observed when illuminated with 408 nm blue light. Modifications to LOV protein expression and purification protocols did not improve binding, nor did reducing the amount of LOV caging by adding more residues of the parent

A

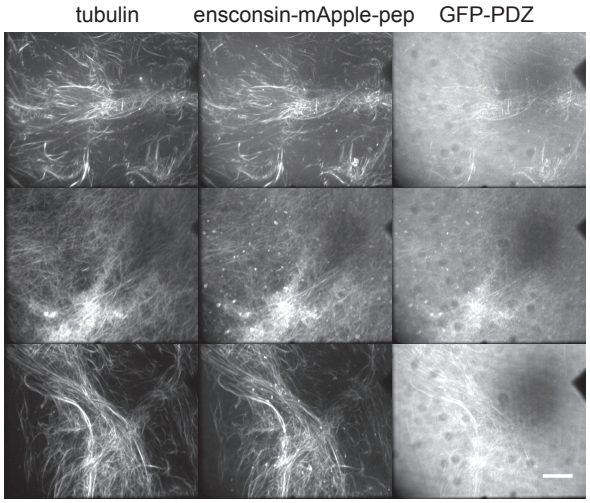

B

Construct	Sequence	Dark Binding	Light Binding
AsLOV2	IDEAAKELPDANL		
ensconsin-mApple-pep	SSADTWV	yes	yes
ensconsin-mApple-LOVpep1	ISSADTWV	no	no
ensconsin-mApple-LOVpep2	IDKAVDTWV	no	no
ensconsin-mApple-LOVpep3	IDSSADTWV	no	no
ensconsin-mApple-LOVpep4	IDESSADTWV	no	no

Figure 2.2: **Test of the LOVpep-PDZ system.**(A) Bovine brain tubulin was polymerized by incubating with GTP and taxol at 37 ℃ for 30 minutes. Purified proteins were added to the solution and imaged between untreated glass coverslips with a spinning disk confocal microscope. Scale bars represent 10 μm. (B) PDZ-pep binding was not observed with a variety of LOVpep constructs using the same assay as in (A).

AsLOV2 protein before the PDZ-binding peptide (Figure 2.2B).

Because this system was reported to work *in vivo*, I suspected the lack of binding was due to some aspect of the protein purification process. For instance, a potential problem was the location of the tag used for purification. The peptide needed to be on the C-terminus for PDZ binding; therefore, the purification tag on the N-terminus did not necessarily isolate the complete translated protein. Throughout the purification process, I consistently observed another abundant protein copurifying with the desired protein with a slightly higher molecular weight than the ensconsin microtubule domain alone but significantly less than that of the desired ensconsin-mApple-LOVpep protein, which might be an incomplete translation product. I suspected that expression of the complete LOV domain was challenging for the bacteria and that the critical peptide was often simply not present due to premature translation termination. I therefore turned to a different peptide-binding domain system that permitted a purification tag on the C-terminus.

SpyTag is a 13-residue peptide, small enough to be potentially caged by a LOV domain (Zakeri et al., 2012; Li, Fierer, Rapoport, & Howarth, 2014). SpyCatcher is also relatively small (129 residues as opposed to roughly 300 for the PDZ domains) and can be readily tagged with GFP or other proteins. SpyTag and SpyCatcher form an irreversible covalent isopeptide bond between lysine and aspartate residues, eliminating the need for continuous illumination once the adduct has been formed and allowing adduct formation to be observed by denaturing gel electrophoresis (Zakeri et al., 2012). SpyTag binds to SpyCatcher regardless of its location in a larger protein, allowing the C-terminal end to be tagged with 6xHis to enable selective purification of the complete protein. I first tested the ability of the tag to associate with SpyCatcher without the LOV domain, using the same *in vitro* polymerized microtubule system from Figure 2.2A. As with the pep-PDZ system, strong colocalization of both the ensconsin-mApple-spy1 and GFP-SpyCatcher was observed. Adding the LOV domain to the construct retained binding in both the light and the dark state (Figure 2.3A, B).

I needed the adduct to only form when illuminated with blue light. I therefore cloned, expressed, and purified three other versions of the LOV protein, each with a shorter peptide than ensconsin-mApple-spy1. Substantial efforts were required to determine a protein purification protocol that retained LOV activity and that adequately separated the desired protein. LOV constructs were expressed and purified in the dark in phosphate buffer, which was critical for protein stability. The addition of 1% NP-40 also seemed to improve protein stability, as did 10% sucrose added as a cryoprotectant. Eventually, relatively clean ensconsin-mAppleLOVspy protein was produced (Figure 2.3C).

Once pure protein was obtained, the ability of the LOVspy proteins to bind to SpyCatcher under light and dark state conditions was tested. Because SpyTag-SpyCatcher binding creates an irreversible covalent bond, I observed formation of the adduct by Coomassie Blue staining of SDS-PAGE gels. To assay the ability of a given construct to bind to SpyCatcher, purified proteins were simply mixed in a clear tube and exposed to blue light prior to denaturing gel electrophoresis. When ensconsin-mApple-LOVspy2 was tested, there was minimal dark state binding but substantially more when the reaction was continuously illuminated with 365 nm light (Figure 2.3D). LOVspy constructs with truncations of the tag did not exhibit any binding to SpyCatcher, even in the lit state.

I then tested the interaction between ensconsin-mApple-LOVspy2 and GFP-SpyCatcher in the presence of microtubules. As in Figure 2.2A, pure proteins were added to a solution of polymerized microtubules. Ensconsin-mApple-LOVspy2 readily bound to microtubules, but GFP-SpyCatcher bound only minimally (Figure 2.3E, time 0 minutes). With continuous illumination with widefield DAPI light, the intensity of both tubulin (visualized with AlexaFluor-647 tubulin added during the polymerization) and ensconsin-mApple-LOVspy2 faded due to photobleaching. In contrast, the intensity of GFP-SpyCatcher increased on microtubules, suggesting that it was binding to ensconsin-mApple-LOVspy2.

At this point, however, it became clear that the LOV strategy was flawed. In a typical *X. laevis* extract reaction, the interphase state is maintained for about 45 minutes before the extract cycles back

Figure 2.3 *(following page)*: **Development of the LOVspy-SpyCatcher recruitment system.** (A) Binding between SpyCatcher and various LOVspy constructs as measured by adduct formation observed on SDS-PAGE gels. (B) The binding of ensconsin-mApple-LOVspy1 was tested by adding purified proteins to *in vitro* polymerized bovine brain tubulin stabilized with taxol in the dark and when illuminated with 408 nm light. Scale bar represents 10 μm. (C) Purified proteins ensconsin-mApple-LOVspy2 and GFP-SpyCatcher, separated via SDS-PAGE and stained with Coomassie Blue. (D, E) Adduct formation over time between ensconsin-mApple-LOVSpy2 and GFP-SpyCatcher at room temperature in the dark and when continuously illuminated with 365 nm light by either (D) separating proteins via SDS-PAGE and staining with Coomassie Blue or (E) observing GFP-SpyCatcher recruitment to microtubules via spinning disk confocal microscopy. Scale bar represents 10 μm.

Figure 2.3: (continued)

A

Construct	Sequence	Dark Binding	Light Binding
ensconsin-mApple-spy1	EAHIVMVDAYKPTK	yes	yes
ensconsin-mApple-LOVspy1	IDEAHIVMVDAYKPTK-6xHis	yes	yes
ensconsin-mApple-LOVspy2	IDEHIVMVDAYKPTK-6xHis	no	yes
ensconsin-mApple-LOVspy3	IDHIVMVDAYKPTK-6xHis	no	no
ensconsin-mApple-LOVspy4	IDAYKPTK-6xHis	no	no

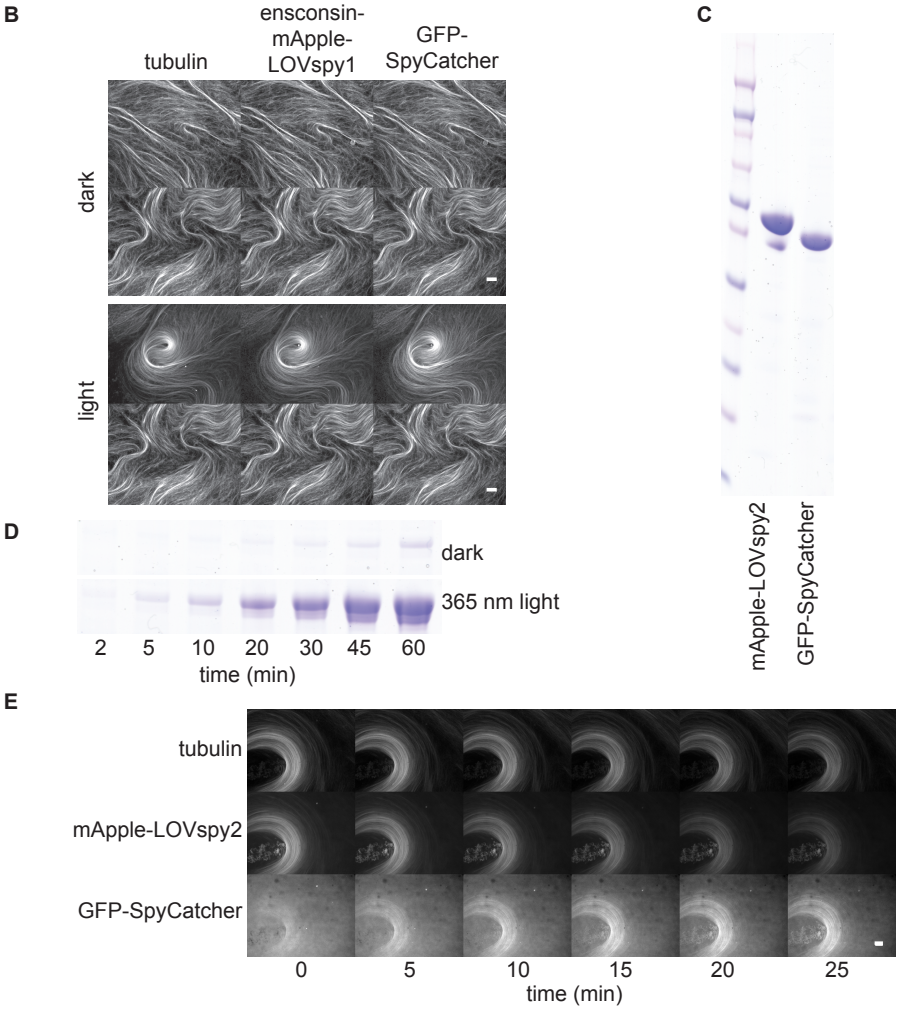

to mitosis, and as such all experimentation must be completed in that time period. Recruitment of SpyCatcher to a supported lipid bilayer would take up a substantial amount of that time and requires continuous illumination, potentially damaging the extract itself. Additionally, a substantial amount of both proteins remained unbound in the test tube reaction/SDS-PAGE assay, suggesting that significant issues remain with purifying active LOV protein. Previous textitin vivo examples of LOV-induced recruitment to biological structures required illumination only for at most a second with blue light (Strickland et al., 2012), also supporting the idea that the purified LOV protein was less active than when expressed endogenously. Lastly, the LOV protein seemed to degrade or lose activity upon storage at -80 °C, even with a variety of cryoprotectants. In the face of these technical challenges, the LOV-based targeting strategy was abandoned, and instead different approaches were pursued to study CPC function.

2.2 Purified CPC subunit localization to microtubule pineapples

I attempted to learn more about CPC behavior by studying its individual components. Work on the CPC has heavily focused on understanding the kinase activity of AURKB and much less on the roles of the other three CPC proteins INCENP, BIRC5, and CDCA8/9. By obtaining pure proteins of these subunits and their domains, I hoped to understand more about the function of the complex as a whole.

We already possessed a clone of GFP-tagged CDCA9, which is the maternally loaded version of CDCA8. CDCA8 is present in very low amounts in the early embryo but becomes much more prominent after the mid-blastula transition when transcription begins. Homology models of both proteins revealed that they consist of a sizeable (~45 residue) extended helix on the N-terminus attached to a globular domain. Crystal structures suggest that CDCA8 binds to INCENP and BIRC5 in a three-helix bundle (Figure 0.3B). Given the similar structural features of CDCA8 and CDCA9, I wondered if CDCA8 had similar function in extracts prepared from unfertilized *X. laevis* eggs. I therefore cloned, expressed, and purified a mApple-tagged version of CDCA8. Keeping these proteins relatively dilute throughout the purification process was critical for preventing aggregation.

Both GFP-CDCA9 and mApple-CDCA8 localize to pineapple microtubules, and especially strongly to the plus ends at the center (Figure 2.4A). Unless the proteins have an as-yet undiscovered microtubule binding domain, they have likely exchanged with endogenous CDCA9 and bound to INCENP, which does bind microtubules. While GFP-CDCA9 may localize slightly more strongly to the center of pineapples than mApple-CDCA8, these differences can also be attributable to different imaging timepoints or small differences in pineapple quality. Further investigation will be required to understand why two isoforms of CDCA8/9 are required for *X. laevis* embryonic development.

I also wanted to investigate the significance of the two domains of CDCA8/9 (globular and helical). I cloned, expressed, and purified fluorophore-tagged versions of the CDCA8 helical and globular domains as well as the globular domain of CDCA9 and examined the localization of these constructs to pineapples. Curiously, all of these constructs localized to microtubules (Figure 2.4B). This wasn't surprising for the helical domain, as it likely exchanged into the CPC by displacing native CDCA9. However, it was surprising that the globular domains of both CDCA8 and CDCA9 localized strongly to microtubules. Either the three-helix bundle isn't as critical for CDCA8/9 incorporation into the CPC as is implied from crystal structures, or CDCA8/9 has alternate microtubule binding mechanisms beyond simply associating with the CPC. Both of these possibilities are worthy of further exploration.

Figure 2.4 *(following page)*: **CDCA8/9 recombinant proteins localize to microtubule pineapples.** Following a 30-minute incubation with the indicated purified protein, microtubule pineapples were formed on glass coverslips coated with casein and visualized with AlexaFluor-647-tubulin on a spinning disk confocal microscope. Images in (C) are zoomed in parts of images highlighted with yellow boxes in (A) and (B). Scale bars represent 10 μm.

Figure 2.4: (continued)

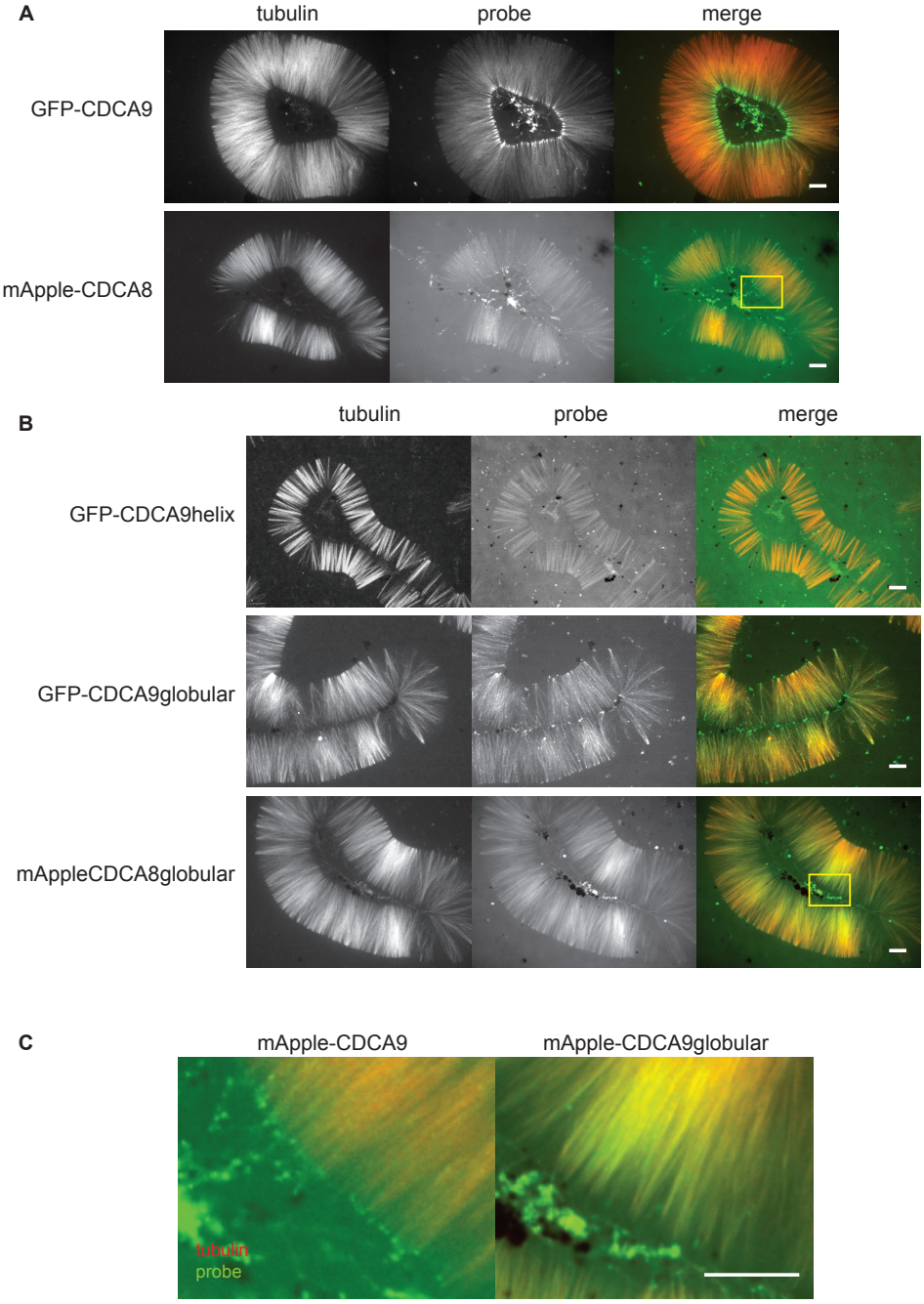

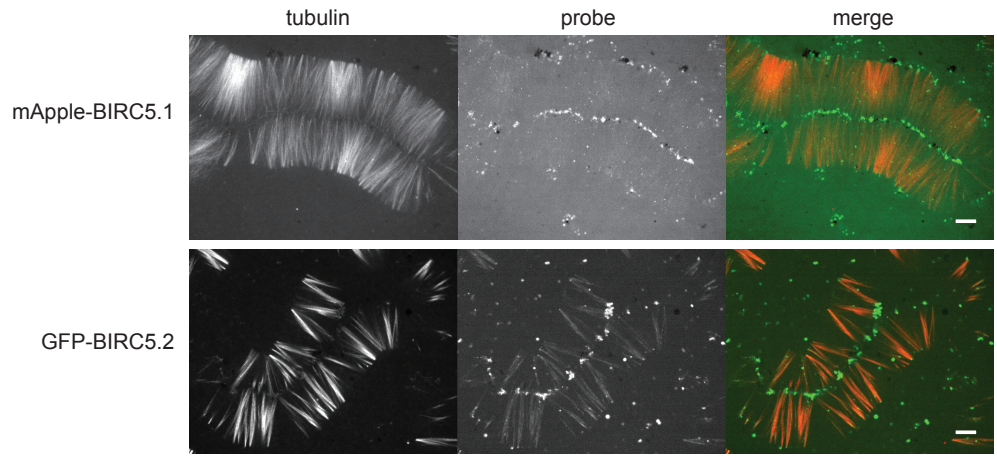

Figure 2.5: **BIRC5 recombinant proteins do not localize to pineapple microtubules.** Pineapples were grown under glass coverslips and imaged as in Figure 2.4 with BIRC5 probes added. Scale bars represent 10 μm.)

Neither the CDCA8 helical domain nor the globular domains of CDCA8/9 seem to localize to the plus ends of microtubules like the full length proteins do (Figure 2.4C). Although there are particles in the middle of the pineapple, they seem to be part of larger clusters unaffiliated with the microtubules that got pushed together as microtubules grew rather than localized to the plus ends of microtubules themselves. There may be some mechanism requiring the whole protein or incorporation into the CPC to be transported to microtubule plus ends. I suspect that the CDCA8/9 subunit does have some functional importance for CPC transport because the helical domain, which I would expect to be incorporated into the CPC, does not localize to the plus ends. Determination of the exact functional domains of CDCA8/9 that are required for CPC incorporation and potentially CPC transport are interesting avenues for future study.

I also investigated recombinant proteins of the other small member of the CPC, BIRC5. Like CDCA8/9, BIRC5 has different maternally loaded and embryonically expressed isoforms in *X. laevis* (which I will refer to as BIRC5.1 and BIRC5.2) that differ in sequence identity by 43%. I expressed and

purified both isoforms with flurophore tags. When purified proteins were added to the pineapple system they did not localize significantly to microtubules but instead formed larger aggregates (Figure 2.5). Although there were larger aggregates in the center of pineapples, these were likely pushed together as pineapple microtubules grew rather than actually being associated with the microtubules. While BIRC5 may only incorporate into the CPC when localized at plus ends, BIRC5's known dimerization properties (Jeyaprakash et al., 2007) and the presence of aggregates outside of pineapples suggests that the recombinant BIRC5 constructs do not exchange with native BIRC5. More work will be required to design appropriate constructs and conditions to generate effective fluorophore-tagged BIRC5 recombinant proteins. One intriguing possibility is that NPMs prevent BIRC5 aggregation until the CPC can be appropriately clustered on microtubule plus ends.

2.3 Attempted purification of the CPC from biological extracts

With purified CPC in hand, one could both examine the structural details of the complex in far greater detail while also more throughly exploring proteins that interact specifically with the CPC. Numerous attempts were made to purify the CPC from either *X. laevis* extracts or from HeLa lysates. While none of these purification methods were ultimately fruitful, a brief discussion of the strategies will hopefully serve as a reference for those making similar attempts in the future.

There are a number of small molecules that inhibit AURKB. I decided to couple one of these inhibitors to a solid substrate, isolate the CPC, and then elute with free inhibitor. I selected barasertib, a highly potent (IC_{50}=0.37 nM in cell free assay) and selective (3000-fold over AURKA) AURKB inhibitor, because the free alcohol provided a handle for attachment to a solid support. The drug was functionalized by reacting the free alcohol with 1,1'-carbodiimidazole, which would likely still preserve AURKB binding based on the crystal structure of this interaction (Figure 0.3). The resulting imidazole was then incubated with a variety of solid supports with amine handles to produce beads tagged

with the complex (Figure 2.6A). I then incubated these beads with HSS, and, after washing, denatured the attached proteins by boiling the beads in an SDS solution, separated via SDS-PAGE, and analyzed by mass spectrometry (Figure 2.6B). Unfortunately, the most abundant proteins were those also most abundant in HSS, with no evidence of enrichment of any CPC proteins (Figure 2.6C). The chemical isolation strategy was therefore abandoned.

Previous purifications of protein complexes from *X. laevis* extracts, including the septins and the gamma tubulin complex (Field et al., 1996; Oegema et al., 1999), have relied on antibodies raised against peptides of subunits of the complex. In this strategy, complexes are isolated from the extract by immunoprecipitation using antibodies attached to a solid support. The complexes are then eluted from the beads by the addition of free peptide against which the antibody was initially raised. I attempted this strategy with antibodies raised against C-terminal peptides of INCENP and CDCA9. For both epitopes, both the native antibody and an antibody specifically purified to be peptide elutable successfully isolated the CPC from the extract, but failed to dissociate from the beads when peptide was added (Figure 2.7A). Antibodies raised against fewer residues or alternate sites within the CPC may be more successful.

The last strategy to isolate *X. laevis* CPC used a cleavable linker to selectively attach the CPC to a solid support. A peptide containing a site cleavable by 3C protease flanked by flexible linkers, a biotin on the N-terminus, and a cysteine on the C-terminus was ordered from a commercial source. The peptide was coupled to an antibody raised against an INCENP C-terminal peptide by first reacting amine groups on the antibody with iodoacetic acid-NHS ester as previously described (Field, Oegema, Zheng, Mitchison, & Walczak, 1998). The cleavable peptide with a C-terminal cysteine was then added to produce the peptide-coupled antibody. When just the antibody was bound to streptavidin coated beads and then reacted with 3C protease overnight, only some of the antibody was eluted (Figure 2.7B). The peptide was extended to include longer flexible linkers to enable better access for the protease. When the new peptide-INCENP antibody coupled beads were incubated in HSS and then incubated overnight with the protease, INCENP and CDCA9 were bound to but not eluted from the beads. This remains the most promising strategy to isolate the CPC from *X. laevis* HSS; with some modification to the length of the peptide to ensure proper exposure to the protease, it is possible that the CPC could be isolated successfully.

An attempt was also made to isolate the CPC from HeLa lysates. As discussed in Chapter 1, CDCA8 was tagged with GFP-3xFLAG using a CRISPR/Cas9 strategy. Lysates were prepared from the tagged cell line as in Chapter 1. Anti-FLAG M2 beads were then used to immunoprecipitate the tagged protein from solution (Figure 2.8A). CDCA8-GFP-3xFLAG and other CPC proteins were readily isolated (Figure 2.8B). However, when proteins bound to the beads were separated by SDS-PAGE and analyzed by mass spectrometry, there were many other nonspecific proteins obtained as well (Figure 2.8C). Addition of another tag on a different CPC subunit may yield a better CPC purification method.

Figure 2.6 *(following page)*: **Attempted CPC purification from HSS using barasertib-coated beads.** (A) Scheme for attaching barasertib to amine-conjugated beads. (B) Proteins isolated from *X. laevis* HSS with barasertib-coupled beads that were then submitted for mass spectrometry analysis. (C) Proteins isolated from HSS treated with DMSO or okadaic acid (OA) with barasertib-coupled beads and washed with low (L) or high (H) salt as well as HSS samples after depletion (sup) were separated via SDS-PAGE, transferred to a nitrocellulose membrane, visualized with Ponceau S stain, and then immunoblotted with antibodies raised against C-terminal peptides of INCENP and CDCA9.

Figure 2.6: (continued)

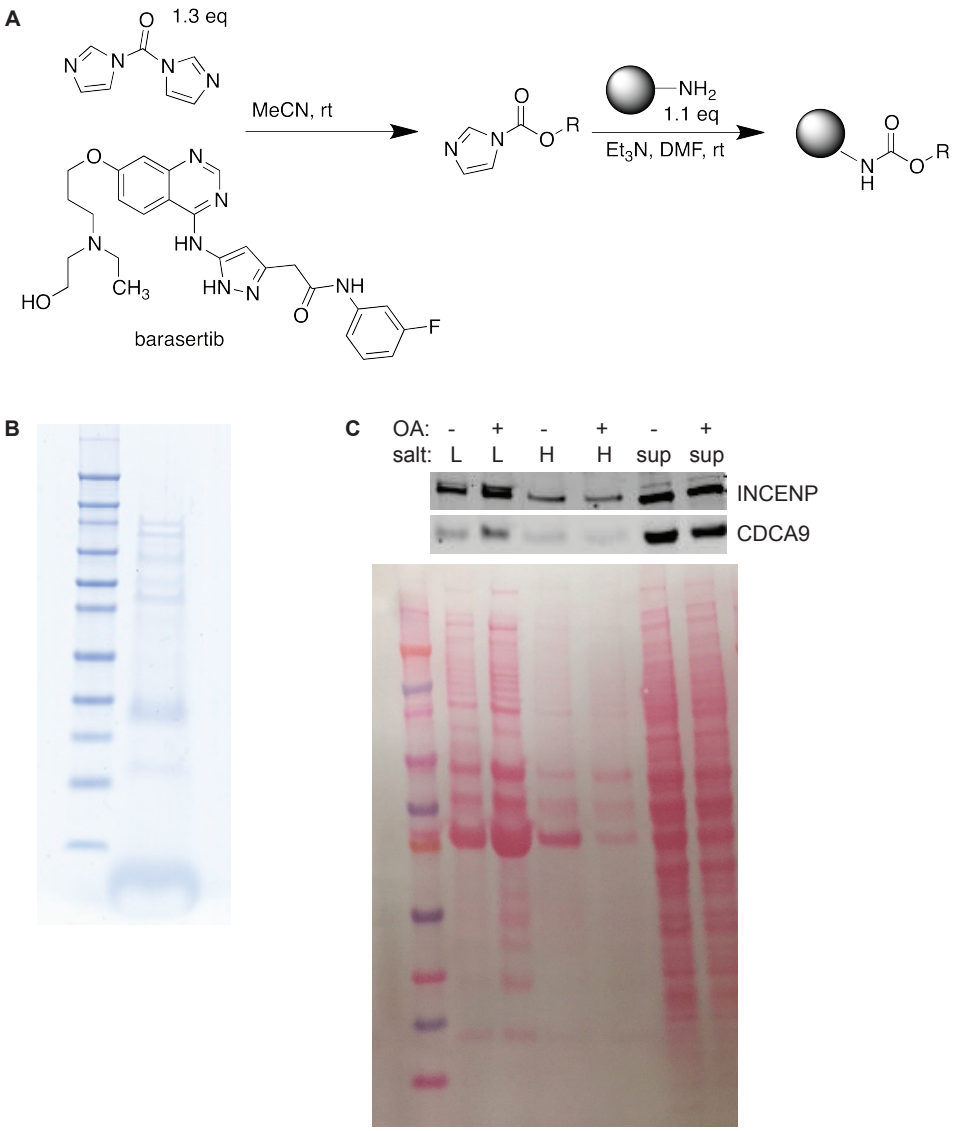

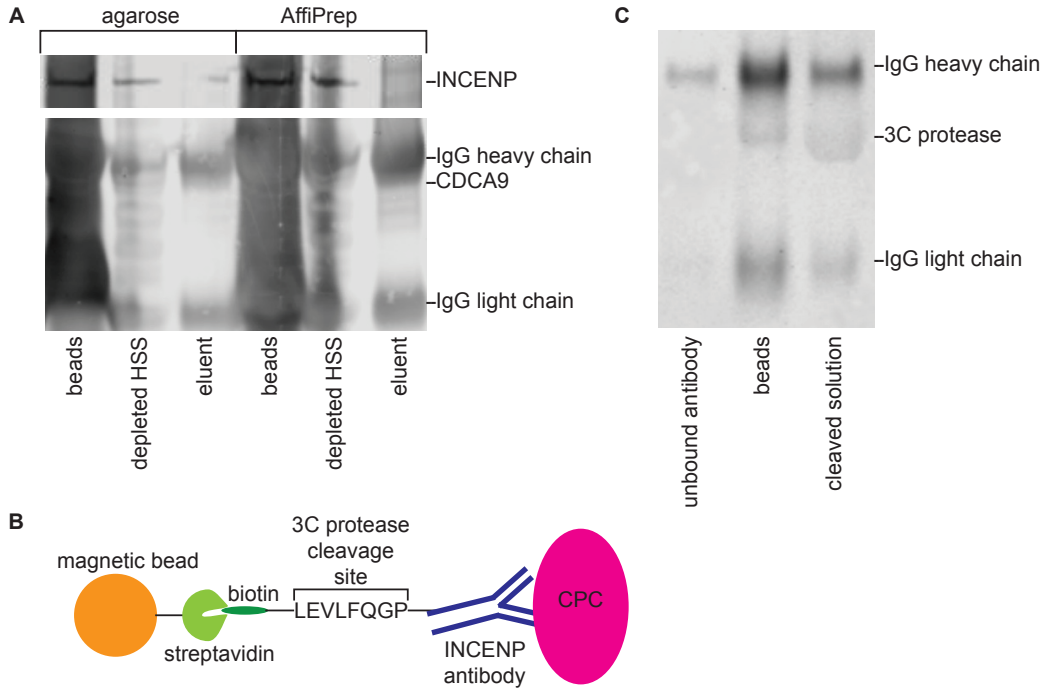

Figure 2.7: **Attempted CPC purification from HSS using antibodies raised against CPC subunits.** (A) CDCA9 antibody was attached to Protein A-conjugated agarose or AffiPrep beads and incubated with HSS. The beads were then washed and incubated with free peptide against which the antibody was originally raised. The proteins were separated via SDS-PAGE and immunoblotted for CDCA9 and INCENP. (B) Scheme of CPC isolation method using streptavidin-coated magnetic beads and a biotinylated peptide with a 3C protease cleavage site conjugated to an antibody against INCENP. (C) IgG antibody was conjugated with a biotinylated peptide containing a 3C protease cleavage site and then attached to streptavidin-coated beads. The beads were then incubated with 3C protease overnight. The proteins in the antibody-bead binding solution, on the beads, and cleaved by 3C protease were separated by SDS-PAGE and immunoblotted for a secondary antibody against IgG.

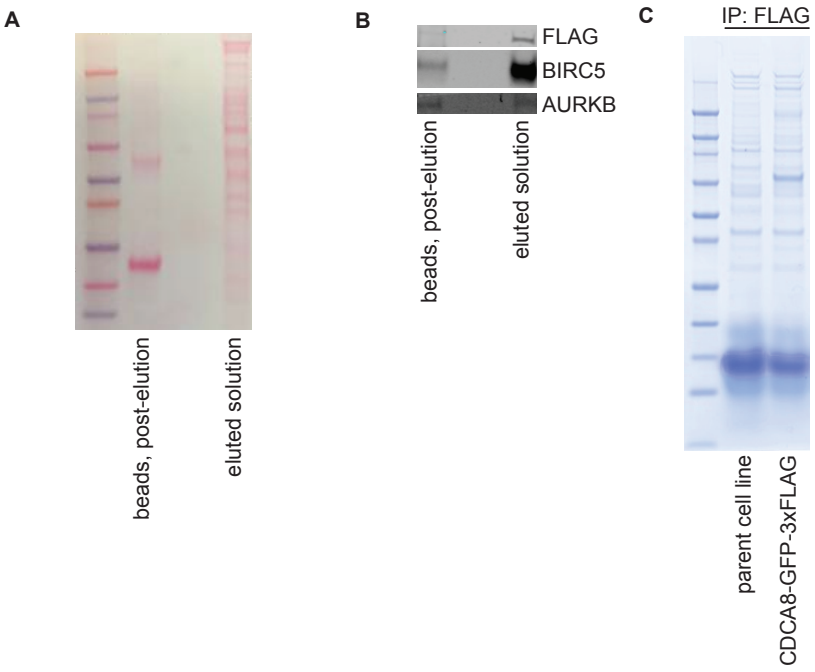

Figure 2.8: (A) Anti-FLAG M2 beads (Sigma) were incubated with lysates of CDCA8-GFP-3xFLAG HeLa cells prepared as described in Chapter 1. The beads were washed and then incubated with free 3xFLAG peptide. The proteins in the bead and eluent solutions were separated by SDS-PAGE, transferred to a nitrocellulose membrane, and stained with Ponceau S. (B) The membrane from (A) was immunoblotted with antibodies against FLAG, BIRC5, and AURKB. (C) The immunoprecipitation described in (A) was repeated using lysates from untagged HeLa cells and the CDCA8-GFP-3xFLAG cell line. The proteins in the eluent solutions were separated by SDS-PAGE and stained with Coomassie Blue.

2.4 Experimental Procedures

Protein Cloning: Proteins were cloned into a pET21a(+) backbone (Novagen) using Gibson assembly as in Chapter 1. Inserts were produced by PCR reactions off of Geneblocks (IDT) using Phusion polymerase master mix (NEB). The backbone was typically cut using restriction enzymes (NEB) and the fragments assembled using the protocol available on the Megason lab wiki. Colonies were expanded and sequenced by Genewiz. Successful clones were transformed into competent Rosetta cells.

Protein Expression and Purification: Proteins were expressed in Terrific Broth following induction by 1 mM IPTG overnight at 16 °C. Bacteria were lysed by sonication in 50 mM sodium phosphate, 200 sodium chloride, 1 mM β-mercaptoethanol, 20 mM imidazole, 1 mM PMSF, 1% Triton X-100, pH 7.7 and centrifuged to pellet any insolubule material. The 6xHis proteins were isolated from the supernatant using HisPur cobalt resin (Thermo) and eluted with the same buffer as the lysis buffer omitting the detergent and adding 300 mM imidazole and 10% glycerol. Proteins were typically purified further on a Sephadex 75 size exclusion column in XB buffer and, after concentration, were stored at -80 °C in 10-20% sucrose. LOV proteins were purified in a darkroom with 1% NP-40 added to the buffers. CDCA8/9 proteins were kept at a low concentration to try to prevent aggregation. The 3C protease expression construct was obtained from Matthew Sonnett and purified as above incubating with glutathione agarose and substituting 10 mM glutathione instead of imidazole in the elution solution. Following concentration, the protease was dialyzed into XB buffer without sucrose overnight at 4 °C.

Pure Microtubule Binding Assays: Microtubules were polymerized by adding purified bovine brain tubulin with small amounts of AlexaFluor 647-labeled bovine brain tubulin and GTP in BRB80 buffer and incubated for 30 minutes at 37 °C, adding taxol at 15 and 30 minutes. Pure proteins were added to the mixture which was sandwiched between untreated coverslips. Images were obtained at the Nikon Imaging Center at Harvard Medical School using a 60X oil Plan Apo 1.49 NA objec-

tive lens (Nikon) on a confocal Nikon Ti motorized inverted microscope equipped with a Yokogawa CSU-X1 spinning disc (Spectral Applied Research Aurora Borealis modification), Perfect Focus, a Prior Proscan II motorized stage, a Spectral Applied Research LMM-5 laser merge module (Ex:Em 488:480/40, 561:620/60, 642:700/75) with AOTF controlled solid state lasers, a Hamamatsu ORCA-AG cooled CCD camera, and driven by Metamorph. Images were prepared for publication using ImageJ.

Extract, HSS, and Pineapple Preparation: *X. laevis* HSS was prepared as described as in Chapter 1. Pineapples were formed as described in Mitchison et al. (Mitchison, Nguyen, Coughlin, & Groen, 2013).

Antibodies and Western Blotting: Antibodies were prepared and blots done as in Chapter 1. Peptide elutable antibodies were prepared by binding antibodies to Protein A-conjugated Affigel (Biorad) and then adding an excess of the peptide to which the antibody was originally raised. The eluted antibody was isolated by concentrating in a 100 kD cutoff filter.

Coupling Barasertib to Solid Support: Barasertib was dissolved in DMSO and added to dichloromethane along with 2 equivalents of 1,1'-carbonyldiimidazole. The solution was stirred at room temperature for 5 hours after which the solvent was removed and diluted in DMSO and added to amino-Affigel (prepared according to Field et al., 1998). The slurry was stirred overnight at room temperature. The beads were then washed with water and S-CSF-XB-phos (see Chapter 1) and incubated with HSS prepared as in Chapter 1. Proteins were eluted off beads by boiling in SDS loading buffer and separated via SDS-PAGE. The lane was submitted to the Taplin Mass Spectrometry facility for analysis.

Attempted CPC Purification Using a Cleavable Peptide: A rabbit random IgG antibody (Jackson) was attached to Protein A-conjugated Affigel. The antibody was reacted with iodoacetic acid-NHS (previously prepared as in Field, Oegema, Zheng, Mitchison, & Walczak, 1998) at a concentration of 50 μg/mL in 200 mM HEPES pH 7.7 buffer twice for 15 minutes each at room temperature. Following washing of the column, the peptide Biotin-Ahx-LEVLFQGPGGSSGGSSC (Genscript), containing a

3C protease cleavage site, was added in the same buffer and the beads incubated in the dark overnight at 4 °C. The beads were washed with the same buffer and eluted into 1 M Tris base pH8 with 0.2 M acetic acid. The eluent was concentrated with a 100 kD cutoff filter. The antibody was then bound to M280 streptavidin beads (Life Technologies) in S-CSF-XB-phos. Following extensive washing, 3C protease was added to the beads and incubated overnight at 4 °C. The eluent was concentrated and separated via SDS-PAGE and immunoblotted with secondary antirabbit secondary antibody (LICOR) along with the beads and concentrated solution from the bead-antibody binding step.

CPC Purification from CDCA8-GFP-3xFLAG HeLa lysates: Lysates of mitotic CDCA8-GFP-3xFLAG HeLa cells were prepared as described in Chapter 1. Anti-FLAG M2 beads (Sigma) were added to the lysate and incubated for 90 minutes at 4 °C. The beads were separated, washed with S-CSF-XB-phos six times, and their protein content analyzed by SDS-PAGE followed by immunoblotting or Coomassie Blue staining followed by mass spectrometry as above for the barasertib purification.

2.5 References

Field, C. M., al-Awar, O., Rosenblatt, J., Wong, M. L., Alberts, B., & Mitchison, T. J. (1996). A purified Drosophila septin complex forms filaments and exhibits GTPase activity. J. Cell. Biol., 133(3), 605-616.

Field, C. M., Groen, A. C., Nguyen, P. A., & Mitchison, T. J. (2015). Spindle-to-cortex communication in cleaving, polyspermic Xenopus eggs. Mol. Biol. Cell, 26(20), 3628-3640.

Field, C. M., Oegema, K., Zheng, Y., Mitchison, T. J., & Walczak, C. E. (1998). Purification of cytoskeletal proteins using peptide antibodies. Methods Enzymol., 298, 525-541.

Halavaty, A. S., & Moffat, K. (2007). N- and C-terminal flanking regions modulate light-induced signal transduction in the LOV2 domain of the blue light sensor phototropin 1 from Avena sativa. Biochemistry, 46(49), 14001-14009.

Harper, S. M., Christie, J. M., & Gardner, K. H. (2004). Disruption of the LOV-J? Helix Interaction Activates Phototropin Kinase Activity. Biochemistry, 43(51), 16184-16192.

Harper, S. M., Neil, L. C., & Gardner, K. H. (2003). Structural basis of a phototropin light switch. Science, 301(5639), 1541-1544.

Jeyaprakash, A. A., Klein, U. R., Lindner, D., Ebert, J., Nigg, E. A., & Conti, E. (2007). Structure of a survivin-borealin-INCENP core complex reveals how chromosomal passengers travel together. Cell, 131(2), 271-285.

Li, L., Fierer, J. O., Rapoport, T. A., & Howarth, M. (2014). Structural analysis and optimization of the covalent association between SpyCatcher and a peptide tag. J. Mol. Biol., 426, 309-317.

Mitchison, T. J., Nguyen, P., Coughlin, M., & Groen, A. C. (2013). Self-organization of stabilized microtubules by both spindle and midzone mechanisms in Xenopus egg cytosol. Mol. Biol. Cell, 24(10), 1559-1573.

Nguyen, P. A., Groen, A. C., Loose, M., Ishihara, K., Wuehr, M., Field, C. M., & Mitchison, T. J. (2014). Spatial organization of cytokinesis signaling reconstituted in a cell-free system. Science, 346(6206), 244-247.

Oegema, K., Wiese, C., Martin, O. C., Milligan, R. A., Iwamatsu, A., Mitchison, T. J., & Zheng, Y. (1999). Characterization of two related Drosophila gamma-tubulin complexes that differ in their ability to nucleate microtubules. J. Cell. Biol., 144(4), 721-733.

Strickland, D., Lin, Y., Wagner, E., Hope, C. M., Zayner, J., Antoniou, C., Sosnick, T. R., Weiss, E. L., & Glotzer, M. (2012). TULIPs: tunable, light-controlled interacting protein tags for cell biology. Nat. Methods, 9, 379-384.

Zakeri, B., Fierer, J. O., Celik, E., Chittock, E. C., Schwarz-Linek, U., Moy, V. T., & Howarth, M. (2012). Peptide tag forming a rapid covalent bond to a protein, through engineering a bacterial adhesin. Proc. Natl. Acad. Sci. U. S. A., 109, E690-E697, SE690/691-SE690/620.

3

Investigation of Potential Chromosomal Passenger Complex-Protein Interactions

This chapter discusses other experiments conducted to explore CPC activity. While nucleophosmin/nucleoplasmin proteins are the most likely candidates for affecting the sedimentation of the CPC, these investigations reveal other proteins with which the CPC may interact. I focus here particularly on myosin II and KIF20AE and how AURKB activity influences these proteins.

3.1 Identification of proteins that may interact with the CPC

I sedimented HSS pretreated with AURKB inhibitor (ZM447439, also referred to as ZM), phosphatase inhibitor (microcystin, MC), or both on sucrose gradients as in Chapter 1. In addition to the CPC structural implications noted in that chapter, I wondered if I could use the sucrose gradients to identify proteins associated with the CPC. In collaboration with Matthew Sonnett (Harvard), I analyzed the fractions from sucrose gradients with quantitative mass spectrometry. We selected four fractions which had either high or low amounts of CPC proteins as determined by immunoblotting: ZM6 and MC11 had low CPC while ZM11 and MC6 had high CPC (Figure 3.1A, red boxes). We wanted to find proteins that followed the same fractionation pattern as the CPC, so we calculated the ratio (ZM11*MC6)/(ZM6*MC11). We counted those proteins enriched at a 1% false discovery rate as hits and obtained 162 candidate proteins (Figure 3.1B). Comfortingly, AURKB was a strong hit. Within this list, prominent classes of proteins included a large number of nuclear pore proteins, several phosphatase subunits, and myosin II subunits (Appendix B). I then selected two of these proteins to investigate in more detail based on important activity in mitosis guided by phosphorylation (myosin II) or previous indications of interaction with the CPC (KIF20AE, based on immunoprecipitations of CPC subunits from *X. laevis* extract done by Timothy Mitchison, personal communication).

3.2 AuroraB kinase activity influences myosin II contractility

Myosin II-induced contractility has already been explored in *X. laevis* actin-intact extract. When drops of mitotic extract are placed in room temperature mineral oil, they visibly initiate gelation-contraction within a few minutes (Field et al., 2011). Cycling the extract into interphase prior to the addition to mineral oil eliminates the contraction. However, the contraction can be restored and dramatically enhanced if phosphatase inhibitors are also added to the extract, unsurprising since myosin II contractility is induced by phosphorylation (Figure 3.2, top). Speckles observed by dark field microscopy

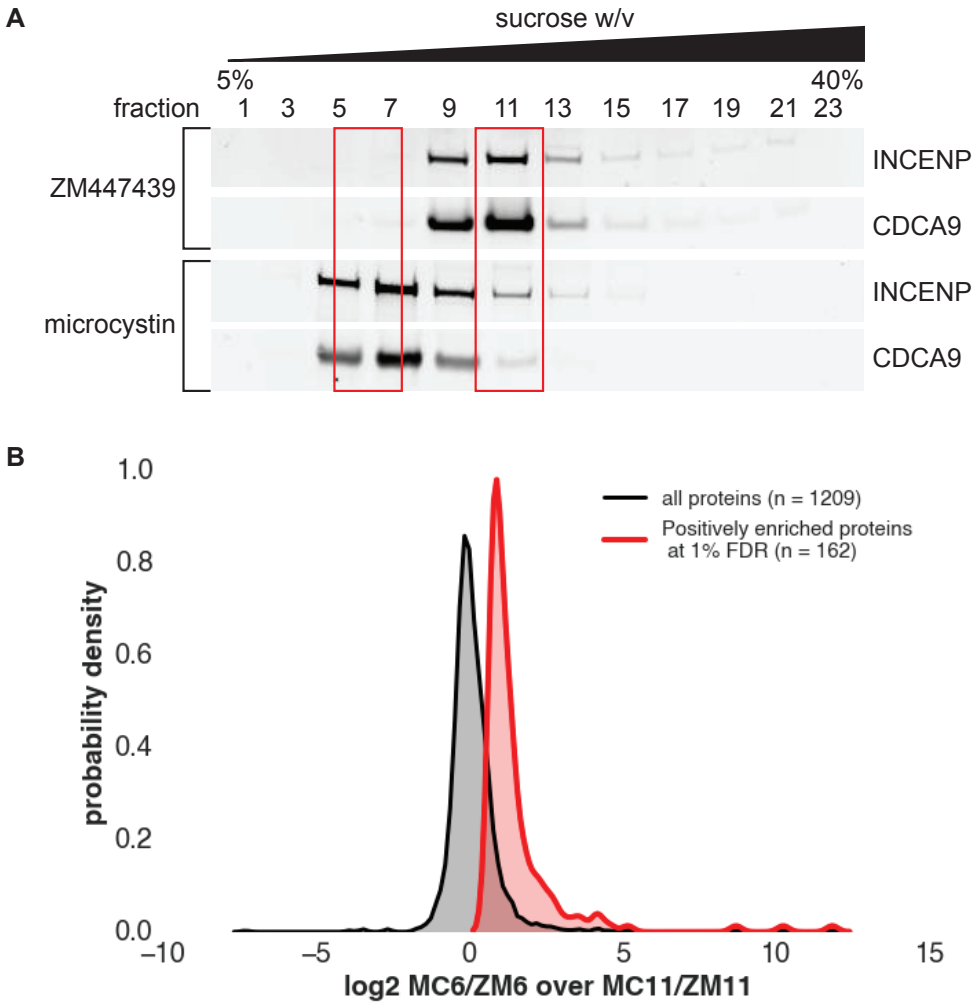

Figure 3.1: **Identification of candidate CPC-interacting proteins from sucrose gradient fractions.** (A) HSS was dosed with either ZM447439 (an AURKB inhibitor) or microcystin (a phosphatase inhibitor) and sedimented on sucrose gradients. Every other fraction was immunoblotted for INCENP or CDCA9. Fractions 6 and 11 from each gradient, highlighted in red boxes, were subjected to quantitative mass spectrometry. (B) 162 proteins were enriched at a 1% false discovery rate (FDR).

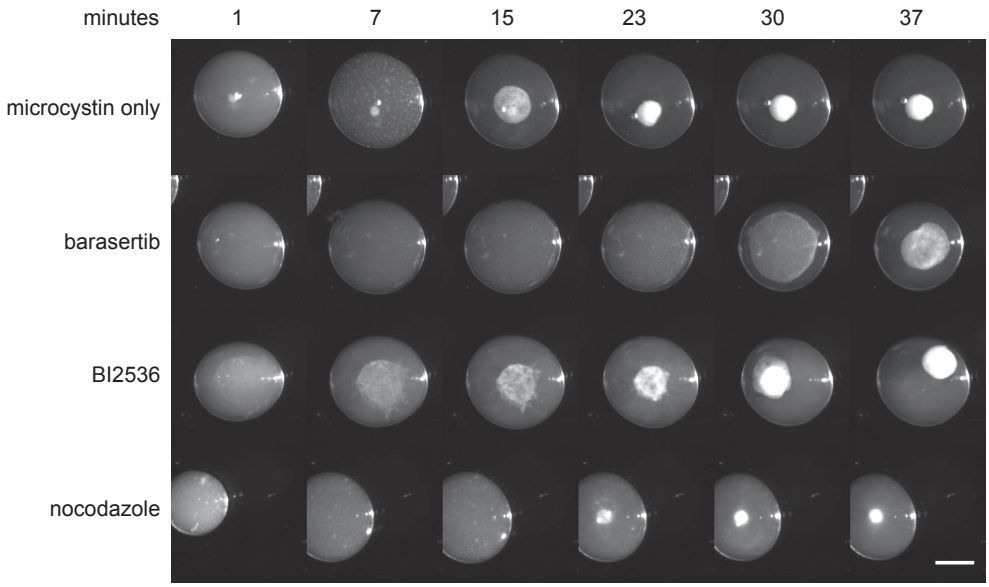

Figure 3.2: **Inhibition of key mitotic kinases influences and inhibits myosin II contractility.** Droplets of interphase *X. laevis* extracts dosed with the phosphatase inhibitor microcystin in room temperature mineral oil, visualized by dark field microscopy over time. Extracts were preincubated with kinase inhibitors against AURKB (barasertib), PLK1 (BI2536), and microtubule polymerization (nocodazole) after the extract was cycled into interphase with calcium prior to microcystin addition. Scale bar represents 500 μm.

formed in the extract, growing larger and then rapidly coalescing to a smaller point in the center.

When I preincubated interphase extract with barasertib to fully inhibit AURKB prior to adding the phosphatase inhibitor, the contraction slowed down (Figure 3.2, second row). This suggests that AURKB phosphorylation of either myosin II or an upstream regulator of myosin is important for myosin II contractility. Such an idea is not unprecedented; AURKB has been reported to phosphorylate both myosin II itself and a kinase immediately upstream of myosin II (Murata-Hori et al., 2000; Dulyaninova & Bresnick, 2004; Vilitkevich et al., 2015). However, myosin II is also regulated by many upstream proteins as well, some of which are regulated by AURKB. For instance, AURKB is required for proper localization and activation of RhoA (Nguyen et al., 2014), the master furrow regulator,

which activates Rho kinase (ROCK) which phosphorylates myosin II. Myosin II also only cosediments primarily with AURKB-inhibited CPC, suggesting that they do not interact directly when AURKB is active (Figure 3.3). It remains unclear which pathway, if any, is the primary route of AURKB-based modulation of myosin II contractility, but myosin II does not seem to be the guiding force behind the change of CPC sedimentation coefficient.

To test if AURKB might be influencing myosin II contractility through upstream regulatory pathways, I inhibited other mitotic kinases to see if their inhibition has similar effects to that of AURKB. I preincubated interphase extract with BI2536, which inhibits PLK1. Although the timing of the contraction was not markedly slowed, the speckles did not form prior to the contraction (Figure 3.2, second from bottom). PLK1 is also an upstream regulator of myosin II; in particular, PLK1 also phosphorylates and activates ROCK (Lowery et al., 2007). It is interesting that PLK1 inhibition has a dramatically different effect on actomyosin contractility than AURKB inhibition, which suggests that PLK1 and AURKB affect myosin II through different regulatory pathways.

Because AURKB and PLK1 both affect actomyosin contractility and interact extensively with microtubules, I wondered if microtubules were necessary for contractility. When microtubule formation was inhibited by the addition of nocodazole, interphase extract droplets treated with phosphatase inhibitor still contracted, albeit slightly more slowly (Figure 3.2, bottom). However, after the first big contraction, there were many subsequent smaller waves of contraction which were not observed in the droplets without nocodazole. I also tested two ROCK inhibitors, Rockout and Y27632, in the same assay, but only Rockout had any appreciable slowing effect. There is some evidence that crosstalk between microtubules and actomyosin networks is mediated by RhoA and ROCK (Birukova et al., 2004), but further work will be required to investigate connections in this system.

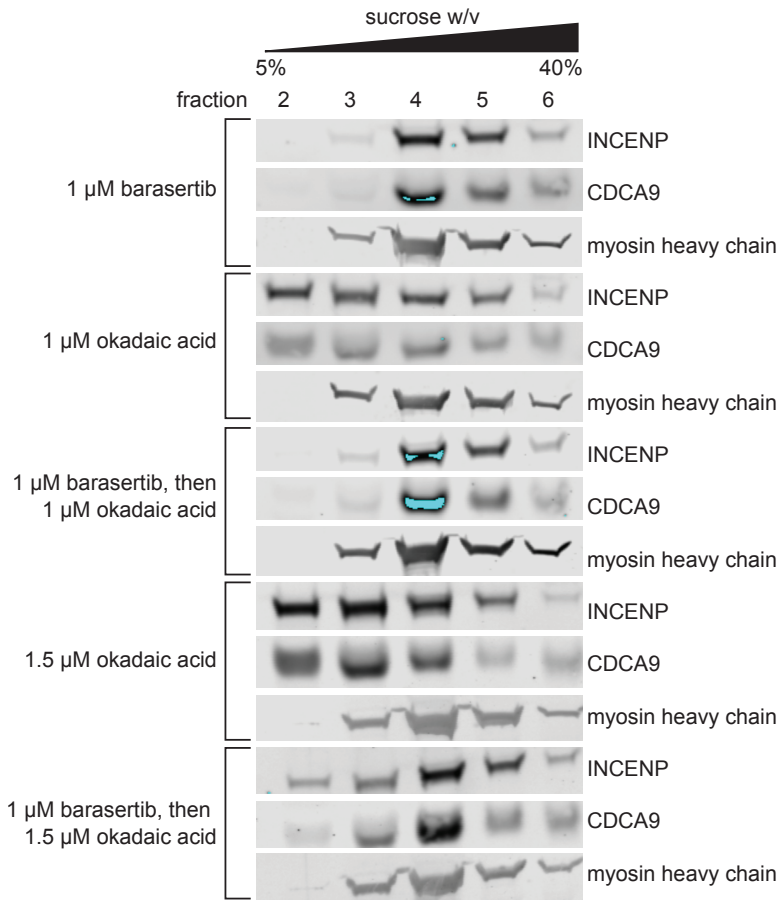

Figure 3.3: **Myosin II heavy chain does not cosediment with the CPC.** Mitotic HSS was dosed with the indicated drugs and sedimented on sucrose gradients as in Chapter 1. Fractions were immunoblotted with antibodies against INCENP, CDCA9, or myosin II heavy chain. Blue indicates oversaturation of the detector.

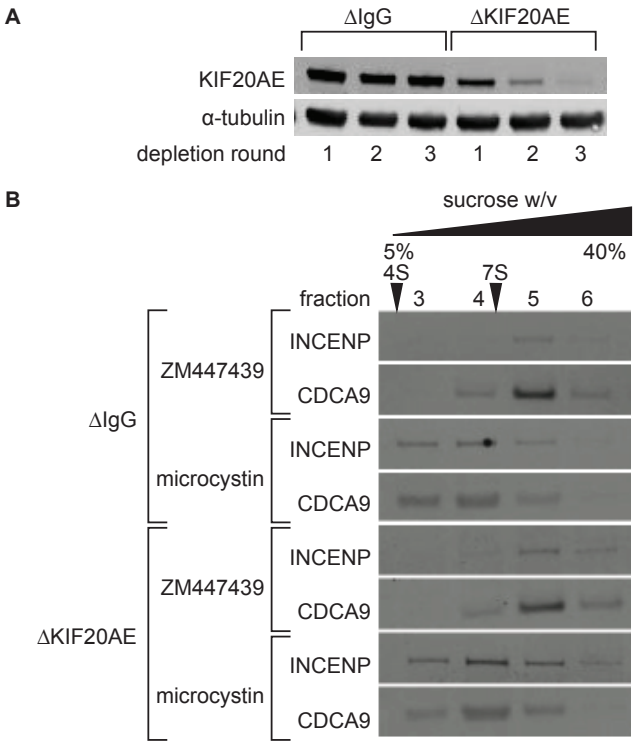

Figure 3.4: **Depletion of KIF20AE from *X. laevis* HSS does not impact CPC sedimentation coefficient.** (A) KIF20AE or random IgG was immunodepleted from mitotic HSS over three rounds. (B) Immunodepleted HSS samples were sedimented on sucrose gradients following drug treatment as in Chapter 1 and the fractions immunoblotted for INCENP and CDCA9 as in Chapter 1.

3.3 KIF20AE may transport the CPC to microtubule plus ends

I also investigated the function of a kinesin, KIF20AE, a maternally loaded paralog of embryonically expressed KIF20A, which was identified as a potential CPC binding partner above. When KIF20AE is depleted from actin-intact egg extracts, the CPC fails to localize to the midzone (Nguyen et al., 2014). I wondered if KIF20AE selectively bound to inactive CPC, causing it to have a higher sedimentation coefficient, and if KIF20AE was responsible for transporting the CPC to the plus ends of microtubules. I depleted KIF20AE from HSS using an antibody raised against a C-terminal portion of KIF20AE (Figure 3.4A). I first used sucrose gradient sedimentation of the depleted HSS to determine how the removal of KIF20AE affected CPC sedimentation coefficients. There was no appreciable difference in sedimentation coefficient between the samples depleted of random IgG and of KIF20AE in the presence of either the AURKB inhibitor ZM447439 or the phosphatase inhibitor microcystin (Figure 3.4B). Therefore, KIF20AE does not influence CPC sedimentation coefficient.

Even though KIF20AE does not seem to affect CPC behavior on sucrose gradients, KIF20AE may be involved in the transportation of the CPC to the plus ends of microtubules. I generated microtubule pineapples (Mitchison, Nguyen, Coughlin, & Groen, 2013) in KIF20AE-depleted extract and imaged with a spinning disk confocal microscope. There was no appreciable morphological difference between pineapples formed in random IgG-depleted extracts versus KIF20AE-depleted extracts, nor was there any significant in CPC localization to the center of pineapples (Figure 3.5A). When I observed the formation of pineapples in normal HSS, the CPC subunit CDCA9 tagged with GFP localized to pineapples before KIF20AE (Figure 3.5B). However, it did not seem to localize to the center of the pineapples until KIF20AE also localized to the center of pineapples. There was very little KIF20AE observed on the microtubule lengths themselves until there was a large amount of protein in the center of the pineapple. Together, these experiments suggest that while KIF20AE is not essential for CPC localization at microtubule midzones, it may interact with the CPC and potentially enhances

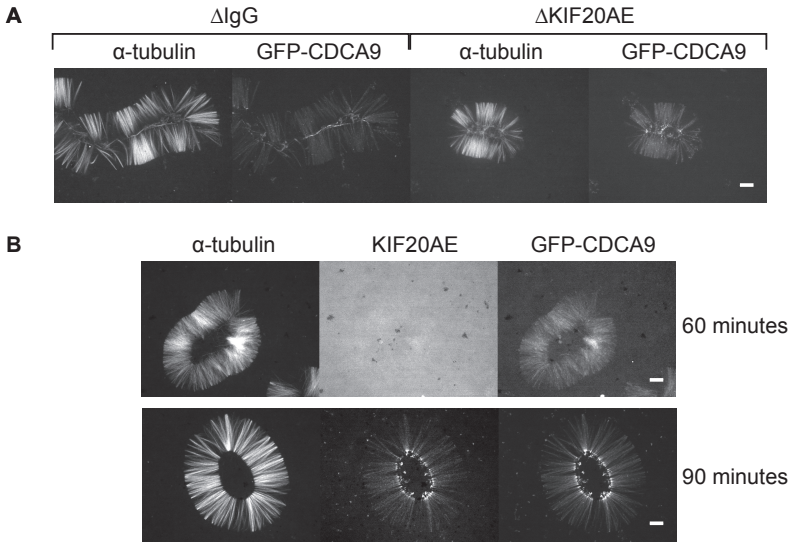

Figure 3.5: **KIF20AE may be partially responsible for CPC transport to microtubule plus ends.** A) Pineapples were formed under coverslips with immunodepleted HSS for 90 minutes and imaged with a 60x spinning disc confocal microscope. Scale bar represents 10 mum. (B) Pineapples were formed and imaged as in Figure 2.4 with mitotic HSS using KIF20AE antibody labeled with Alexafluor-568, α-tubulin and GFP-CDCA9 probes as before. Scale bars represent 10 μm.

its localization.

While neither myosin II or KIF20AE impacted the behavior of the CPC in sucrose gradient sedimentation experiments, both have interesting interactions with the CPC, either as a downstream element regulated by AURKB function in the case of myosin II or as an upstream motor protein helping position the complex. There is substantial opportunity to further investigate the mechanism and significance of these interactions.

3.4 Experimental Methods

Materials: Inhibitors for sucrose gradients (barasertib (Apex Bio), ZM447439 (Tocris), okadaic acid (Enzo), microcystin-LR (Calbiochem), nocodazole (Sigma), BI2536 (Selleck)) were typically used as supplied and stored in solutions in DMSO. Antibody against myosin II heavy chain B was produced by Aaron Straight using a C-terminal peptide according to the method in Field et al. (Field, Oegema, Zheng, Mitchison, & Walczak, 1998); the production of the antibody against KIF20AE was described in Nguyen et al. (Nguyen et al., 2014).

Sucrose Gradient Sedimentation, Immunoblotting, Mass Spectrometry, and Pineapple Formation and Imaging: Sucrose gradient sedimentation and immunoblotting were performed as described in Chapter 1. For mass spectrometry of sucrose gradients, fractions were half the size of those in Chapter 1. Mass spectrometry samples were prepared as in Chapter 1, omitting the immunoprecipitation step. HSS and pineapples were formed as in Chapter 2.

Contraction Assays: X. laevis crude extract was prepared as described in Chapter 1 and cycled into interphase by adding calcium and incubating at room temperature for 10 minutes. Inhibitors were added and the extract incubated on ice for an additional 10 minutes prior to adding 1 µL droplets to room temperature mineral oil. Drops were side-illuminated and imaged with a dissecting scope and Metamorph. Images were processed using ImageJ.

KIF20AE Depletion: Protein A-coated Dynabeads (Life Technologies) were charged with antibody against KIF20AE as in Chapter 1. The beads were split into three aliquots. Each aliquot was added to *X. laevis* HSS and incubated for 45 minutes for a total of three rounds. Small portions of the depleted HSS were reserved for immunoblotting; the rest was subjected to pineapple formation or sucrose gradient sedimentation.

3.5 References

Birukova, A. A., Smurova, K., Birukov, K. G., Usatyuk, P., Liu, F., Kaibuchi, K., Ricks-Cord, A., Natarajan, V., Alieva, I., Garcia, J. G. N., & Verin, A. D. (2004). Microtubule disassembly induces cytoskeletal remodeling and lung vascular barrier dysfunction: Role of Rho-dependent mechanisms. J. Cell. Physiol., 201(1), 55-70.

Dulyaninova, N. G., & Bresnick, A. R. (2004). The long myosin light chain kinase is differentially phosphorylated during interphase and mitosis. Exp. Cell Res., 299(2), 303-314.

Field, C. M., Oegema, K., Zheng, Y., Mitchison, T. J., & Walczak, C. E. (1998). Purification of cytoskeletal proteins using peptide antibodies. Methods Enzymol., 298, 525-541.

Field, C. M., Wuhr, M., Anderson, G. A., Kueh, H. Y., Strickland, D., & Mitchison, T. J. (2011). Actin behavior in bulk cytoplasm is cell cycle regulated in early vertebrate embryos. J. Cell. Sci., 124(12), 2086-2095.

Lowery, D. M., Clauser, K. R., Hjerrild, M., Lim, D., Alexander, J., Kishi, K., Ong, S.-E., Gammeltoft, S., Carr, S. A., & Yaffe, M. B. (2007). Proteomic screen defines the Polo-box domain interactome and identifies Rock2 as a Plk1 substrate. EMBO J., 26(9), 2262-2273.

Mitchison, T. J., Nguyen, P., Coughlin, M., & Groen, A. C. (2013). Self-organization of stabilized microtubules by both spindle and midzone mechanisms in Xenopus egg cytosol. Mol. Biol. Cell, 24(10), 1559-1573.

Murata-Hori, M., Fumoto, K., Fukuta, Y., Iwasaki, T., Kikuchi, A., Tatsuka, M., & Hosoya, H. (2000). Myosin II regulatory light chain as a novel substrate for AIM-1, an Aurora/Ipl1p-related kinase from rat. J. Biochem., 128(6), 903-907.

Nguyen, P. A., Groen, A. C., Loose, M., Ishihara, K., Wuehr, M., Field, C. M., & Mitchison, T. J. (2014). Spatial organization of cytokinesis signaling reconstituted in a cell-free system. Science, 346(6206), 244-247.

Vilitkevich, E. L., Khapchaev, A. Y., Kudryashov, D. S., Nikashin, A. V., Schavocky, J. P., Lukas, T. J., Watterson, D. M., & Shirinsky, V. P. (2015). Phosphorylation regulates interaction of 210-kDa myosin light chain kinase N-terminal domain with actin cytoskeleton. Biochemistry, 80(10), 1288-1297.

4

Conclusion

In this work, I have presented my efforts to understand how structure influences CPC behavior. The most notable discovery is the interaction between inactive CPC and the nucleophosmin/nucleoplasmin family of proteins. However, there is opportunity for future insights from other tools I developed and from preliminary investigations into other proteins that may interact with the CPC.

4.1 Potential experimental directions and ramifications of the inactive CPC-NPM interaction

NPM proteins only bind inactive CPC. As pentamers/decamers, they are large enough to potentially influence CPC sedimentation. To test this hypothesis, NPM family members would need to be removed from HSS and the depleted HSS subjected to centrifugation on sucrose gradients. However, NPM2 is highly abundant in cells, and there is also substantial NPM1 and NPM3. Depletion of all of these proteins would require three separate antibodies raised ideally against the whole protein, and even then successfully removing all of the protein will be challenging. Antibodies used to deplete NPM proteins might also deplete the CPC in the basal or AURKB-inhibited state, preventing comparison of the CPC sedimentation coefficients in inhibited and active AURKB forms in NPM-depleted extracts. Creative solutions will need to be developed to test whether NPM binding and unbinding is the causal agent of the observed shift of CPC sedimentation upon phosphorylation.

Likewise, testing whether NPM binding influences CPC diffusion velocity in live HeLa cells will be challenging. NPM proteins are similarly abundant and reportedly have a wide range of activities, including chaperoning histones. Knocking out NPMs using a CRISPR/Cas9 strategy would likely prevent cell growth, although there may be opportunities to deplete NPMs by targeting for degradation with small molecules or other non-genetic methods of depletion. The CPC also cannot be easily removed to observe its effect on NPM behavior; as a critical complex for mitotic regulation, removing or inhibiting the complex and its kinase will halt cell growth and propagation. As with HSS, different strategies must be developed to overcome these technical hurdles.

The potential for NPMs to chaperone the CPC is intriguing. The single alpha helix recently discovered in the middle of INCENP is likely prone to destabilization and/or proteolysis; NPMs may shield this section until the complex is activated. Alternatively, NPMs might directly inhibit AURKB activity. NPMs may also indirectly prevent AURKB activity by blocking the oligomerization of the

CPC required to activate AURKB until the proper point in mitosis. Preventing unwanted protein aggregation is a common function for chaperone proteins.

What triggers the dissociation of NPM from the CPC is not clear. NPMs are only associated with the CPC when AURKB is not active. For AURKB to be activated, it must be phosphorylated by another molecule of AURKB. However, if NPMs inhibit AURKB activity and all CPC molecules are bound to NPMs in the basal state of cells and extracts, it is unclear how the first NPM-CPC interaction would be broken to initiate the positive feedback loop between CPC units. The dissociation of NPMs may involve phosphorylation or other posttranslational modifications of NPMs or CPC subunits by other mitotic kinases present in the midzone between microtubule asters that are not inhibited by NPMs. Alternatively, NPM dissociation could be triggered by the proximity of other CPC units; clustering at the plus ends of microtubules or on beads is known to promote AURKB activity. Proximity sensing could involve structural recognition of other CPC and/or NPM subunits or other proteins associated with the CPC.

Understanding the causes and effects of the interaction between the CPC and NPMs will potentially profoundly effect how we view CPC behavior and its effect on mitosis. Future work will likely start with understanding the structural basis of the CPC-NPM interaction but will probably expand to include the associative and dissociate mechanisms as well as broader effects on mitosis.

4.2 Potential future directions for understanding CPC behavior

I also attempted and described here a number of other experiments to advance understanding of the CPC. Based on my work, there are a number of outstanding questions, including but not limited to:

- Can AURKB and/or the CPC initiate cleavage furrow formation when targeted to the cortex independent of RhoA?
- Does AURKB phosphorylate myosin II or the kinase directly upstream of myosin II, or does AURKB only influence contractility through RhoA?

- Why do organisms with large eggs like *X. laevis* and zebrafish have separate maternally loaded and embryonically expressed paralogs of CDCA8/9 and BIRC5 but not of INCENP and AURKB?
- What is the function of the globular and helical subunits of CDCA8/9?
- Can CDCA8/9 localize to microtubules and microtubule plus ends without incorporation into the CPC, and if so how does this localization occur and what is the purpose of the microtubule-binding domain in INCENP?
- Does KIF20AE transport the CPC to microtubule plus ends, and if so what subunits or subunit domains are critical for this interaction?
- How extended or compact is the CPC, and in particular the single alpha helix region of INCENP?

Although the tools and strategies developed here were insufficient to answer these questions, they may provide a useful starting point for others interested in exploring CPC structure and behavior. Of these, isolating the CPC from biological sources using an antibody against CPC subunits conjugated with a protease-cleavable peptide and understanding subunit behavior by using purified proteins to identify subunit- and subunit domain- interacting proteins and to image subunit localization in *X. laevis* extract are likely the most tractable routes.

A

Supplementary Tables and Figures for Chapter 1

Supplementary tables of mass spectrometry data and supplementary figures for Chapter 1. Only first pages of tables are shown; full tables are contained as supplemental material to the dissertation available online or by emailing a request to timothy_mitchison@hms.harvard.edu.

Figure A.1 *(following page)*: **Supplementary Table 1 for Chapter 1.** Immunoprecipitation-mass spectrometry results from HSS treated with barasertib (AURKB inhibitor) or okadaic acid (phosphatase inhibitor) using antibodies against INCENP and CDCA9. Results were normalized to immunoprecipitations using random IgG from the same HSS samples and to the amount of target protein (INCENP or CDCA9) in each sample.

Figure A.1: (continued)

Gene Symbol (Uniprot)	Gene Description	Number of Peptides	Normalized Count Ratio, BA-treated/OA-treated, INCENP IP	Normalized Count Ratio, BA-treated/OA-treated, CDCA9 IP
PARD3	Partitioning defective 3 homolog	5	2.474994756	8.697175544
NPM3	Nucleoplasmin-3	2	2.405681316	6.661699932
GTSF1	Gametocyte-specific factor 1	1	2.236301427	0.775935678
DNAJB7	DnaJ homolog subfamily B member 7	8	2.162327788	0.965817275
PRPF3	U4/U6 small nuclear ribonucleoprotein Prp3	2	2.017025245	1.267400889
CDCA8	Borealin	40	2.004798004	1
CHMP2B	Charged multivesicular body protein 2b	4	1.931166003	0.788212734
ARL3	ADP-ribosylation factor-like protein 3	6	1.866088371	0.656794161
MAEL	Protein maelstrom homolog	2	1.765452049	0.503087001
TARDBP	TAR DNA-binding protein 43	4	1.60818247	0.777034032
NPM2	Nucleoplasmin-2	20	1.547715608	4.057774669
ATP1B3	Sodium/potassium-transporting ATPase subunit beta-3	3	1.533274526	0.272057006
DNAJC7	DnaJ homolog subfamily C member 7	22	1.473377773	0.655109447
PKP3	Plakophilin-3	1	1.387849429	0.818220868
DNAJA4	DnaJ homolog subfamily A member 4	8	1.35884855	0.728634341
PLRG1	Pleiotropic regulator 1	4	1.317577176	0.901486749
AURKB	Aurora kinase B	36	1.230605708	0.933060413
DNAJA2	DnaJ homolog subfamily A member 2	20	1.190518707	0.653949275
DNAJA1	DnaJ (Hsp40) homolog, subfamily A, member 1, isoform CRA_b	6	1.187330823	0.752044041
RAE1	mRNA export factor	7	1.14195376	0.842161824
ESD	S-formylglutathione hydrolase	13	1.133493701	0.788114631
CBX3	Chromobox protein homolog 3	5	1.109155105	2.580111271
INCENP	Inner centromere protein	60	1	0.584650302
BTRC	F-box/WD repeat-containing protein 1A (Fragment)	4	0.980907675	0.265015983
CEP55	Centrosomal protein of 55 kDa (Fragment)	1	0.92407618	1.12812844
ARFGAP3	ADP-ribosylation factor GTPase-activating protein 3	2	0.906643634	1.486159811
RBM25	RNA-binding protein 25	6	0.90351428	0.569444584
NPM1	Nucleophosmin	10	0.872043551	2.381989902
SNX33	Sorting nexin-33	2	0.862896614	0.799100869
SNRNP70	U1 small nuclear ribonucleoprotein 70 kDa	4	0.839554792	0.688489078
HSF2	Heat shock factor protein 2	1	0.838279524	1.078562325
NONO	Non-POU domain-containing octamer-binding protein	6	0.800317044	0.945136082
BIRC5	Baculoviral IAP repeat-containing protein 5	14	0.774594837	0.437560831
EIF4G2	Eukaryotic translation initiation factor 4 gamma 2 (Fragment)	8	0.766681831	0.607428096
MAD1L1	Mitotic spindle assembly checkpoint protein MAD1	8	0.763562022	0.681403592
ZNF638	Zinc finger protein 638	3	0.755275916	1.012439318
DYNC1LI1	Cytoplasmic dynein 1 light intermediate chain 1	6	0.754386917	1.027324168
CHMP4B	Charged multivesicular body protein 4b	6	0.745532342	0.558651515
MYEF2	Myelin expression factor 2	7	0.742540886	0.590210949
NAP1L1	Nucleosome assembly protein 1-like 1	23	0.739643499	1.701587174
RAB21	Ras-related protein Rab-21	1	0.735018567	0.165934504
CENPE	Centromere-associated protein E	9	0.72955041	0.726595597
DDX3X	ATP-dependent RNA helicase DDX3X	11	0.716667807	1.0732268
UPK3A	Uroplakin-3a	1	0.715480475	0.12257524
ARF1	ADP-ribosylation factor 1	16	0.714099691	0.529090919
HGS	Hepatocyte growth factor-regulated tyrosine kinase substrate	14	0.712045395	0.092230999
TTC27	Tetratricopeptide repeat protein 27	3	0.703724741	2.907987685
EDF1	Endothelial differentiation-related factor 1	2	0.703637115	0.79397556
HIC2	Hypermethylated in cancer 2 protein	15	0.703354024	0.397733063
SCAMP2	Secretory carrier-associated membrane protein 2	2	0.702244067	0.206917974
KIF2C	Kinesin-like protein KIF2C	12	0.687624914	2.516504904
EEA1	Early endosome antigen 1	32	0.681226715	0.142642718
CNNM4	Metal transporter CNNM4	1	0.67118955	0.173161353
SMAP2	Stromal membrane-associated protein 2	2	0.666155411	0.6856548
ARF4	ADP-ribosylation factor 4	3	0.661052462	0.674927588
UFD1L	Ubiquitin fusion degradation protein 1 homolog	6	0.643807214	0.872103887
TIAL1	Nucleolysin TIAR	2	0.638241788	0.679770703
SFPQ	Splicing factor, proline- and glutamine-rich	3	0.632297607	0.878493428
UPF1	Regulator of nonsense transcripts 1	4	0.63087203	0.773414782
ATP6V1F	V-type proton ATPase subunit F	1	0.628214539	0.493906605
NUP98	Nuclear pore complex protein Nup98-Nup96	7	0.619246315	0.892037381
DIAPH3	Protein diaphanous homolog 3	3	0.618831274	0.545725894
CXADR	Coxsackievirus and adenovirus receptor	3	0.617120402	0.119808578
EPCAM	Epithelial cell adhesion molecule	6	0.616524904	0.11947848
RALB	Ras-related protein Ral-B	2	0.608504574	0.16162688
RAB2A	Ras-related protein Rab-2A	3	0.602730402	0.491224493
PRPF40A	Pre-mRNA-processing factor 40 homolog A	8	0.594560019	0.500482305
LNPEP	Leucyl-cystinyl aminopeptidase	10	0.593955864	0.105436838
FBL	FBL protein (Fragment)	2	0.593526164	0.430758073

Figure A.2 *(following page)*: **Supplementary Table 2 for Chapter 1.** Immunoprecipitation-mass spectrometry results from *X. laevis* crude mitotic extract treated with ZM447439 (AURKB inhibitor) or no drug using antibodies against INCENP and CDCA9. Results were normalized to immunoprecipitations using random IgG from the same HSS samples and to the amount of target protein (INCENP or CDCA9) in each sample. This data was collected and prepared by Timothy Mitchison.

Figure A.2: (continued)

Gene name	Protein	Peptides	Counts: AURKB	Counts: AURKB IP + ZM	ZM/control
nap1l1	Nucleosome assembly protein 1-like 1	2	115.564	948.311	8.2
NPM2	Nucleoplasmin-2	5	214.96	1299.26	6.0
CBX3	Chromobox protein homolog 3	2	125.296	695.632	5.6
NPM2	Nucleoplasmin-2	5	224.359	1239.91	5.5
nap1l1	Nucleosome assembly protein 1-like 1	6	471.83	2253.59	4.8
		1	81.1258	316.01	3.9
PPP1R12C	Protein phosphatase 1 regulatory subunit 1	1	42.3259	103.687	2.4
RANBP3	Ran-binding protein 3	2	138.458	338.968	2.4
MTDH	Protein LYRIC	1	22.3882	45.5446	2.0
CEP120	Centrosomal protein of 120 kDa	2	56.4194	112.17	2.0
POLDIP2	Polymerase delta-interacting protein 2	1	36.9105	66.8187	1.8
INHBA	Inhibin beta A chain	1	79.7694	139.241	1.7
ADAP2	Arf-GAP with dual PH domain-containing pr	1	87.292	141.531	1.6
IPO7	Importin-7	1	12.223	18.9399	1.5
AKR1B1	Aldose reductase	1	38.6068	59.6196	1.5
ASCC2	Activating signal cointegrator 1 complex sul	1	34.908	53.7572	1.5
		1	53.8205	82.1642	1.5
MDH2	Malate dehydrogenase, mitochondrial	1	82.732	120.247	1.5
glod5	Glyoxalase domain-containing protein 5	1	34.1418	49.2411	1.4
tf	Serotransferrin	1	77.7965	111.664	1.4
PGK1	Phosphoglycerate kinase 1	1	60.1419	84.4427	1.4
ACAA1	3-ketoacyl-CoA thiolase, peroxisomal	1	22.2334	31.1998	1.4
NDUFS8	NADH dehydrogenase [ubiquinone] iron-sul	1	40.5874	56.8778	1.4
MRPL12	39S ribosomal protein L12, mitochondrial	2	142.784	200.083	1.4
STUB1	E3 ubiquitin-protein ligase CHIP	2	125.619	175.876	1.4
		1	96.2978	134.065	1.4
TIMM13	Mitochondrial import inner membrane tran	1	55.4068	77.1315	1.4
CLPP	Putative ATP-dependent Clp protease prote	2	78.0376	107.076	1.4
PCK2	Phosphoenolpyruvate carboxykinase [GTP],	1	81.7631	112.128	1.4
tpx2	Targeting protein for Xklp2	2	43.6917	59.1066	1.4
ECHS1	Enoyl-CoA hydratase, mitochondrial	1	65.6946	88.7202	1.4
GAPDH	Glyceraldehyde-3-phosphate dehydrogenas	4	352.161	474.254	1.3
COX6A1	Cytochrome c oxidase subunit 6A1, mitocho	1	48.3661	64.9388	1.3
SLC25A11	Mitochondrial 2-oxoglutarate/malate carrie	1	42.4696	57.0078	1.3
GRPEL1	GrpE protein homolog 1, mitochondrial	1	77.0579	103.233	1.3
DOCK6	Dedicator of cytokinesis protein 6	1	70.3321	94.0245	1.3
AGK	Acylglycerol kinase, mitochondrial	1	36.9498	49.3947	1.3
		1	29.4893	39.4082	1.3
PLK1	Serine/threonine-protein kinase PLK1	2	58.6455	78.1422	1.3
		1	87.5544	116.534	1.3
mrpl45	39S ribosomal protein L45, mitochondrial	1	56.9995	75.7735	1.3
GCSH	Glycine cleavage system H protein, mitocho	1	90.8345	120.699	1.3
PGK1	Phosphoglycerate kinase 1	6	310.543	410.48	1.3
ACADL	Long-chain specific acyl-CoA dehydrogenase	9	446.955	590.034	1.3
IDH3B	Isocitrate dehydrogenase [NAD] subunit bet	2	108.823	143.546	1.3
ACADM	Medium-chain specific acyl-CoA dehydroge	1	45.4427	59.9014	1.3
CYP27C1	Cytochrome P450 27C1	1	33.1511	43.6617	1.3
CHCHD6	Coiled-coil-helix-coiled-coil-helix domain-co	2	138.831	182.384	1.3
		2	105.224	138.148	1.3

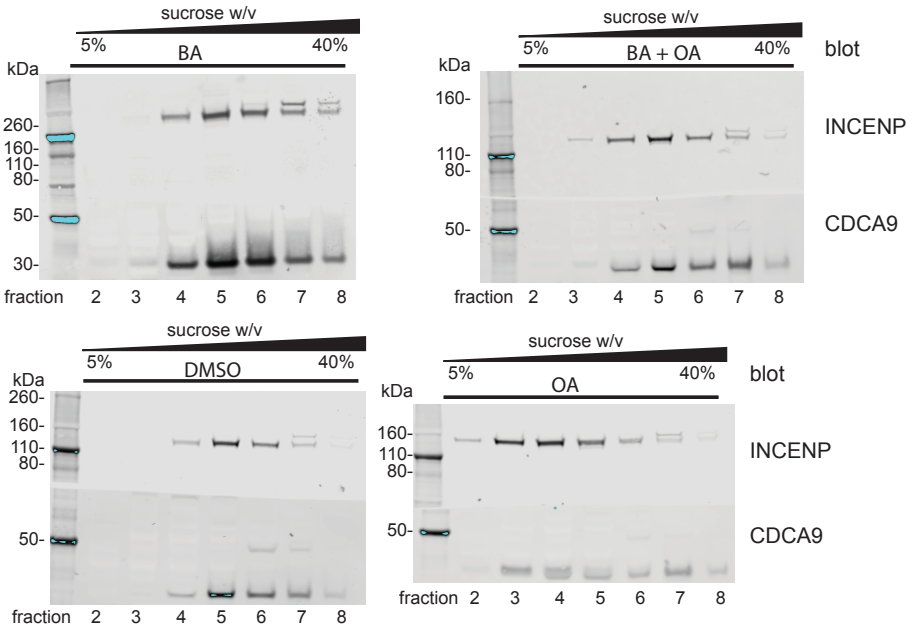

Figure A.3: **Supplementary Figure 1 for Chapter 1.** Full blot of sucrose gradients in Figure 1D.

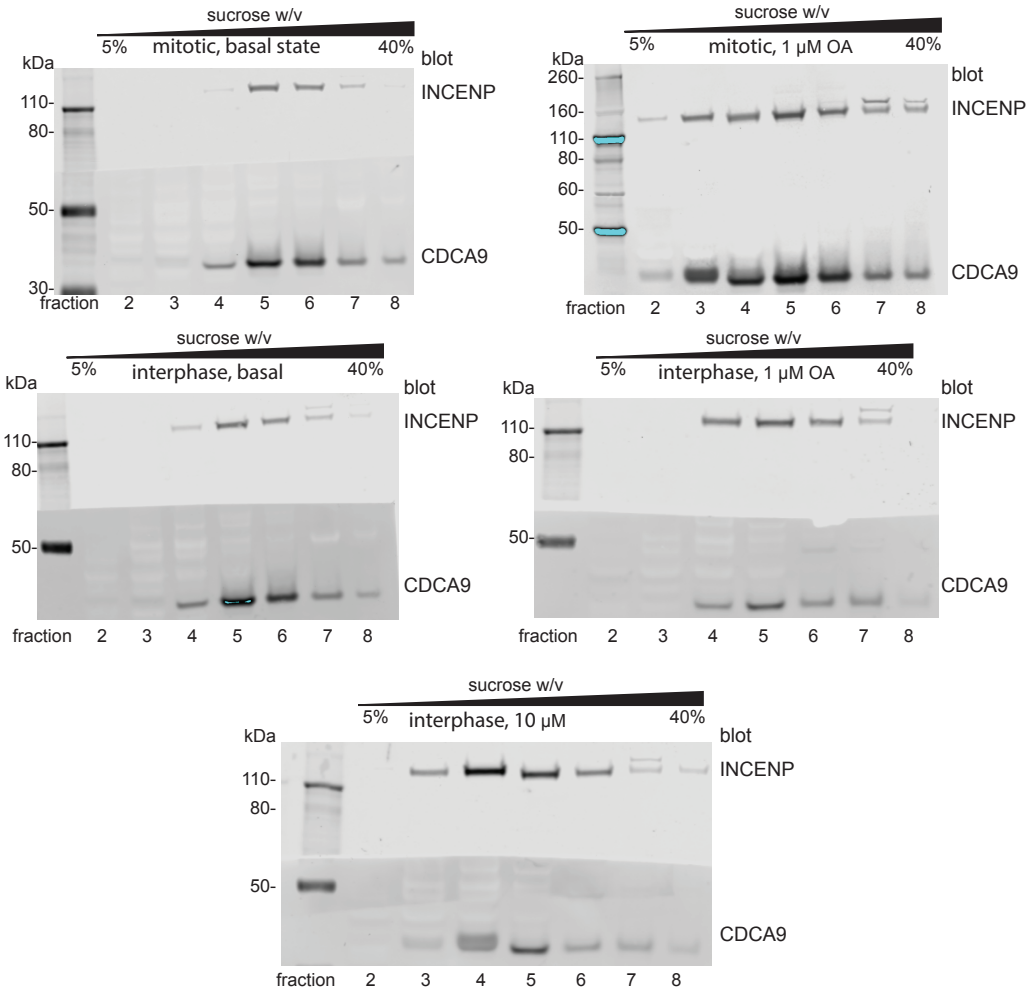

Figure A.4: **Supplementary Figure 2 for Chapter 1.** Full blot of sucrose gradients in Figure 2B.

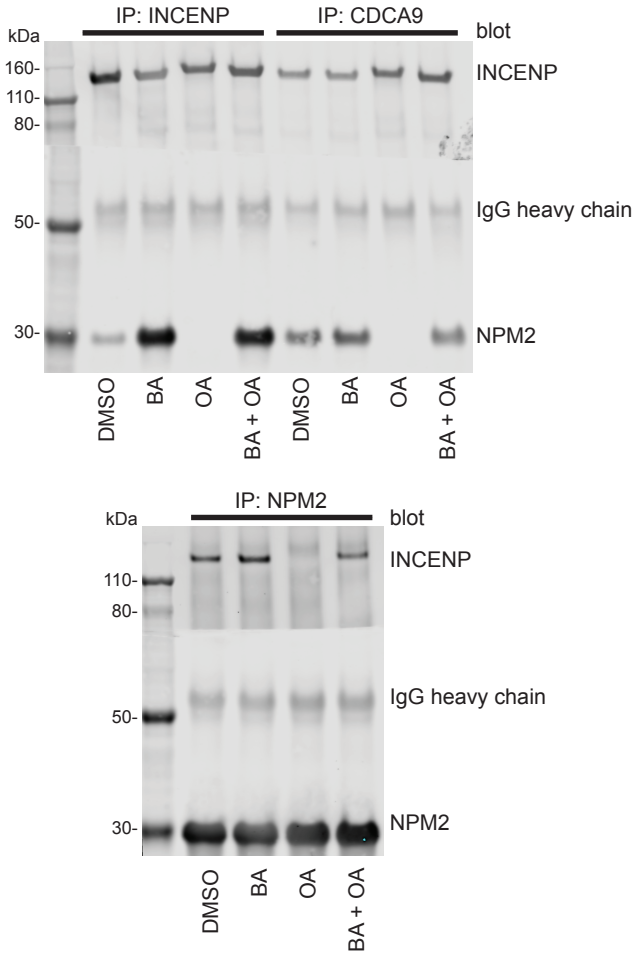

Figure A.5: **Supplementary Figure 3 for Chapter 1.** Full blot of immunoprecipitation-western blotting experiment in Figure 5B.

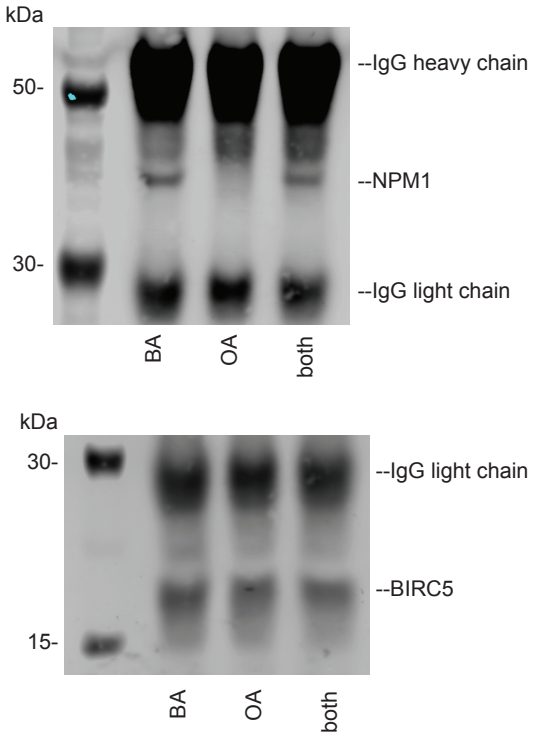

Figure A.6: **Supplementary Figure 4 for Chapter 1.** Full blot of immunoprecipitation-western blotting experiment in Figure 5C.

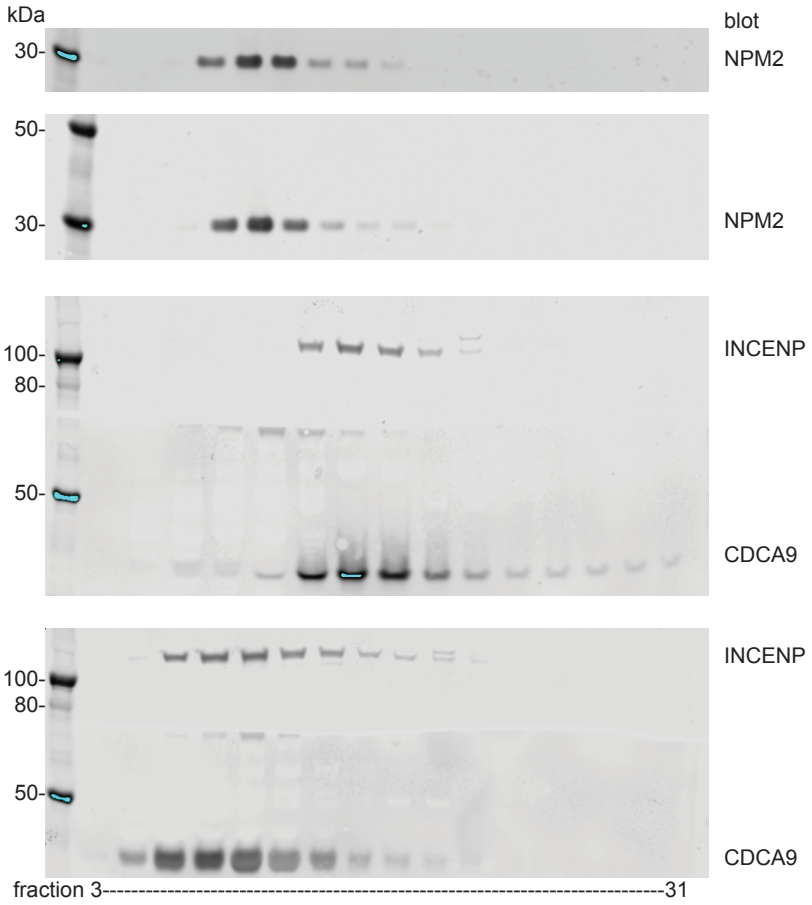

Figure A.7: **Supplementary Figure 5 for Chapter 1.** Full blot of sucrose gradients in Figure 5D.

B

Supplementary Table for Chapter 3

Supplementary tables of mass spectrometry data for Chapter 3. Only first pages of tables are shown; full tables are contained as supplemental material to the dissertation available online or by emailing a request to timothy_mitchision@hms.harvard.edu.

Figure B.1 *(following page)*: **Supplementary Table 1 for Chapter 3.** Mass spectrometry results of sucrose gradient fractions. HSS was treated with ZM447439 (AURKB inhibitor) or microcystin (phosphatase inhibitor) and sedimented on 5-40% sucrose gradients. Individual fractions were subjected to quantitative mass spectrometry and normalized by total protein count. The list of hits was generated by calculating the value of (ZM11*MC6)/(ZM6*MC11) for each protein. 162 proteins were identified as hits at a 1% false discovery rate.

Figure B.1: (continued)

Gene Symbol	Description	Number of peptides	(ZM6*MC11)/(ZM11*MC6)	ZM_6	ZM_11	MC_6	MC_11
Aurora kinase B	AURKB	1	3639.426399	0.10380596	77.8969622	57.5615426	11.8685519
Casein kinase II subunit alpha	CSNK2A1	1	1200.421163	0.00333129	81.0068146	4.46558465	90.4593624
Myosin-9	MYH9	1	587.0576386	0.49664875	259.287567	100.10512	89.0241609
Condensin complex subunit 2	NCAPH	2	413.4909239	0.0150617	199.23657	6.14506222	196.587264
NUMA1 variant protein (Fragment)	NUMA1 VAR	1	36.11309225	0.53394982	10.836538	6.21925714	3.49513494
Myosin-9	MYH9	1	27.36317986	0.69450494	20.0921999	10.6167301	11.2247419
Myosin regulatory light polypeptide 9	MYL9	2	24.14667491	2.27329948	46.6609677	18.7888608	15.9712977
FLJ00279 protein (Fragment)	FLJ00279	9	22.59065443	28.949648	794.132836	269.030069	326.679497
Myosin-9	MYH9	20	22.25593948	88.7415298	2050.31057	777.260335	806.888103
Microtubule-associated protein 4	MAP4	2	20.31190844	27.335457	1.08435057	24.8382432	0.04850802
Serine/threonine-protein phosphatase 2A 55 kDa regulat	PPP2R2D	1	17.08326318	0.43224546	15.6917418	6.09688827	12.9562142
FLJ00279 protein (Fragment)	FLJ00279	12	16.51892472	68.5020315	1200.62824	455.053959	482.821084
Myosin-9	MYH9	39	16.35023727	226.278959	4409.15826	1606.88962	1915.02083
Myosin light polypeptide 6	MYL6	4	12.91506693	8.15074874	267.667257	64.7028914	164.522299
Nucleoporin p54	NUP54	2	12.07632976	38.7218452	110.692591	108.185333	25.6091952
Nucleoporin p58/p45	NUPL1	1	10.5021969	13.9007354	40.4465358	37.314066	10.3379868
Serine/threonine-protein phosphatase 2A 55 kDa regulat	PPP2R2A	3	9.030509828	13.3638365	129.194649	77.5885443	83.061297
Transcriptional regulator ATRX	ATRX	1	7.949503944	3.64647733	3.24914604	5.33208283	0.59765777
		1	7.380882755	14.3429032	2.69954921	12.6738634	0.32318775
Vacuolar protein sorting-associated protein 13C	VPS13C	1	6.932410461	0.4830554	62.0185238	3.22735586	59.7705245
Calcium/calmodulin-dependent protein kinase type II sut	CAMK2D	1	6.651176797	0.58960192	23.358317	3.4623709	20.623281
Tubulin-specific chaperone A	TBCA	1	6.643625587	15.5207631	2.05234815	11.7389371	0.23364774
Transportin-3	TNPO3	1	6.330223101	2.89743771	6.22972316	5.45329131	1.85222747
Nuclear pore glycoprotein p62	NUP62	4	5.657123804	90.9352813	222.448038	196.400277	84.9263732
E3 ubiquitin-protein ligase HUWE1 (Fragment)	HUWE1	1	5.643205893	0.27122264	48.4763351	1.35569587	42.9378422
Eukaryotic translation initiation factor 4E transporter	EIF4ENIF1	1	5.454224385	5.46241436	2.20927197	7.40641099	0.54921115
Nuclear pore complex protein Nup98-Nup96	NUP98	2	5.356681974	45.1502705	58.7802398	89.2744197	21.6971239
Serine/arginine repetitive matrix protein 2 (Fragment)	SRRM2	1	5.244622535	0.97508856	40.2714018	3.88331278	30.5802352
Fructose-bisphosphate aldolase A	ALDOA	4	5.171283093	11.0313484	798.226828	53.1320005	743.456522
Protein transport protein Sec31B	SEC31B	1	5.145638814	0.42115191	17.3445547	2.51602351	20.1372324
Chromodomain-helicase-DNA-binding protein 4	CHD4	1	4.707032985	0.48223366	28.1982295	2.07251372	25.7462804
Nuclear pore complex protein Nup88	NUP88	2	4.656762294	22.4876233	73.9796103	58.9497963	41.6453697
Cell division cycle 5-like protein	CDC5L	1	4.634929956	0.39136558	33.2269855	2.57655742	47.1959758
Oxysterol-binding protein 1	OSBP	2	4.632386058	7.02691668	120.298596	21.0407645	77.7593325
Serine/threonine-protein phosphatase 4 regulatory subu	PPP4R2	1	4.572930891	38.6281509	43.3484872	62.1549465	15.252853
Disks large-associated protein 5	DLGAP5	5	4.351537079	60.8029736	130.667281	192.502407	95.0682527
Nuclear pore complex protein Nup214	NUP214	8	4.318885845	70.6282002	248.352803	152.490248	124.154159
Myosin-10	MYH10	11	4.244779536	68.1660377	1063.35332	124.383033	457.104552
Epidermal growth factor receptor substrate 15	EPS15	1	4.070782532	7.8062687	10.7246406	10.8210651	3.65200494
Serine/threonine-protein phosphatase 2A catalytic subur	PPP2CA	1	3.836634319	5.51210305	40.2751682	16.6345709	31.6797124
UDP-N-acetylglucosamine transferase subunit ALG13 hor	ALG13	1	3.717163886	17.3287169	17.0445295	38.266996	10.1258449
Septin-11	11-Sep	2	3.596584835	1.17292939	143.996296	4.63524838	158.220283
Glutamine synthetase	GLUL	1	3.579441834	0.70154737	9.72268585	2.73931154	10.6060915
Coatomer subunit gamma-1	COPG1	1	3.509413273	0.6405309	27.8021254	2.12796299	26.3188841
Ras suppressor protein 1	RSU1	1	3.494007177	11.2110954	4.43153022	13.3931321	1.51517929
HCG1741805, isoform CRA_a	HCG_174180	2	3.384704056	5.33239436	44.6998437	9.76039421	24.1729915
Clathrin light chain B	CLTB	3	3.366327982	9.2632914	497.821191	19.594702	312.816959
Myristoylated alanine-rich C-kinase substrate	MARCKS	2	3.363877249	16.4862749	6.15217459	13.8555669	1.53705807
GDP-mannose 4,6 dehydratase	GMDS	7	3.358506415	9.59698124	1226.60833	35.338934	1344.86449
Disks large-associated protein 5	DLGAP5	1	3.324837312	30.8488385	16.2978938	62.1996041	9.88347995
DnaJ homolog subfamily C member 9	DNAJC9	1	3.305194385	11.5455149	9.70795953	20.2675902	5.15608133
Serine/threonine-protein phosphatase 2A catalytic subur	PPP2CA	3	3.289804153	27.0614013	165.270745	76.2234985	141.502638
Serine hydroxymethyltransferase, cytosolic	SHMT1	11	3.283555915	15.7578787	2168.27178	55.7555469	2336.46688
Spectrin alpha chain, non-erythrocytic 1	SPTAN1	1	3.264490765	0.17073515	39.4066542	0.65870319	46.5715761
TMSB4X protein (Fragment)	TMSB4X	1	3.072059703	44.5009385	8.95605093	49.2116254	3.2239288
Adenosylhomocysteinase	AHCY	18	3.057961256	63.2639842	6088.18477	196.638334	6188.2449
Kinesin-like protein KIF20A	KIF20A	3	3.037849551	43.7989995	29.7476569	91.9039439	20.5473804
Cystathionine beta-synthase	CBS	1	3.021177171	3.54025337	2.60788069	5.62263857	1.37093653

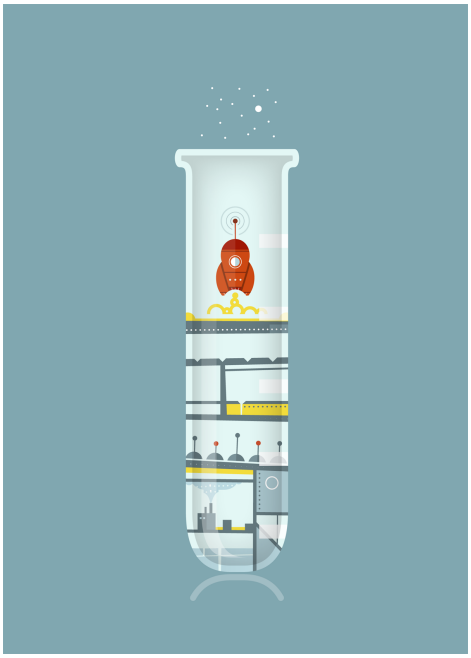

This thesis was typeset using LaTeX, originally developed by Leslie Lamport and based on Donald Knuth's TeX. The body text is set in 11 point Egenolff-Berner Garamond, a revival of Claude Garamont's humanist typeface. The above illustration, *Science Experiment 02*, was created by Ben Schlitter and released under CC BY-NC-ND 3.0. A template that can be used to format a PhD dissertation with this look & feel has been released under the permissive AGPL license, and can be found online at github.com/suchow/Dissertate or from its lead author, Jordan Suchow, at suchow@post.harvard.edu.